Allostery governs Cdk2 activation and differential recognition of CDK inhibitors

A DISSERTATION

SUBMITTED TO THE FACULTY OF THE GRADUATE SCHOOL

OF THE UNIVERSITY OF MINNESOTA

BY

Abir Majumdar

IN PARTIAL FULFILLMENT OF THE REQUIREMENTS

FOR THE DEGREE OF

DOCTOR OF PHILOSOPHY

Nicholas M. Levinson

May, 2021

Acknowledgements

It feels like an immense act of hubris to call this "my" work. However, administrative stipulations dictate that I must do so to receive my degree. These are the people I will forever be grateful to:

My advisor, Dr. Nicholas Levinson, welcomed me into his brand new laboratory five years ago, despite my having next to no bench experience. He then proceeded to do something even more ridiculous: he actually taught me how to be a good scientist. Nick's unceasing enthusiasm for kinase biology, his incredible ability to hone in on minuscule details, and his constant willingness to hear me out (even on the days we didn't see eye to eye) left their mark on me as a student. Joining his lab was easily one of the best decisions I've ever made; thank you, Nick.

My thesis committee was invaluable in helping me identify many of the scientific questions addressed in this dissertation. In the latter part of my time here, I regret that I absolutely underused the formidable intellect and many years of accumulated knowledge that comprise my committee as a whole. However, each member of my committee was individually influential in their own right: Dr. Carol Lange taught me how to think like a cancer biologist, Dr. Sivaraj Sivaramakrishnan taught me how to think mechanistically about kinase biology, and Dr. Kevin Wickman (in his capacity as department chair) taught me (in my capacity as department gadfly) how to think more

like a leader. Thank you, Carol, Shiv and Kevin.

The team at the BTC always made me feel welcome to walk in when I had questions. A special thank you to Dr. Andrew Thompson, who taught me how to run and analyze DEER experiments from start to finish, and Dr. Joseph Muretta, who taught me the intricacies of FRET.

Science can be an incredibly isolating experience, but the folks in the Levinson Lab ensured that it never really felt that lonely. Thank you to Soreen Cyphers, Dr. Emily Ruff, Dr. Kaya Erbil, Dr. David Burban, Dr. Eric Lake, Damien Rasmussen, Tiffany Engel, Apoorva Limaye and Zach Baker for the fun conversations, the help with my experiments, and putting up with the sound of my jingly keys.

The support staff at the department of pharmacology handled the logistics and paperwork to the point where I barely noticed having to do any at all. Thank you to Eric Zhang, Jim Shoemaker and Hannah Salen for all of the work you did in the background.

Without the custodial staff at NHH, our workplace would be a literal trash heap. Thank you for coming in at night and keeping our lab clean. In particular, I'd like to thank Asegedech and Kan for always checking to see how I was doing and why I was in so late.

Finally none of this would have been possible without the support of my friends and family. A huge thank you to:

- My friends for checking in on me and letting me vent about ponderous scientific things that may not have made any sense.
- My parents, Ramanath and Radha Majumdar, for your constant support throughout my many years of school.
- My sister, Manjari, for keeping me grounded and never failing to make me laugh.

- My diabetic cat, Tucker, and my reactive dog, Doug, for always keeping me on my toes at home.

- My partner, Marcheta Fornoff, who has heroically stuck by my side for the entirety of my time in graduate school. Thank you for helping me celebrate the triumphs, sharing the burden of the bad days, and putting up with my awful sense of time. I hope you will forgive all of the calls and messages I missed while I was in the basement of NHH.

Financial support for this work came from the National Institutes of Health Cancer Biology Training grant (no. T32 CA009138, A.M.), which supported me personally, and the National Institutes of Health (no. R01 GM121515, N.M.L.), which supported the lab.

Significant portions of this dissertation have previously appeared in the following publication: Majumdar, A., Burban, D.J., Muretta, J.M. *et al.* Allostery governs Cdk2 activation and differential recognition of CDK inhibitors. *Nat Chem Biol* **17**, 456–464 (2021). https://doi.org/10.1038/s41589-020-00725-y

Dedication

This work is dedicated to the patients whose illnesses we often invoke to justify our own publicly funded research, but whose health outcomes we leave to the mercy of insidious "market forces."

You deserve so much better.

Abstract

Cyclin-dependent kinases (CDKs) are the master regulators of the eukaryotic cell cycle. To become activated, CDKs require both regulatory phosphorylation and binding of a cognate cyclin subunit. Using a series of DEER and NMR experiments, we studied the activation process of the G1/S kinase Cdk2 in solution. We show that catalytically inactive Cdk2 readily adopts multiple active-like states for efficient dephosphorylation, and that regulatory phosphorylation on the activation loop enhances allosteric coupling with the cyclin subunit. We then used DEER and FRET experiments to measure the binding of multiple CDK inhibitors and developed a thermodynamic model that describes the allosteric coupling between regulatory phosphorylation, cyclin binding and inhibitor binding. We reveal that the allosteric coupling between these biochemical effectors is responsible for the differential recognition of Cdk2 and Cdk4 inhibitors. Finally, we used sequence analysis, DEER, FRET and activity assays to identify and measure the effects of mutating an allosteric hub that has diverged between Cdk2 and Cdk4. We demonstrate that this hub controls the strength of allosteric coupling, and that the altered architecture and allosteric wiring of Cdk4 leads to compromised activity toward generic peptide substrates and comparative specialization toward its primary substrate retinoblastoma (RB).

Contents

Acknowledgements **i**

Dedication **v**

Abstract **vi**

List of Figures **x**

List of Acronyms **xii**

1 Introduction **1**

1.1 An introduction to the protein kinase fold 1

1.2 An introduction to cyclin dependent kinase 2 3

1.3 The implication of Cdk2 in cancers 6

1.4 The role of the architecture of the CDK core in allosteric regulation . . 7

2 Allostery governs activation of Cdk2 **9**

2.1 Background 9

2.1.1 Cyclin and phosphorylation synergistically affect the Cdk2 activation loop 12

2.1.2 How to determine how much of the kinase is in a particular conformational state . . . 14
2.2 Results . . . 21
2.2.1 Cdk2 samples catalytically inactive Aloop-out states . . . 27
2.3 Methods . . . 32

3 Allostery governs inhibitor binding in Cdk2 35
3.1 Background . . . 35
3.1.1 A note on the Cdk2 FRET experiment . . . 42
3.2 Results . . . 42
3.2.1 Cdk2 inhibitors drive conformational shifts upon binding . . . 42
3.2.2 Inhibitor and cyclin binding are allosterically coupled . . . 50
3.3 Methods . . . 59

4 Allostery manifest in the architecture of Cdk2 63
4.1 Background . . . 63
4.2 Results . . . 65
4.2.1 The autoinhibitory hub of Cdk2 differs from that of Cdk4 . . . 65
4.2.2 A divergent hub controls allosteric coupling in Cdk2 . . . 67
4.3 Methods . . . 81

5 Conclusion and Discussion 83
5.1 Summary . . . 83
5.2 The role of cyclins in the conformational balance of CDKs . . . 85
5.3 The importance of considering the conformational equilibrium in drug discovery . . . 86

5.4 Towards an understanding of the role of hub mutations in the evolution of the eukaryotic cell cycle 88
Bibliography 90

Appendix A. A brief comparison of Cdk2 and AurA DEER results 102

List of Figures

1.1 The x-ray structure of PKA 2

1.2 The role of CDKs in the eukaryotic cell cycle 4

1.3 The x-ray structures of Cdk2 and pCdk2:cyclinA 5

1.4 Cdk2/cyclinE-implicated cancer survival curves 6

2.1 X-ray structure of the Cdk2:cyclinA dimer of dimers 10

2.2 Catalytic activity of Cdk2 in four biochemical states 11

2.3 A simple Cdk2 fluorescence experiment 13

2.4 A basic illustration of the Zeeman effect. 15

2.5 MTSSL structure 17

2.6 The four pulse DEER experiment 18

2.7 Cdk2 A-loop B factors and label modeling 19

2.8 Validation of the Cdk2 A-loop DEER construct 20

2.9 Validation of the Cdk2 αC-helix DEER construct 21

2.10 Cdk2/Cdk2:cyclinA MTSSL rotamer modeling 22

2.11 Cdk2/Cdk2:cyclinA DEER results 23

2.12 pCdk2/pCdk2:cyclinA MTSSL rotamer modeling 24

2.13 pCdk2/pCdk2:cyclinA DEER results 25

2.14 K03861 structure 26

2.15 Allosteric two state model for cyclin binding 27
2.16 PRE data mapped onto x-ray structures of Cdk2 28
2.17 PRE results for Aloop-out states of Cdk2 29
2.18 The three Aloop-out states of Cdk2 31
2.19 DEER fits of the three Cdk2 Aloop-out states 31
3.1 Flavopiridol structure 37
3.2 Roscovitine structure 38
3.3 Dinaciclib structure 39
3.4 AZD5438 structure 39
3.5 Palbociclib structure 40
3.6 Ribociclib structure 41
3.7 Abemaciclib structure 41
3.8 Apo Cdk2/Cdk2:flavopiridol DEER results 43
3.9 Cdk2:dinaciclib/Cdk2:roscovitine DEER results 44
3.10 Cdk2:inhibitor A-loop DEER spectra 45
3.11 Cdk2:inhibitor αC-helix DEER spectra 46
3.12 Allosteric two state model for the Cdk2:inhibitor DEER experiments . . 47
3.13 Cdk2:dinaciclib/Cdk2:roscovitine x-ray structures 48
3.14 Cdk2:AZD5438 x-ray structure 48
3.15 Cdk2:cyclinA:flavopiridol/Cdk2:cyclinA:ADP x-ray structures 49
3.16 DEER spectra of Cdk4 inhibitors bound to Cdk2:cyclinA 50
3.17 Cdk2 FRET labeling schematic 51
3.18 A representative FRET inhibitor binding titration 52
3.19 Allosteric two state model for the Cdk2:inhibitor FRET experiments . . 52
3.20 Cdk2/pCdk2:inhibitor FRET titrations 53
3.21 Cdk2 inhibitor β values 54

3.22 Cdk2/pCdk2:cyclinA microscopic equilibrium constants 55
3.23 Cdk2:inhibitor microscopic equilibrium constants 56
3.24 pCdk2:inhibitor microscopic equilibrium constants 57
3.25 pCdk2:cyclinA:inhibitor IC_{50} values 58
3.26 Visualization of DEER constraints for ATSM 61
3.27 Representative error surface for FRET global fits 62
4.1 Sequence alignment of CDKs 1-9 64
4.2 pCdk2:cyclinA and pCdk4:cyclinD x-ray structures 66
4.3 Comparison of the core residues of Cdk2 and Cdk4 67
4.4 Phylogenetic tree of Cdk1/2/4/6 across metazoans 69
4.5 Structures of the divergent allosteric hub 70
4.6 Phylogenetic tree of the Cdk2 hub residue A151 70
4.7 Validation of the $Cdk2^{cdk4hub}$ construct 72
4.8 Conformational equilibrium values for WT pCdk2 and mutants 73
4.9 $pCdk2^{cdk4hub}$ DEER data 74
4.10 $pCdk2^{L148R}$ DEER data 74
4.11 Cyclin affinities for WT Cdk2, $Cdk2^{L148R}$ and $Cdk2^{cdk4hub}$ 75
4.12 Comparison of Cdk2:cyclinA:inhibitor K_D values 77
4.13 Comparison of Cdk2:inhibitor K_D values 78
4.14 Comparison of IC_{50} values for pCdk2 and pCdk4 79
A.1 The continuum of Cdk2 conformations 103
A.2 The continuum of Aurora A conformations 104

Acronyms

A-loop activation loop. 1

ATSM allosteric two-state model. 51

CAK Cdk activating kinase. 4

CDK cyclin-dependent kinase. 3

CLL chronic lymphocytic leukemia. 36

CML chronic myelogenous leukemia. 6

DEER double electron-electron resonance. 14

DFG aspartate-phenylalanine-glycine. 47

EPR electron paramagnetic resonance. 14

FRET Förster resonance energy transfer. 36

KAP kinase associated phosphatase. 28

MTSSL 1-oxyl-2,2,5,5-tetramethylpyrroline-3-methyl)methanethiosulfonate. 16

NMR nuclear magnetic resonance. 27

NSCLC non-small-cell lung cancer. 38

PRE paramagnetic relaxation enhancement. 27

Chapter 1

Introduction

1.1 An introduction to the protein kinase fold

Protein kinases are an indispensable component of cellular function. Their role is simple: catalyze the transfer of the γ-phosphate from ATP to a peptide substrate, a task that, when performed correctly, forms the basis for much of the signalling transduction in living cells[1]. Despite the relatively uncomplicated nature of *what* they do, the ubiquity of protein kinases in cellular signalling and the disastrous consequences of uncontrolled kinase expression and activity require a nuanced understanding of *how* different kinases in the >500-member kinase family work.

At the time of this writing, it has been thirty years since the x-ray structure of a protein kinase was first reported[2]. A seminal work, the structure (of cAMP protein kinase, commonly known as PKA) illustrated the basic fold of a kinase (Figure 1.1): one lobe containing five antiparallel β-sheets and an α-helix (the "αC-helix"), a larger lobe composed mostly of α-helices, and, in between, an ATP-binding cleft and a long, unstructured loop across which the substrate docks (the "activation loop," or "A-loop")[3].

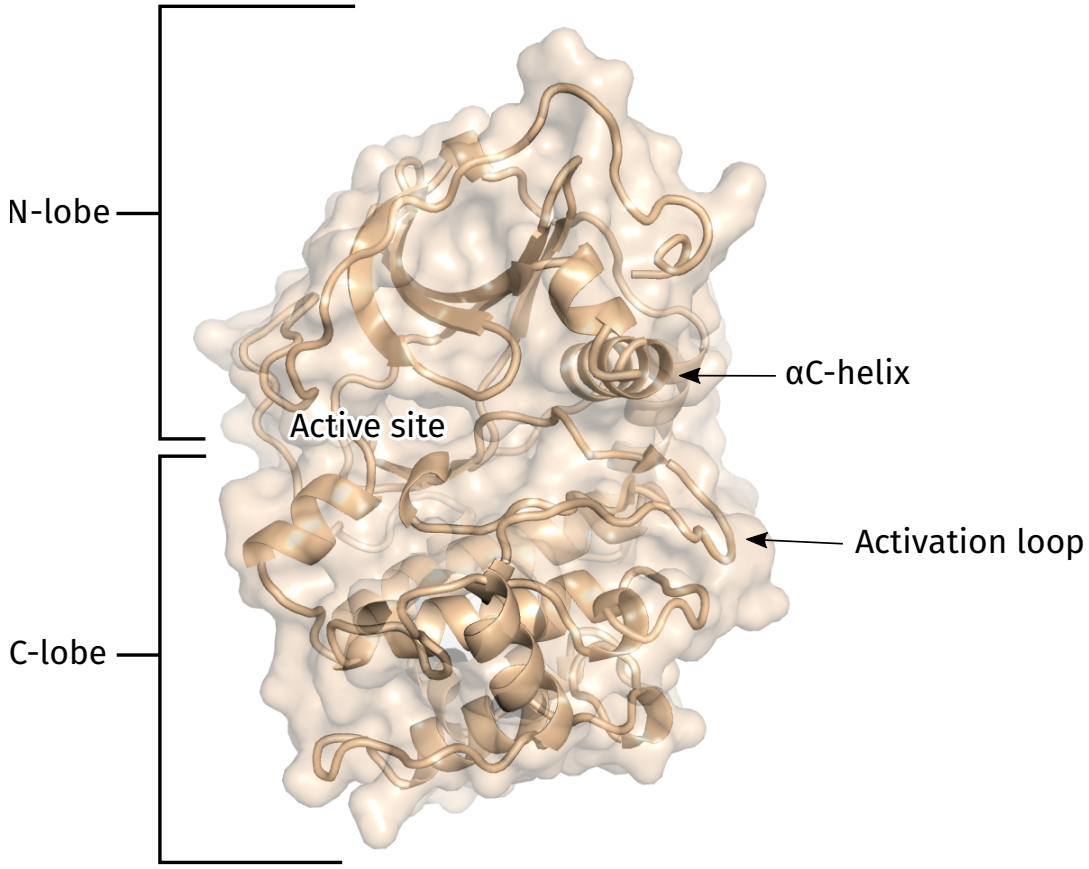

Figure 1.1: The first reported x-ray structure of a protein kinase, PKA (PDB: 2CPK). The structure depicts a bilobal fold with several key domains conserved across all protein kinases.

Structures of other kinases soon followed, demonstrating that despite the significant differences in the amino acid sequences of protein kinases, the kinase fold itself is highly conserved. To date, roughly half of the human kinome has been characterized structurally and deposited to the Protein Data Bank[4], providing a framework for comparing structures across the kinase family, identifying the structural basis for behaviors unique to particular kinases and even designing inhibitors for kinases implicated in human disease.

These structures have also raised at least as many interesting questions as they have answered. Protein kinases represent a constant and delicate thermodynamic balancing act exquisitely dependent on protein structure. Consider the following:

- a kinase must be able to perform its function, but only when and where called upon to do so by the cellular environment (a kinase must have *control mechanisms*).
- a kinase must be able to bind the same phosphodonor as the other kinases (Mg^{2+}-ATP), but it must be able to distinguish and bind its own phosphoacceptor substrate (a kinase must have *specificity*).
- a kinase must be able to maintain its own structure, but be malleable enough so as to undergo the structural transitions necessary for the previous two conditions (a kinase must be *dynamic*).

These conditions have imposed a set of challenges that evolution has dealt with in both dramatic and subtle ways. This work represents a small dent[5] in the understanding of how one particular kinase, Cdk2, works.

1.2 An introduction to cyclin dependent kinase 2

The cyclin-dependent kinases (CDKs) are a subfamily in the CMGC group of kinases. Grouped together because of their dependence on a cyclin binding partner for activity, the human CDKs comprise at least twenty members, four of which have been identified as the central regulators of the cell cycle in all eukaryotes. Cdk1 orchestrates progression through mitosis, Cdk2 controls the G1/S transition, and Cdk4 and Cdk6 trigger cell cycle entry in response to growth factor signaling[6] (Figure 1.2).

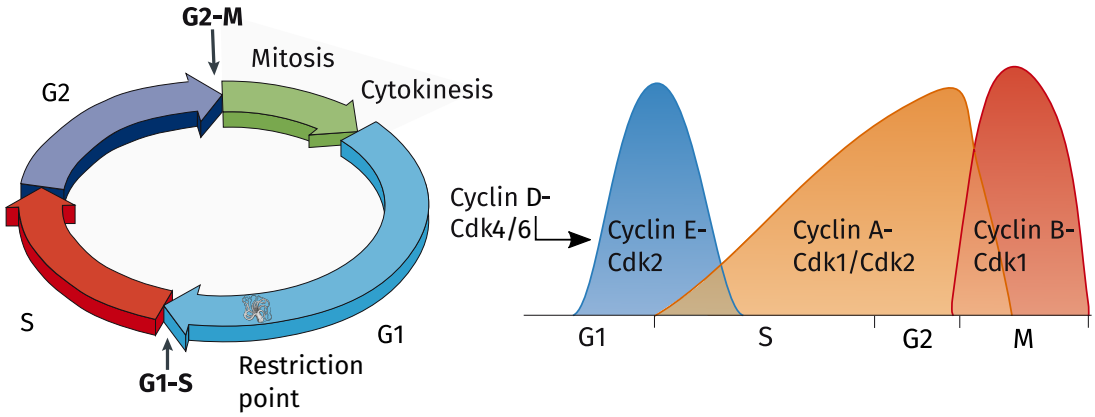

Figure 1.2: CDKs 1,2,4 and 6 comprise the regulatory checkpoints for the eukaryotic cell cycle. Adapted from [7].

The CDKs are inactive as monomeric kinases and require two separate steps for activation. In the canonical model developed for Cdk2, the kinase is first phosphorylated on the A-loop on a specific site (T160 in Cdk2) by a Cdk activating kinase (CAK) complex[8], and is subsequently activated by binding of a cognate cyclin subunit[9]. While CAK is active throughout the cell cycle, the expression of each cyclin subunit is restricted to a specific cell cycle stage, ensuring coordinated progression through the cell cycle.

Cdk2 has been extensively characterized by crystallography, allowing for the identification of its conformational endpoints. Monomeric Cdk2 adopts an autoinhibited conformation in which the αC-helix swings out of the active site, breaking a catalytically-important salt bridge ("αC-out"), and the A-loop folds into the active site, blocking substrate binding ("Aloop-in;" Figure 1.3, left)[10]. Cyclin binding triggers rotation of the αC-helix into the active site ("αC-in") and refolding of the A-loop into an extended conformation that permits substrate binding ("Aloop-out;" Figure 1.3, right)[11]. Cyclin binding also buries the phosphorylated T160 residue, blocking dephosphorylation and inactivation of the kinase[12]. This is thought to facilitate the abrupt switch-like

activation of Cdk2 at the G1/S boundary.

The numerous static x-ray structures of Cdk2 have provided key insights into the allosteric effects of both cyclin binding and phosphorylation on Cdk2 activation, as well as a wealth of information about the stable conformational states of the kinase. *The extent to which* cyclin and phosphorylation act through allostery, and *how* Cdk2 transitions between these macrostable states, however, remains an open question, and is the topic of chapter 2.

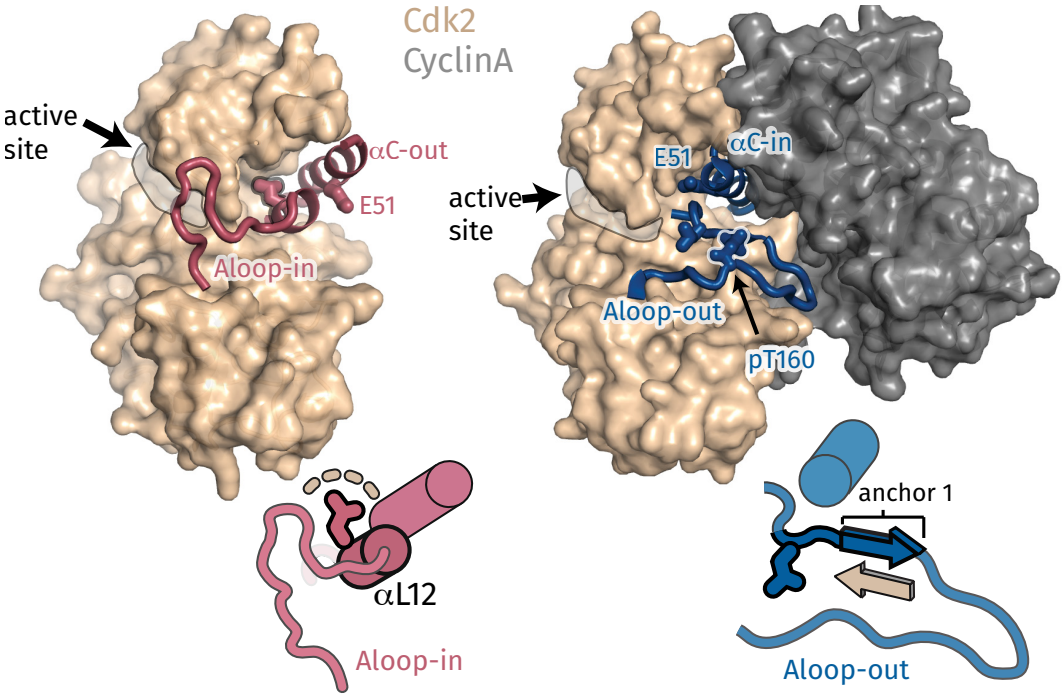

Figure 1.3: X-ray structures of Cdk2 in the Aloop-in/αC-out and Aloop-out/αC-in states (PDB: 1HCK and 1JST), accompanied by schematics of the respective A-loop and αC-helix conformations. The segment of the A-loop highlighted in the schematics refolds from a helix (αL12) in the Aloop-in state to an anchoring β-strand in the Aloop-out state. Adapted from [13].

1.3 The implication of Cdk2 in cancers

Pathogenesis at the level of individual unregulated proteins is often extremely difficult due to the complex network of protein interactions required for cellular function. However, there have been some indisputable triumphs in identifying oncogenic drivers in the kinase field, the most salient of which is the identification of BCR-ABL as the cause of chronic myelogenous leukemia (CML). The road to treatment for this disease spanned some forty years, from the initial description of the Philadelphia Chromosome[14], to the identification of the specific deregulated tyrosine kinase[15] to the development of imatinib, the first FDA-approved protein kinase inhibitor[16], and many other significant breakthroughs along the way[17]. At the time of this writing, there are 62 FDA-approved small molecule kinase inhibitors for the treatment of cancer and inflammatory diseases[18].

Although Cdk2 is not a classic oncogene, it has been implicated in several types of cancer, most commonly through the overexpression of its binding partner cyclinE[19,20] (Figure 1.4 a,b) and low molecular weight isoforms thereof[21]. More recently, high expression of Cdk2 itself has been shown to be a possible driver of glioblastoma[22] (Figure 1.4c).

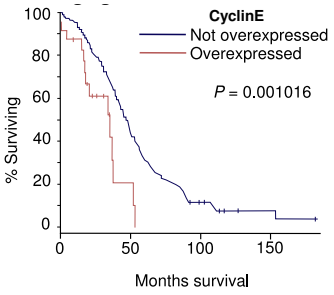

(a) High grade serous ovarian cancer; adapted from [19].

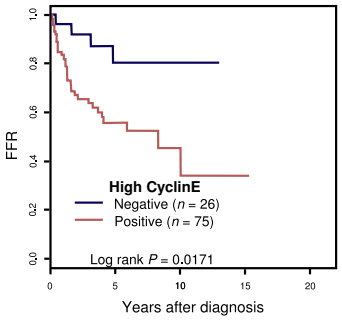

(b) Triple negative breast cancer; adapted from [20].

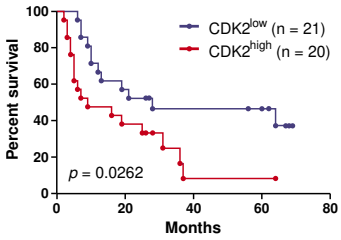

(c) Glioblastoma; adapted from [22].

Figure 1.4: Survival curves showing that high expression of cyclinE or Cdk2 is correlated with worse long term outcomes in cancer patients.

Although a number of inhibitors have been developed for Cdk2, all of them have failed out of clinical trials due to a lack of efficacy and/or off-target toxicity. Although there are many theories as to why these inhibitors have not been met with the same degree of success as with other kinases, a true mechanistic understanding of how the inhibitors bind to and interact with the intrinsic allosteric regulation of the kinase itself has not been contended with. This is the focus of chapter 3.

1.4 The role of the architecture of the CDK core in allosteric regulation

The CDKs share a high degree of sequence conservation across the subfamily, and several members have been shown to compensate for one another in cells. However, there are significant differences in both the expression profile of the cyclins, as well as sequential divergence in the residues that comprise the core of the kinase. For example, the activation pathway of Cdk4/6 differs from that of the other cell cycle CDKs[23]. Expression of the cognate cyclin, cyclinD, is gradual rather than switch-like, and, unlike with Cdk2:cyclinA which is effectively trapped in the phosphorylated state as a complex, Cdk4:cyclinD complexes are continually phosphorylated and dephosphorylated on the A-loop. Reversible A-loop phosphorylation allows the activity of Cdk4:cyclinD complexes to be tuned by growth factors, which shift the balance towards phosphorylation by enhancing CAK activity. Reversible phosphorylation is possible because Cdk4, unlike other CDKs, does not switch to the active state when cyclinD binds[24,25], leaving the activation loop accessible to phosphatases[23]. Thus, the degree to which cyclin binding is coupled to kinase activation has diverged between Cdk1/2 and Cdk4/6 in a manner that reflects a biological requirement for altered activation dynamics. The role of key sequential differences in the activation and inhibitor binding profiles between Cdks 1,2

and 4 comprise the focus of chapter 4.

Chapter 2

Allostery governs activation of Cdk2

2.1 Background

The requirement of both a cyclin subunit and phosphorylation on T160 for activation of Cdk2 is well-documented[8,9,26]. However, the *extent* to which each of these modulators individually contributes to Cdk2 activation, why they are only able to activate Cdk2 in concert, and whether Cdk2 is able to adopt an active-like conformation without them is unclear. This gap in understanding arises from the following technical challenges:

- The x-ray structure of the unphosphorylated Cdk2 monomer depicts the kinase in the canonical Cdk2/Src-like autoinhibited state, in which the αC-helix is rotated out of the active site, and the activation loop has formed a β-hairpin and a short helical turn (αL12 helix) for stability (Figure 1.3). Given the propensity for x-ray crystallography to force its subject into a single conformational state, it is impossible to judge how dynamic Cdk2 is in the absence of its modulators.

- The x-ray structure of the unphosphorylated Cdk2:cyclin complex is that of a symmetric dimer of dimers ($P6_222$ space group; figure 2.1), a structure that forms at the high protein concentration needed for crystallization. This likely forces the kinase into an active-like conformation and therefore does not permit insight into the conformation of the unphosphorylated kinase bound to cyclin *at physiological concentrations*.

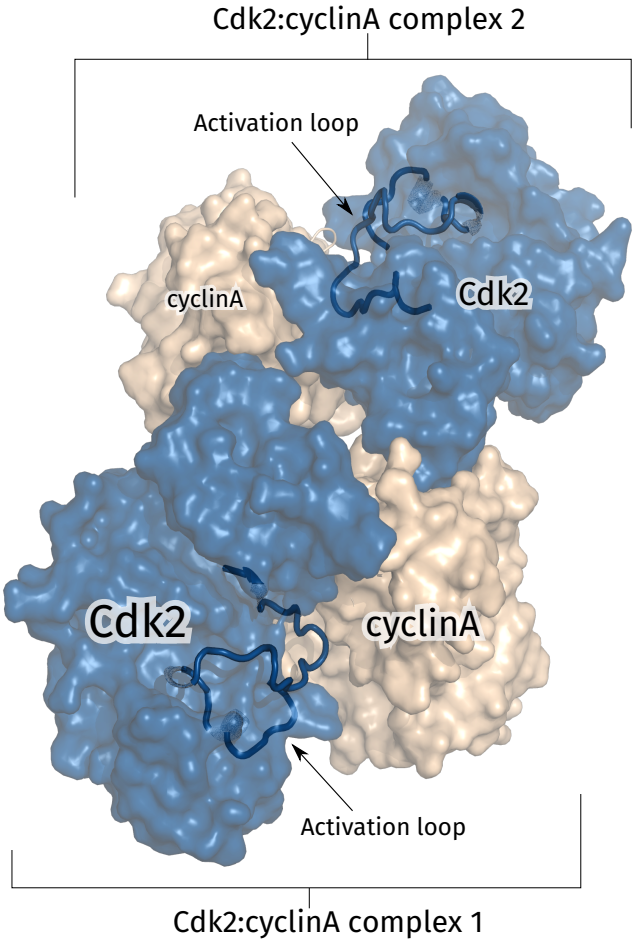

Figure 2.1: The x-ray structure of the unphosphorylated Cdk2:cyclinA complex (PDB: 1FIN), which forms a dimer of dimers. The presence of a second complex likely influences the conformational state of the first, thus confounding attempts to ascertain the effect of cyclin alone.

- In kinase activity assays, neither the unphosphorylated Cdk2:cyclin complex, nor the phosphorylated Cdk2 monomer has appreciable kinase activity, thus making it difficult to directly measure the individual contributions of cyclin binding and phosphorylation to Cdk2 activation (Figure 2.2).

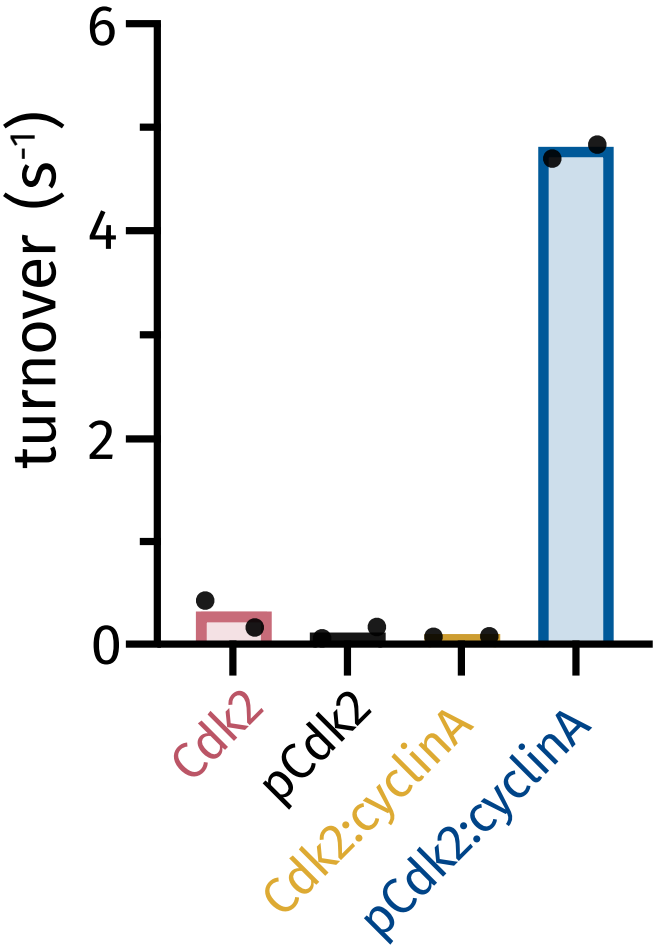

Figure 2.2: Neither the phosphorylated Cdk2 monomer (black), nor the unphosphorylated Cdk2:cyclin complex (yellow) have sufficient kinase activity to differentiate the effects of cyclin binding and phosphorylation.

Operating under the assumption that the key determinant for activity is not the conformational state of any single Cdk2 molecule, but rather the conformation of the ensemble of protein molecules, we chose to circumvent these challenges by using biophysical spectroscopy tools (fluorescence and EPR) to track important structural domains of Cdk2 while subjecting the samples to physiologically-relevant biochemical conditions.

2.1.1 Cyclin and phosphorylation synergistically affect the Cdk2 activation loop

We probed the local environment of the Cdk2 activation loop in four biochemical states: unphosphorylated monomer ("Cdk2"), phosphorylated monomer ("pCdk2"), unphosphorylated complex ("Cdk2:cyclinA") and phosphorylated complex ("pCdk2:cyclinA"). We chose this experiment because of its relative simplicity: conjugate an environmentally-sensitive fluorophore to an engineered cysteine on the A-loop of the kinase, excite the fluorophore and measure the emission spectra.

We labeled a "cys-lite1" mutant of Cdk2 (with the endogenous, solvent-exposed C177 mutated to a serine) with the solvatochromic fluorophore acrylodan on two residues on either side of the T160 phosphorylation site: R157C and E162C. Acrylodan, which conjugates to the cysteines by a thioether bond, is highly sensitive to the polarity of its surrounding environment. These changes are reflected in the energy of the excited state, which manifests as a change in the fluorophore's emission wavelength (Stokes shift)[27]. In the context of this experiment, an increase in the emission wavelength (redshift) can generally be associated with greater exposure to the solvent or polar residues, and a decrease in emission wavelength (blueshift) can be associated with a more hydrophobic environment.

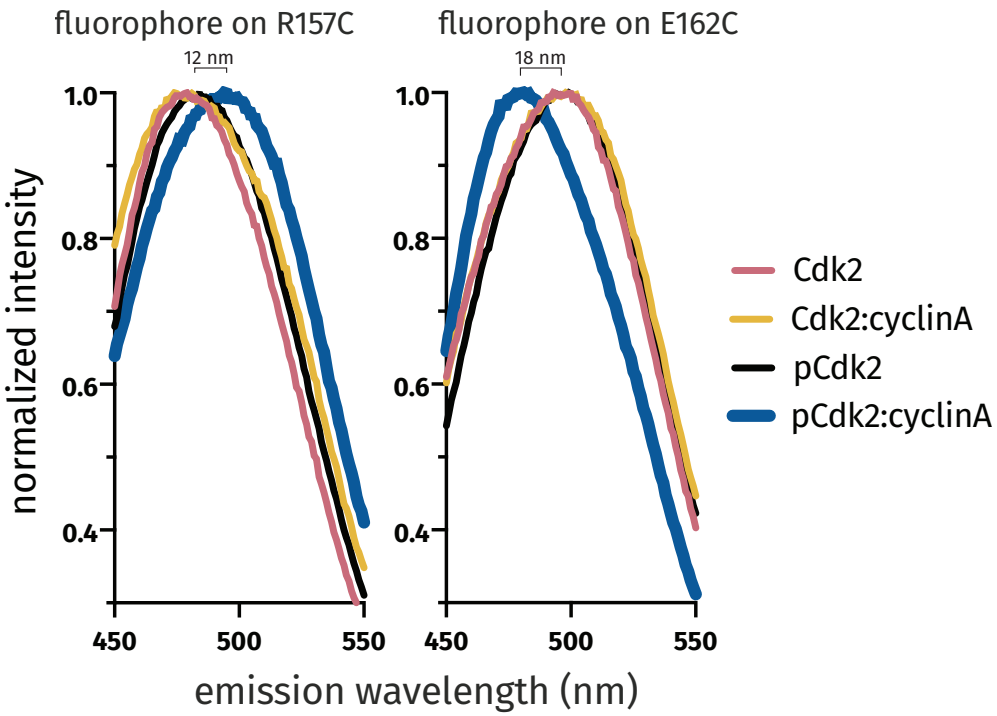

Figure 2.3: Emission spectra of acrylodan conjugated to two different sites on the A-loop of Cdk2 (R157C, left; E162C; right). The fluorophore was excited at 370 nm. Only the pCdk2:cyclinA samples (blue) exhibited large Stokes shifts, suggesting that cyclin and phosphorylation together affect the A-loop differently than either alone.

In both sets of spectra, the emission profile of the pCdk2:cyclinA sample was markedly different from that of the others; the R157C sample exhibited a redshift of approx. 12 nm, while the E162C spectrum blueshifted by 18 nm (Figure 2.3). While it is difficult to deduce the structure of a protein domain based on the emission profile of a conjugated dye (due to the complex set of electronic effects that contribute to a Stokes shift), the qualitative differences pointed to a profound result that is not immediately obvious in the x-ray structures of Cdk2: cyclin-binding and phosphorylation on T160 together affect the local environment of the tip of the A-loop in a way that neither can achieve alone. This result led us to study the conformational balance of Cdk2 in a more

quantitative fashion.

2.1.2 How to determine how much of the kinase is in a particular conformational state

Due to the ensemble nature of protein kinases in cells, it is often enough to measure the steady state average of kinase activity or structure to reap useful information about the biochemical state. However, in order to develop a quantitative model that ties the biochemical state to kinase conformation, it is necessary to be able to break down the ensemble into its constituent subpopulations. We thus chose double electron-electron resonance (DEER) spectroscopy to track conformational changes of Cdk2 in solution. DEER, which was used to obtain the bulk of the results in this chapter, is one of several types of experiments that comprise electron paramagnetic resonance spectroscopy (EPR), and is an underused technique in structural biology. The fundamental concepts required to understand the method are summarized below.

The Zeeman effect

(EPR) spectroscopy is a method used to study the properties of materials with unpaired electrons. EPR exploits a phenomenon called the Zeeman effect, which describes the energy gap between the ground and excited states that unpaired electrons can occupy in the presence of a magnetic field $\mathbf{B}_0$ because they possess an intrinsic angular momentum (called *spin*). An unpaired electron in the ground state can be promoted to the higher energy state by absorbing a photon of energy equal to the gap between the two states (Figure 2.4):

$$h\nu = g_{\mathrm{e}}\mu_{\mathrm{B}}B_0 \tag{2.1}$$

where g_e is the g-factor for an electron, μ_B is the Bohr magneton and B_0 is the strength of the magnetic field. A simple example of an EPR experiment is one in which the number of unpaired electrons in a sample are counted; this is typically done by exposing the sample to a fixed microwave radiation source and a magnetic field of variable strength, and integrating the absorption spectrum that results.

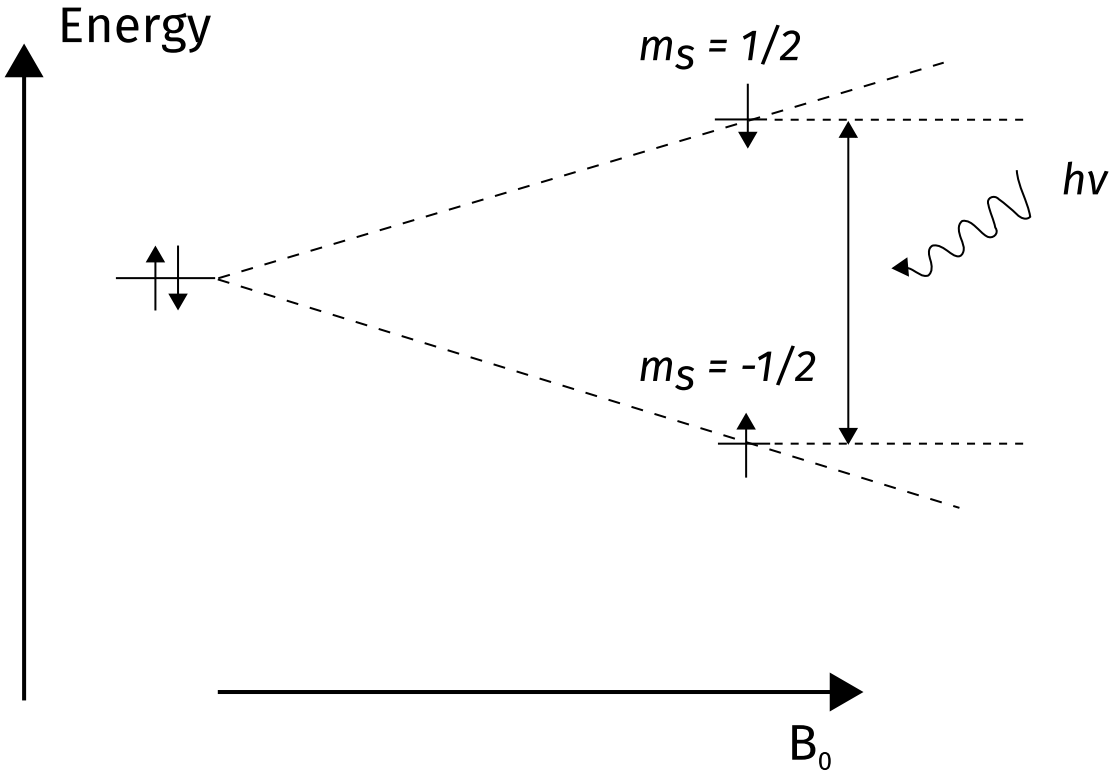

Figure 2.4: A basic illustration of the Zeeman effect.

Double electron-electron resonance

DEER spectroscopy combines the basic concept of EPR with the phenomenon of magnetic dipolar coupling, a through-space interaction that occurs when two (for our purposes, but in principle this is true in a pairwise fashion for any n >1) unpaired electrons are in relatively close proximity. The dipolar coupling between two electrons, ω_{ab}, is

described by

$$\omega_{\mathrm{ab}} = \frac{1}{r_{\mathrm{ab}}^3} \frac{\mu_{\mathrm{B}}^2 g_{\mathrm{a}} g_{\mathrm{b}}}{\hbar} (3\cos^2\theta_{\mathrm{ab}} - 1) \tag{2.2}$$

where r_{ab} represents the distance between the two electrons (notice that ω_{ab} drops off in a manner inversely proportional to the third power of the distance), μ_{B} is the Bohr magneton, g_{i} is the g factor for each electron, and θ_{ab} is the angle between the dipolar axis and the magnetic field.

DEER in protein structural biology makes use of the Zeeman effect, dipolar coupling and some amount of mathematical wizardry to back out the distances between two parts of a protein, and thereby ascertain its conformational states. In practice, this involves the following:

1. Preparation of a purified protein sample with two spin labels (each of which contains one unpaired electron) conjugated to each protein molecule. There are several stable nitroxide spin labels available for this purpose, the most commonly used being MTSSL (Figure 2.5). The use of MTSSL requires formation of a disulfide bond to engineered cysteine residues on the protein. This requires the removal of labile, endogenous cysteine residues (a more challenging alternative is to introduce the unnatural amino acid *p*-acetyl-L-phenylalanine and label with a hydroxylamine spin label[28]). For higher quality data, the buffer should be deuterated and the labeled sample must be rapidly frozen.

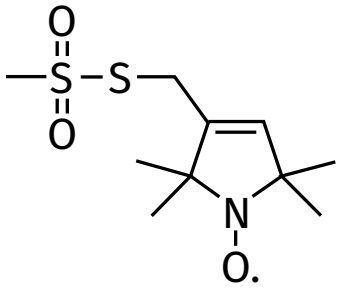

Figure 2.5: The chemical structure of (1-oxyl-2,2,5,5-tetramethylpyrroline-3-methyl)methanethiosulfonate (MTSSL), the nitroxide spin probe used to label Cdk2 in the DEER experiments.

2. Application of the DEER technique to the sample, in which the frozen sample is placed inside a resonant cavity and exposed to a fixed magnetic field as well as a specific pulse sequence of microwave radiation (Figure 2.6). The different microwave pulses provide the energy needed to excite one population of spins (arising from the Zeeman effect) and measure their effect (due to dipolar coupling) on nearby spins (i.e. measure what happens to one unpaired electron on the protein when the other unpaired electron on the protein is excited). The recorded measurement is the amplitude of the spin echo of the second population of spins, which is caused by the refocusing of their magnetization.

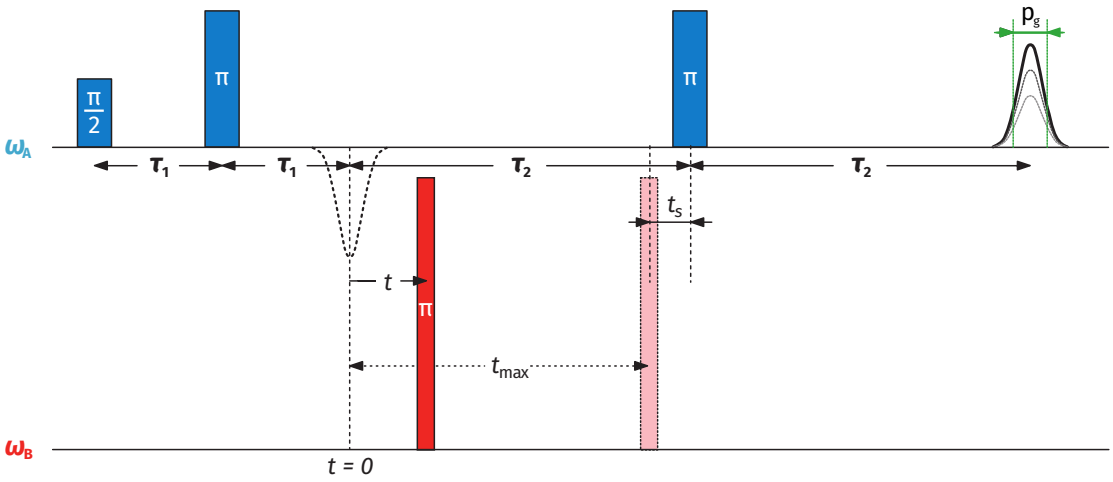

Figure 2.6: The four pulse DEER experiment. Adapted from [29].

3. Fitting of the DEER data to interspin distance distributions, which is an ill-posed problem (i.e. there is no unique solution to a particular set of primary data in DEER). This requires the user to iteratively generate distributions for known distances and convolve each distribution with the kernel function (Eq. 2.3) to match the form of the primary data in the time domain:

$$K(t,r) = \int_0^1 \cos\left[\frac{(3\theta^2-1)C_i t}{r_{\mathrm{ab}}^3}\right] d\theta \tag{2.3}$$

where C_i is the proportionality constant $\frac{\mu_{\mathrm{B}}^2 g_{\mathrm{a}} g_{\mathrm{b}}}{\hbar}$ from Eq. 2.2, t is time, and θ is the angle between the dipolar axis and the magnetic field. The final step in DEER analysis is to fit the generated, convolved distribution to the primary data.

The practical Cdk2 DEER experiment

Given the uneven geometry of the kinase fold, the locations of catalytic residues that must not be perturbed, and the propensity for some domains of the kinase to be more dynamic than others, some care was required in the spin labeling of Cdk2. We chose to

track the movements of the activation loop and αC-helix not only due to their importance in Cdk2 activity, but also because they appear to move the most across different x-ray structures, therefore maximizing our chance of capturing the active-inactive conformational transition in Cdk2.

On the activation loop of Cdk2, the residues between 154 and 161 move the farthest distance, determined from measuring the C_α-C_α distances for each residue across the Cdk2 and pCdk2:cyclinA x-ray structures. We immediately ruled out P155 and T160 because of their special properties: P155 due to the special role of prolines in protein conformation[30] and T160 phosphorylation in Cdk2 activity. We also excluded the residues immediately preceding and succeeding P155 and T160 due to their proximity to the important residues. We ultimately chose R157C (Figure 2.7) as the labeling site for MTSSL: it was located in an appropriate region of the activation loop, it replaces a relatively bulky (albeit polar) residue with a bulky spin label and it had already been validated as a construct that responds to cyclin and phosphorylation in the acrylodan experiments. Further validation demonstrated that the Cdk2 R157C construct labeled with MTSSL, could bind to cyclinA, and was catalytically active (Figure 2.8).

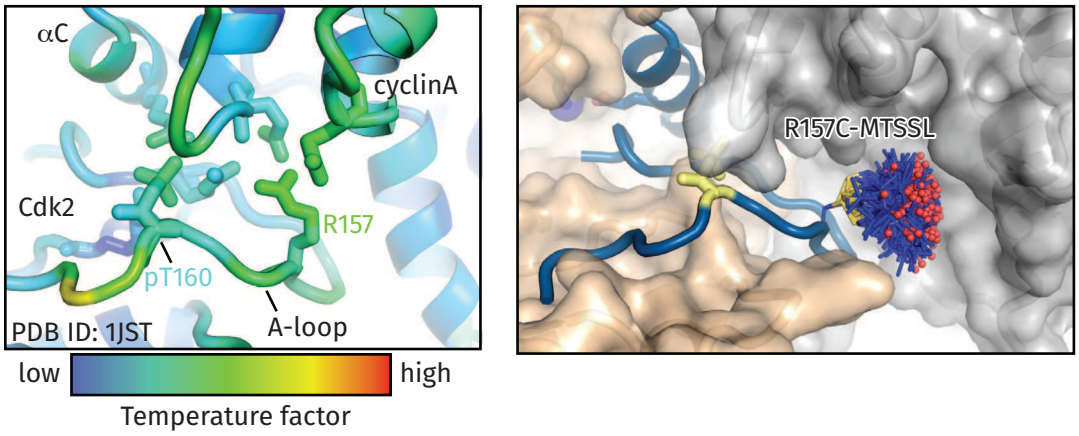

Figure 2.7: Crystallographic temperature factors (left) and spin label conformational modeling (right) of the A-loop labeling site residue R157.

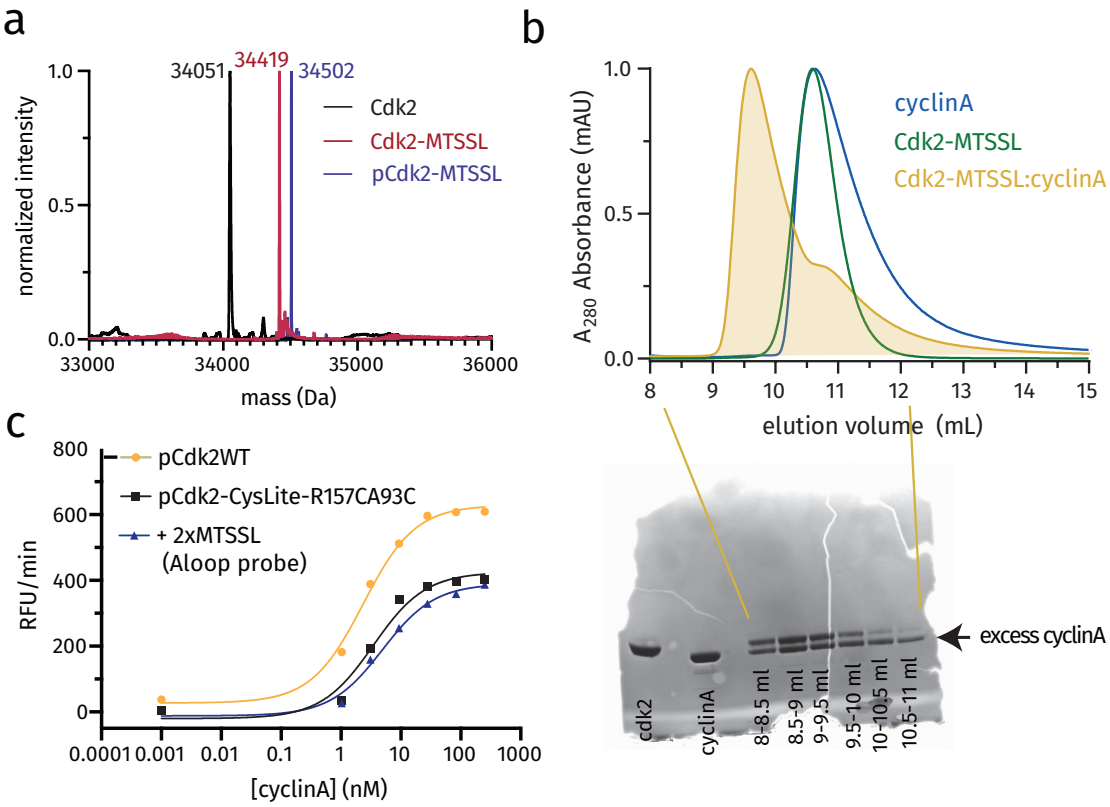

Figure 2.8: **a)** Mass spectra of unphosphorylated Cdk2 (DEER A-loop construct) without (black) and with (red) two MTSSL spin probes (+368 Da). The mass spectrum of phosphorylated Cdk2 with two MTSSL probes is shown in blue. **b)** Size exclusion chromatography traces for unphosphorylated, spin-labeled monomeric Cdk2 (DEER A-loop construct; green) and Cdk2:cyclinA dimer (yellow) as well as free cyclinA (blue), demonstrating that the spin-labeled kinase binds the cyclinA subunit. The SDS-PAGE gel shows fractions from the Cdk2:cyclinA dimer run confirming formation of the 1:1 complex and demonstrating that the sample was prepared with excess cyclinA. Protein samples used for reference Cdk2 and cyclinA markers (lanes 1 and 2) had been previously validated. This analysis was performed on the sample used for the DEER experiment. **c)** Kinase activity assays showing catalytic activation of pCdk2 WT, the unlabeled DEER A-loop construct (pCdk2-Cyslite$_2$-R157CA93C), and the DEER A-loop construct labeled with 2 MTSSL spin labels. We confirmed that the spin labels remained on the kinase in the kinase activity assay buffer by mass spectrometry.

For the αC-helix, our choice for labeling site was essentially limited to S46C, which is located at the tip of the helix, unlikely to rotate into the active site of the kinase, and

distant from the critical residues R50 and E51. Cdk2 S46C was also validated by mass spectroscopy and activity assays; the presence of the spin label did not significantly affect the ability of cyclinA to bind and activate spin-labeled pCdk2 (Figure 2.9).

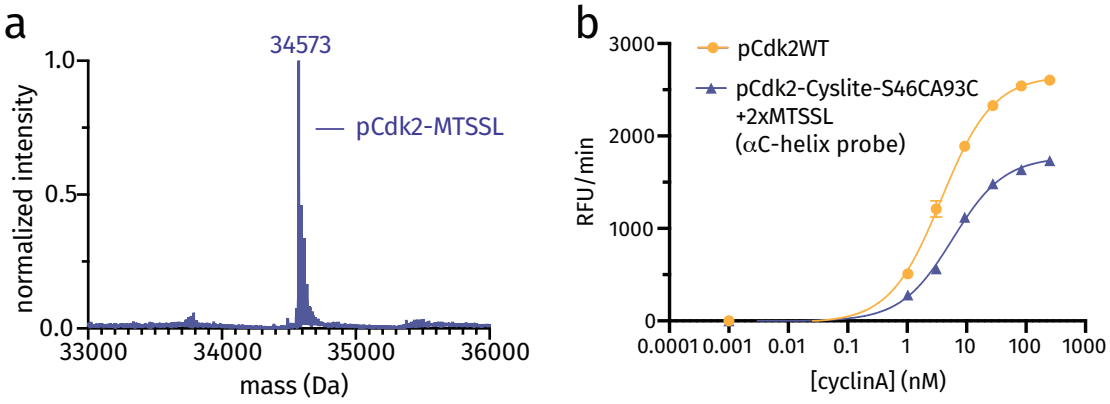

Figure 2.9: **a)** Mass spectrum of the phosphorylated Cdk2 αC-helix construct with two MTSSL labels on S46C and A93C. Expected mass: 34,573 Da. **b)** Kinase activity assays showing catalytic activity of the αC-helix probe construct compared to WT Cdk2. The activity of the +2xMTSSL sample was measured with protein previously used in the DEER experiment itself.

As for the choice of reference spin label, we chose A93C on the αD-helix, which remains immobile across the different x-ray structures of Cdk2. The aforementioned validation experiments were performed with the A93C construct.

Having chosen labeling sites, we proceeded with the DEER experiments to ascertain the conformational states of Cdk2 in solution.

2.2 Results

One pair of spin labeling sites (A93C, R157C) was used to track the A-loop between the Aloop-in and the Aloop-out states. A second pair of labeling sites (A93C, S46C) was used to track the αC-helix between αC-out and αC-in states. Assignment of peaks in the spin-spin distance distributions[31] to these structural states was achieved by reference

to calculations performed on x-ray structures[32] (Figure 2.10).

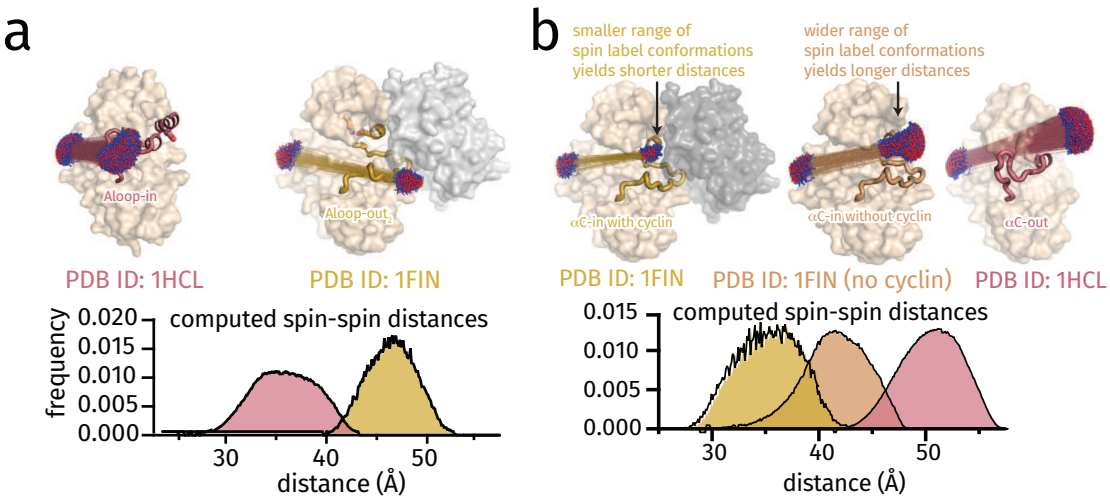

Figure 2.10: MTSSL rotamers visualized on the x-ray structures of Cdk2 using the PyMOL plugin MtsslWizard. Calculated ensemble distance distributions were used to assign conformational states to Gaussian populations from the DEER experiments measuring **a)** the A-loop of Cdk2 and Cdk2:cyclinA, showing that Cdk2 samples the Aloop-out$_1$ state, and that Cdk2:cyclinA adopts the Aloop-out$_2$ state **b)** the αC-helix of Cdk2 and Cdk2:cyclinA, showing that the MTSSL probe is more constrained in the presence of cyclin, leading to different Gaussian centers for the αC-in conformation

In experiments tracking the A-loop, monomeric unphosphorylated Cdk2 ("Cdk2") exhibited one predominant short-distance peak assigned to the Aloop-in state, and a minor longer-distance peak corresponding to an Aloop-out state (Figure 2.11). This demonstrates that monomeric Cdk2 samples the Aloop-out state to a substantial degree (13 ± 6%), as suggested by a recent molecular dynamics study[33]. Addition of cyclinA ("Cdk2:cyclinA") resulted in the Aloop-out peak becoming dominant, but a subpopulation sampling the Aloop-in state was still present, indicating an incomplete shift to the Aloop-out state (Figure 2.11).

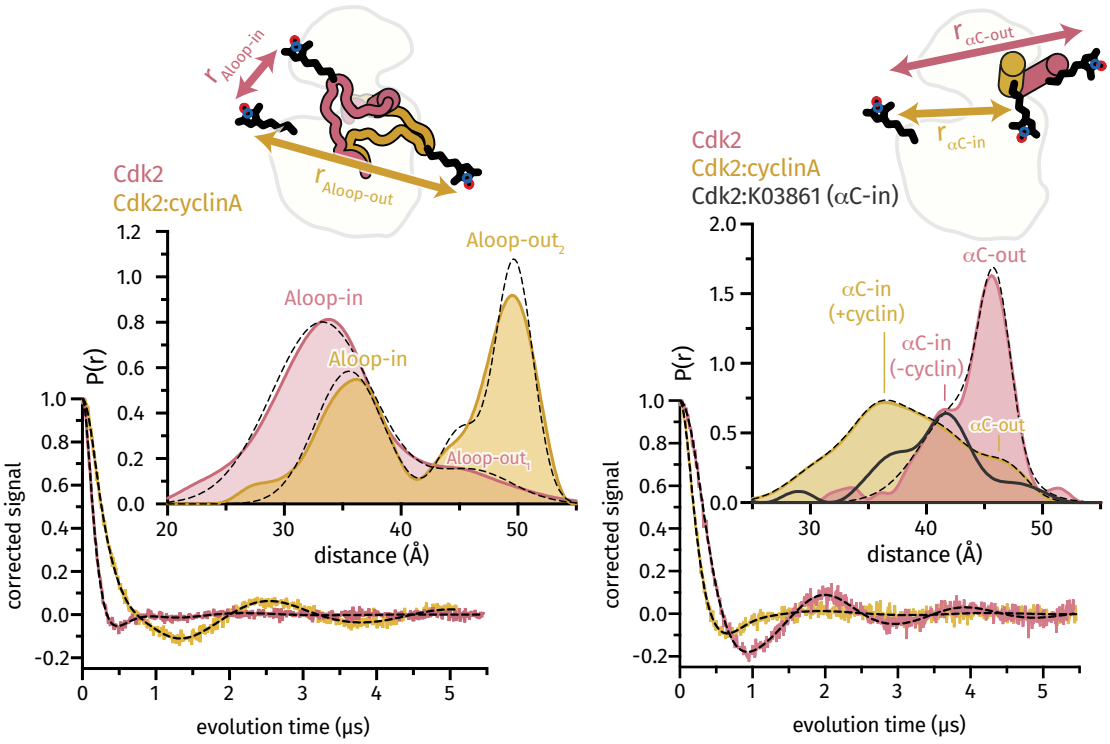

Figure 2.11: DEER experiments tracking the A-loop (left) and αC-helix (right). Tikhonov-derived distance distributions are shown for monomeric Cdk2 and Cdk2–cyclinA dimer in the unphosphorylated state. Dashed black lines represent Gaussian fits to the DEER data. Peak assignments are based on spin–spin distance calculations (Figure 2.10). The spin labeling schemes are represented schematically. Data for the αC-in inhibitor K03861 are shown in dark gray. P(r) is the probability of distance r.

DEER data collected on T160-phosphorylated monomeric Cdk2 ("pCdk2") were similar to the unphosphorylated case, although the Aloop-in peak was shifted and broadened (Figure 2.13), consistent with local disorder around the labeling site observed in the x-ray structure of phosphorylated Cdk2[34]. However, addition of cyclinA to this sample ("pCdk2:cyclinA") led to nearly homogeneous adoption of the Aloop-out state (Figure 2.13), indicating that phosphorylation enhances the cyclin-driven conformational shift.

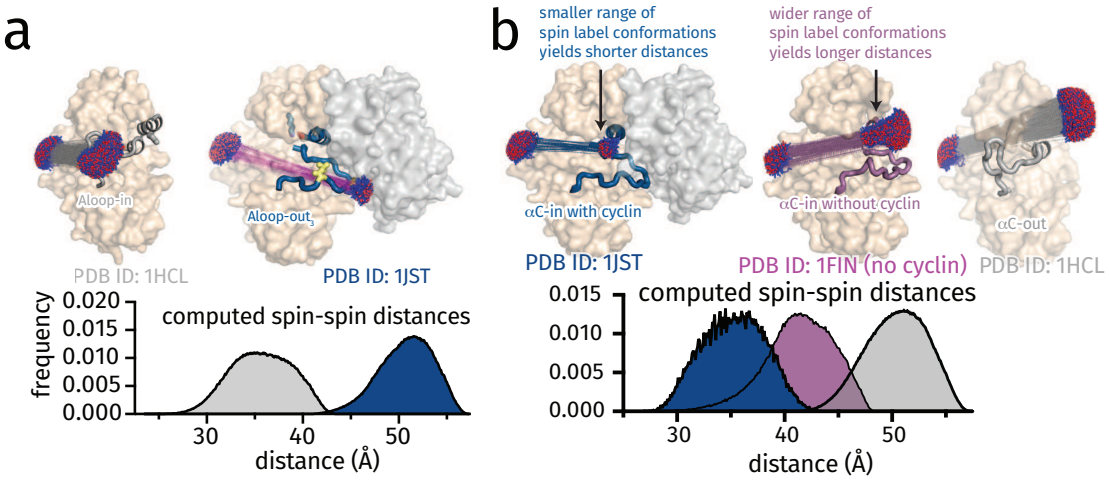

Figure 2.12: MTSSL rotamers visualized on the x-ray structures of Cdk2 using the PyMOL plugin MtsslWizard. Calculated ensemble distance distributions were used to assign conformational states to Gaussian populations from the DEER experiments measuring **a)** the A-loop of pCdk2 and pCdk2:cyclinA, showing that pCdk2 has a similar Aloop-out subpopulation to Cdk2 and that pCdk2:cyclinA adopts the Aloop-out$_3$ state **b)** the αC-helix of pCdk2 and pCdk2:cyclinA, showing that pCdk2:cyclinA is mostly shifted to the αC-in state.

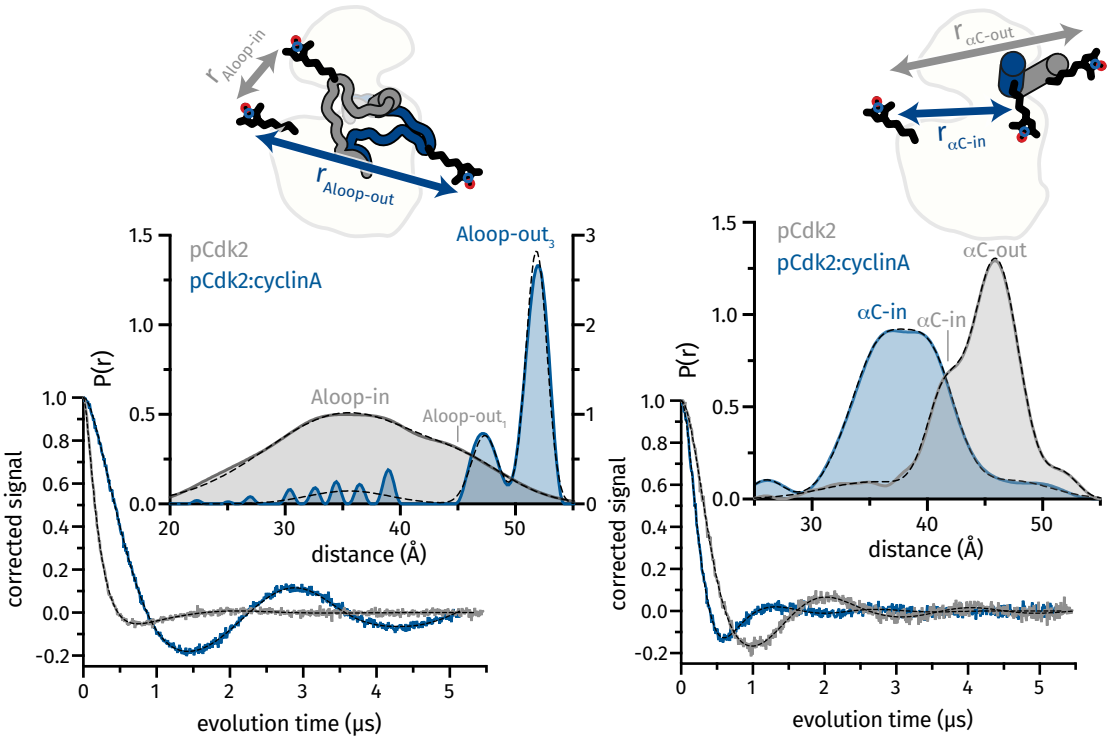

Figure 2.13: DEER experiments tracking the A-loop (left) and αC-helix (right). Tikhonov-derived distance distributions are shown for monomeric Cdk2 and Cdk2–cyclinA dimer in the phosphorylated state. Dashed black lines represent Gaussian fits to the DEER data. Peak assignments are based on spin–spin distance calculations (Figure 2.12). The spin labeling schemes are represented schematically. P(r) is the probability of distance r. Data for phosphorylated Cdk2 monomer are plotted on a different y axis scale for clarity.

The experiments tracking the αC-helix revealed conformational shifts that were correlated to those of the A-loop, with a subpopulation of monomeric Cdk2 sampling the αC-in state, and a larger cyclin-driven shift to the αC-in state when the kinase is phosphorylated (Figure 2.11, 2.13). The inhibitor K03861, which has an αC-in binding mode14, was used to confirm the assignment of the αC-in peak in monomeric Cdk2 (Figure 2.14).

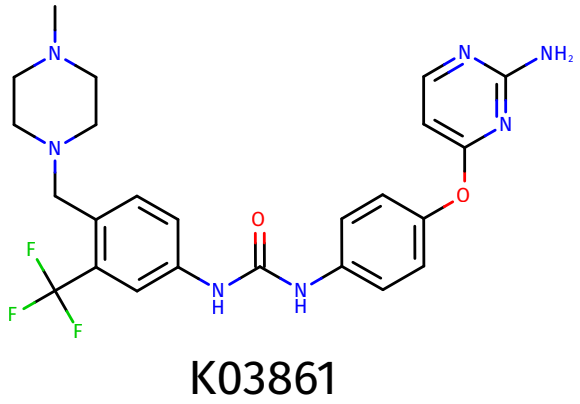

Figure 2.14: The structure of the DFG-out Cdk2 inhibitor, K03861[35].

These results are consistent with an allosteric conformational shift model[36] (Figure 2.15), in which the kinase transitions in a concerted manner between Aloop-in/αC-out and Aloop-out/αC-in states. The cyclin-driven population shift is described by the allosteric coupling parameter α. The value of α can be estimated from the DEER data to be 9 for unphosphorylated Cdk2, and 36 for phosphorylated Cdk2, indicating that phosphorylation on T160 increases the cyclin-driven conformational shift by $\sim$4-fold.

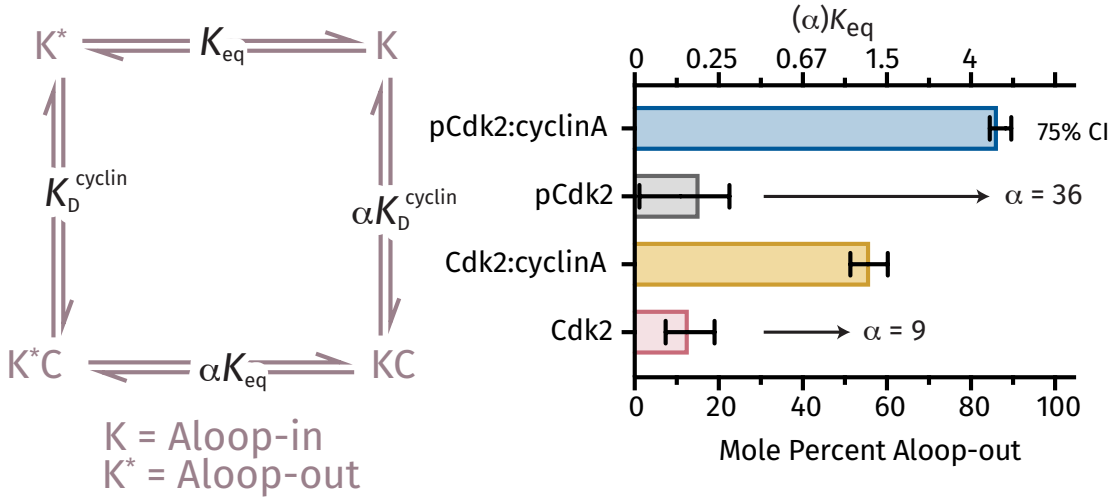

Figure 2.15: Allosteric two-state model for cyclin binding to Cdk2, with K and K* representing the Aloop-in and Aloop-out states of the kinase, C representing the cyclin subunit, K_{eq} the Aloop-in/out equilibrium constant, and K_D^{cyclin} and αK_D^{cyclin} representing microscopic equilibrium constants for cyclin binding to Aloop-out and Aloop-in states, respectively. The coupling parameter α represents the fold change in K_{eq} on cyclin binding. The bar graph summarizes the values of K_{eq} and α derived from Gaussian fits of the DEER data. Error bars represent 75% CIs, calculated from 50,000 simulations of Gaussian fits to the primary data.

2.2.1 Cdk2 samples catalytically inactive Aloop-out states

We used paramagnetic relaxation enhancement (PRE) NMR experiments[37] to further probe the A-loop movements [i]. The A-loop of Cdk2 is invisible in NMR spectra due to exchange broadening. Nonetheless, by incorporating a spin label on the same A-loop site used for DEER, the position of the A-loop can be inferred through the effects of the paramagnetic label on the spin relaxation of nearby elements of the kinase. In monomeric Cdk2 the observed PRE effects were localized to the αG helix, the β3-αC loop, the CMGC insert region and the αEF and αF helices, and were not affected by phosphorylation (Figures 2.16 & 2.17). PRE calculations (see Methods) revealed that

[i]The NMR experiments were performed by Dr. David Burban of the Levinson Lab

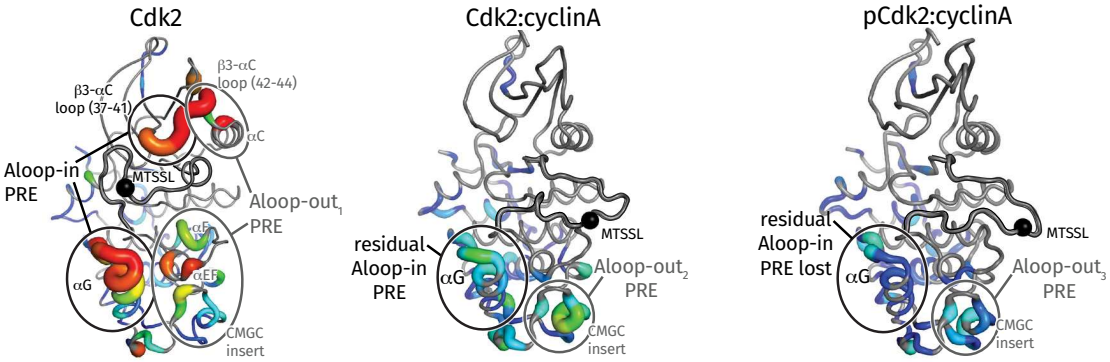

Figure 2.16: NMR PRE data for monomeric unphosphorylated Cdk2 (left), the unphosphorylated Cdk2:cyclinA dimer (middle) and the phosphorylated Cdk2:cyclinA dimer (right) are mapped onto the respective X-ray structures. Ovals represent assignments of PRE effects to specific structural states based on PRE calculations and black spheres represent the R157C spin labeling site.

the effects on the αG helix and part of the β3-αC loop were consistent with the Aloop-in state, but the other effects were not. Calculations performed on three Aloop-out x-ray structures of Cdk2, differing in the position of the labeled segment of the A-loop, indicated that these latter PRE effects were most consistent with the conformation observed in the structure of Cdk2 bound to KAP (kinase associated phosphatase)[38]. This structure is a rare example of a CDK adopting an Aloop-out state in the absence of a cyclin subunit. Rather than being induced by KAP binding, it appears that Cdk2 dynamically samples this Aloop-out state in which the T160 site is presented for efficient dephosphorylation.

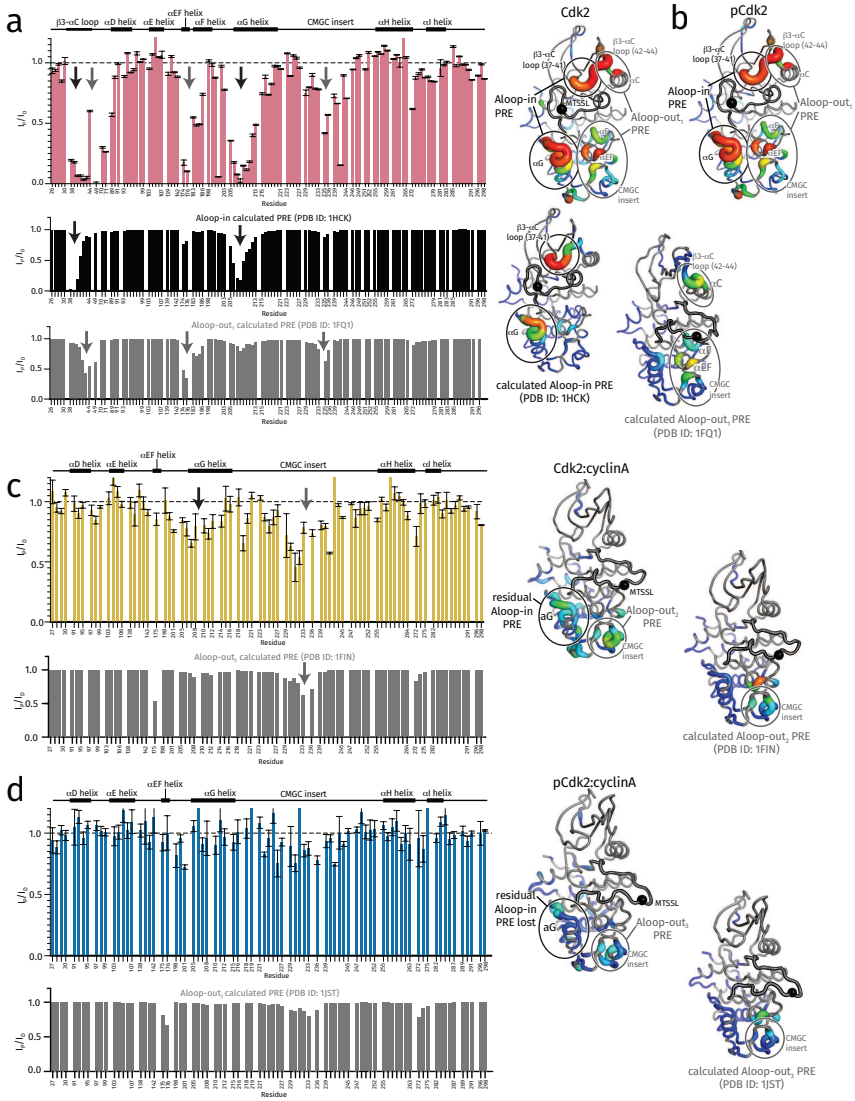

Figure 2.17: **a)** Plots of the PRE I_p/I_d values for monomeric Cdk2, as well as calculated I_p/I_d for the Aloop-in state (black, based on the apo 1HCK x-ray structure) and the Aloop-out$_1$ state (gray, based on the KAP-bound 1FQ1 structure). The experimental and calculated PRE effects are shown mapped onto the x-ray structure on the right. PRE effects on the C-terminal half of the β3-αC loop, CMGC insert, αEF-helix and αF-helix demonstrate that monomeric Cdk2 samples the Aloop-out$_1$ state. Error bars represent the standard error calculated from the signal-to-noise ratio of the entire spectrum. **b)** The PRE effects for phosphorylated monomeric Cdk2 are mapped onto the x-ray structure. **c)** Experimental and calculated PRE I_p/I_d values for Cdk2:cyclinA. The PRE effect on the CMGC insert is consistent with adoption of the Aloop-out$_2$ state observed in the 1FIN x-ray structure. The PRE signature on the αG helix is consistent with an Aloop-in subpopulation. Error bars represent the standard error calculated from the signal-to-noise ratio of the entire spectrum. **d)** Experimental and calculated PRE I_p/I_d.

For the Cdk2:cyclinA dimer, the PRE effects were more muted (Figure 2.16). In the unphosphorylated dimer, they were localized predominantly to the CMGC insert region, as predicted by PRE calculations, although there was a remnant of the αG helix PRE effect seen in monomeric Cdk2 (Figure 2.17), consistent with the dimer sampling the Aloop-in state as indicated by the DEER experiments. In the phosphorylated Cdk2:cyclinA dimer, both the residual αG PRE effect and the CMGC insert PRE effect largely disappeared, and calculations confirmed this to be consistent with the homogeneous adoption of the Aloop-out conformation seen in the x-ray structure of the phosphorylated dimer[12].

Together with the DEER results, the PRE experiments help clarify that Cdk2 can sample multiple Aloop-out states. These Aloop-out states all share the characteristic β-sheet formed in the N-terminal segment of the A-loop (anchor 1), but they differ in the positioning of the C-terminal segment of the A-loop (Figure 2.18). In the Aloop-out state adopted by monomeric Cdk2 (termed "Aloop-out$_1$"), this segment of the A-loop is anchored onto the C-terminal lobe of the kinase through a second β-sheet interaction (anchor 2). This feature is common in activated kinases[39], but in Cdk2 the β-sheet is out of register, and instead stabilizes an inactive conformation in which the T160 residue is presented for dephosphorylation. In the unphosphorylated Cdk2:cyclinA dimer, anchor 2 is also formed, but its register is shifted by two amino acids, allowing more extensive interactions with the cyclin subunit, while simultaneously blocking the substrate binding site ("Aloop-out$_2$"). Finally, in the phosphorylated Cdk2:cyclinA dimer, anchor 2 is broken, and the A-loop is further shifted toward the cyclin subunit and locked in place by ionic interactions of the pT160 residue with three arginine residues ("Aloop-out$_3$"). Only in this Aloop-out$_3$ state is the peptide substrate binding site formed. Kinase activity assays confirmed that this is the only state that demonstrates appreciable kinase activity 2.2. Comparison of the long-distance subpopulations measured by DEER

revealed that these experiments also distinguish between the three Aloop-out states (Figure 2.19). This provides a simple explanation for why monomeric Cdk2 remains catalytically inactive when phosphorylated on T160, as the Aloop-out$_1$ conformation cannot support substrate binding.

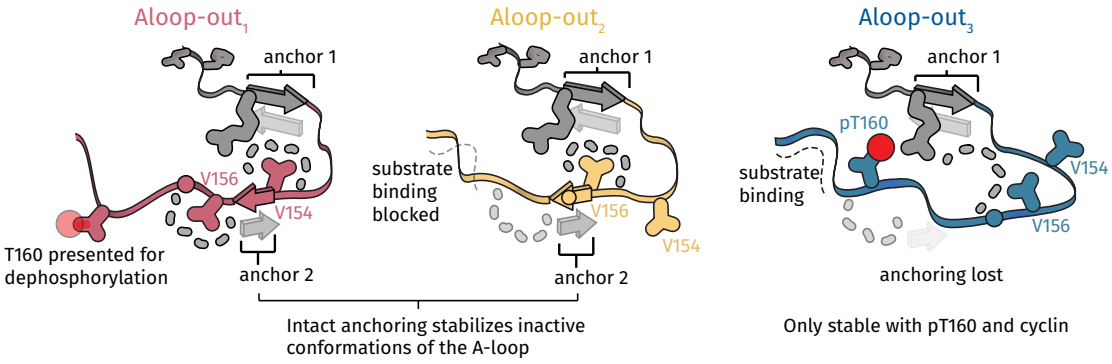

Figure 2.18: Schematics representing the three Aloop-out states detected in the PRE experiments. The spin labeling site on the A-loop is shown as a circle.

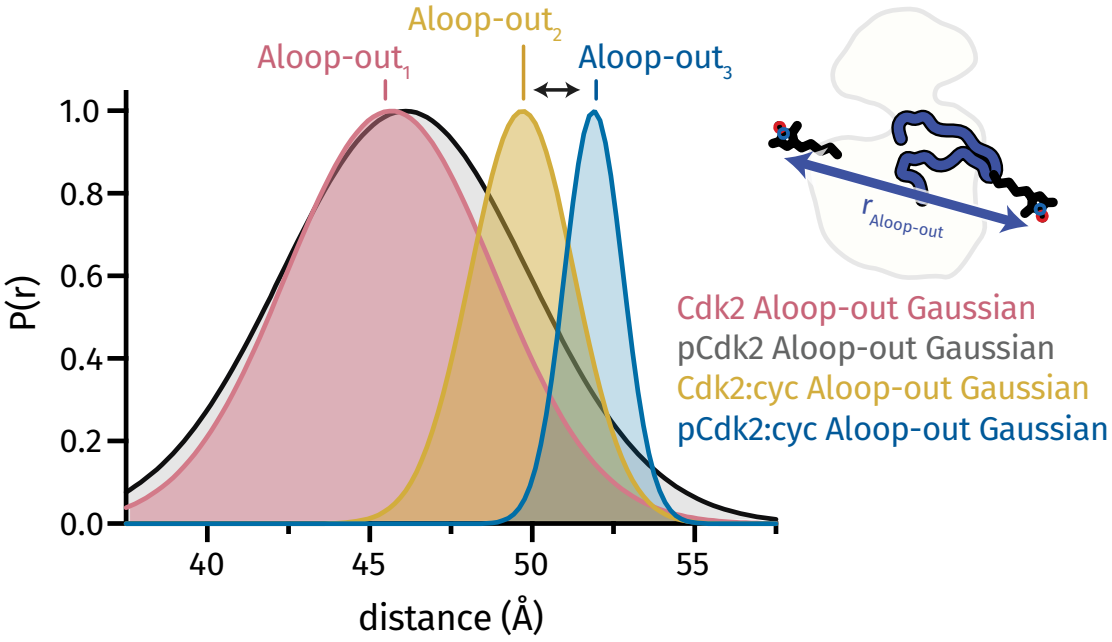

Figure 2.19: The Aloop-out Gaussian fits to the DEER experiments shown in Figures 2.11 & 2.13, highlighting the detection of the three different Aloop-out states.

2.3 Methods

Expression and purification of Cdk2 and cyclinA

Human Cdk2 (residues 1-298 with a TEV-cleavable N-terminal hexahistidine tag in pCDFduet) and mutants were expressed in BL21(DE3) *Escherichia coli* overnight at 18 °C. Coexpression with yeast CAK was used to prepare T160-phosphorylated Cdk2, and mass spectrometry confirmed homogeneous single phosphorylation in these samples (see Figures 2.8 and 2.9). Harvested cell pellets were lysed using an Emulsiflex C3 homogenizer (Avestin). Lysates were clarified by centrifugation and loaded onto HisTrap HP IMAC columns (GE), washed with lysis buffer (50 mM Tris pH 8.0, 500 mM NaCl, 10% glycerol) and eluted with elution buffer (1x PBS, 500 mM imidazole, 10% glycerol). Imidazole was immediately removed by desalting using a HiPrep 26/10 column (GE), and the hexahistidine tag was cleaved overnight with TEV protease (1:10 TEV:6HisCdk2 w/w). Protein was further purified using a Superdex 75 10/300 GL size exclusion column (GE).

Bovine CyclinA3 (residues 171-432 with a non-cleavable C-terminal hexahistidine tag) was expressed overnight in BL21(DE3)pLysS *Escherichia coli.* Cell pellets were lysed as above, lysates clarified, loaded onto HisTrap HP columns, and eluted using a 0-500 mM linear imidazole gradient (50 mM Tris pH 8.25, 300 mM NaCl, 10% glycerol). CyclinA was stabilized with the immediate addition of 100 mM $MgCl_2$ and further purified using a HiLoad 16/600 Superdex 200 size exclusion column (50 mM Tris pH 8.25, 100 mM $MgCl_2$, 5 mM 2-mercaptoethanol).

DEER spectroscopy

DEER samples were prepared by labeling "Cys-lite2" constructs of Cdk2 (C118A, C177S, A93C, and either R157C or S46C for A-loop and αC-helix experiments, respectively) with a 2.25-fold excess of MTSSL spin label, at a protein concentration of 50-100 μM. Labeled kinase was purified by size exclusion chromatography and concentrated to 60-80 μM, buffered in 1x PBS pH 7.4, 10 mM $MgCl_2$ and 10% d_8-glycerol in D_2O and rapidly frozen in 1.1 mm ID/1.6 mm OD glass capillary tubes. For samples containing inhibitors, deuterated DMSO was used and inhibitor concentrations were 250 μM. DEER spectra were acquired at 65 K using the standard deadtime-free four-pulse sequence ($\pi/2$ = 16 ns and π = 32 ns)[40] on an Elexsys E580 spectrometer (Bruker) equipped with an EN5107 resonator operating at Q-band frequencies (∼34 GHz). The pump frequency was set to the maximum of a two-pulse echo detected field sweep and the observe frequency was set to 24 G up-field. DEER waveforms were analyzed using Venison, a custom program written in Python based on DeerAnalysis 2017. Briefly, distance distributions were fit to the background-corrected waveforms using unconstrained Tikhonov regularization, with smoothing parameter λ chosen using the L-curve and leave-one-out cross validation (LOOCV). Features of the spectrum that were tightly coupled to the background model and contributed to unstable populations that were both distinct from the primary distance populations and beyond the limit of sensitivity of the 6 μs evolution time (∼58 Å) were suppressed by incorporating them into the background model. Tikhonov regularization was repeated on the corrected waveform. The Tikhonov distribution was used to initialize fitting of the waveforms to a sum of Gaussians model in order to determine the population centers of the spin-spin distances, as well as the widths and mole fractions. The appropriate number of Gaussian subpopulations was determined by selecting the fewest number of Gaussian centers that met

the RMSD minimization threshold calculated by the Bayesian information criterion[41]. Confidence intervals for Gaussian fits were calculated with Monte Carlo simulations of Gaussian fits to the background-corrected waveforms. All uncertainties quoted in main text and figures represent 75% confidence intervals.

Predicted spin-spin distance distributions were calculated from x-ray structures using the PyMOL plugin mtsslWizard[32] with the thorough conformational search setting for generating MTSSL spin probe ensembles. Calculated distance distributions agreed well with experiment, allowing unambiguous assignment of peaks in the experimental distance distributions to individual structural states (Figures 2.10 and 2.12). In particular, these calculations confirmed that the Aloop-out$_1$, Aloop-out$_2$, and Aloop-out$_3$ states should give rise to increasingly longer spin-spin distances in A-loop DEER experiments, and that the 41 Å peak observed in the αC-helix DEER experiments with monomeric Cdk2 corresponds to the αC-in state.

Chapter 3

Allostery governs inhibitor binding in Cdk2

3.1 Background

Having determined the intrinsic conformational balance of Cdk2 and how it is modulated by cyclin and phosphorylation, we next turned our focus to how small-molecule inhibitors interact with the dynamic kinase. Across the spectrum of inhibitors developed specifically to target the Cdks, there has been a significant number of preclinical and clinical studies to determine their potency, efficacy and toxicity profiles both *in vitro* and *in vivo*. As is true of the majority of drug discovery efforts, most of these drug candidates have failed in clinical trials (with the exception of the Cdk4/6 inhibitors palbociclib, ribociclib and abemaciclib). Despite having glimpses into the biochemical preferences of Cdk2 inhibitors through crystallography and ITC studies[42], there has not been a quantitative evaluation of how phosphorylation and/or cyclin-binding affect Cdk2:inhibitor affinities, how the presence of inhibitors affect the Cdk2:cyclin affinity and the extent to which the inhibitors drive conformational shifts in Cdk2.

We thus sought to develop a quantitative model accounting for the Aloop-in/out equilibrium, cyclin affinity and inhibitor affinity in both phosphorylated and unphosphorylated Cdk2. We used DEER and Förster resonance energy transfer (FRET) experiments to measure Cdk2 conformation and centered our study around the following seven inhibitors because they represent a variety of chemical scaffolds, intended targets and clinical outcomes:

1. **Flavopiridol** (alvocidib; Figure 3.1) was the first Cdk inhibitor tested in clinical trials[43]. The compound was derived from rohitukine, a natural product first described in the late 1970s[44], synthesized in the late 1980s[45] and investigated for its potential anti-inflammatory effects. Flavopiridol, which subsitutes a 2-chlorophenyl group for a methyl in rohitukine, was soon discovered to inhibit the Cdks[46,47] and determined to have antitumor properties[48]. Flavopiridol is a multi-Cdk inhibitor that has been crystallized bound to the Cdk2:cyclinA complex in the active-like state, and has been shown to have a higher affinity for the pCdk2:cyclinA complex than the monomer[42]. The compound has been tested in numerous clinical trials against leukemias, lymphomas and various solid tumors, but the inhibitor has not been approved mostly due to a lack of efficacy and dose-limiting toxicities[43]. Flavopiridol was found to be partially effective against chronic lymphocytic leukemia (CLL), but was also linked to tumor lysis syndrome in a significant number of patients[49]. For the purposes of this study, we have classified flavopiridol as a Cdk2 inhibitor.

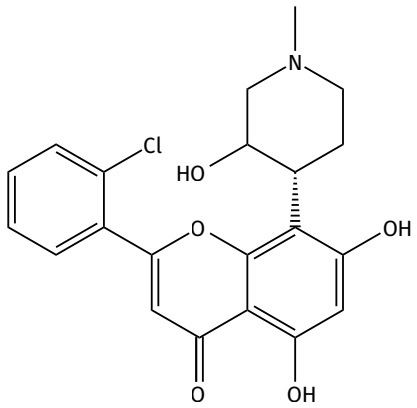

Figure 3.1: The chemical structure of the multi-Cdk inhibitor flavopiridol.

2. **Roscovitine** (seliciclib; Figure 3.2) was derived from the weak Cdk inhibitor olomoucine, itself a derivative of adenine[50]. Roscovitine is a sub-μM inhibitor of Cdks 1,2,5,7 and 9[51], and has been crystallized with both monomeric Cdk2 in the Cdk2/Src-like inactive state[52] and in the pCdk2:cyclinA complex in an active-like state[53]. The compound has been tested in small scale clinical trials for Cushing disease and non-small cell lung cancer, but these studies were terminated due to unacceptable toxicities[54] or unspecified reasons. For the purposes of this study, we have classified roscovitine as a Cdk2 inhibitor.

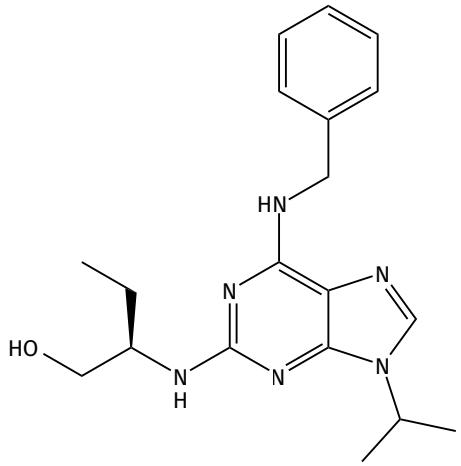

Figure 3.2: The chemical structure of the multi-Cdk inhibitor roscovitine.

3. **Dinaciclib** (Figure 3.3) was developed through the optimization of pyrazolo[1,5-a]pyrimidine-based structures using *in vivo* screening against an ovarian carcinoma xenograft model[55]. Dinaciclib is a low nM inhibitor of Cdks 1,2,5 and 9[56]. Dinaciclib has failed in clinical trials for advanced breast cancer[57], non-small-cell lung cancer (NSCLC)[58] and CLL[59], among others, due to dose-limiting toxicities including tumor lysis syndrome[60]. The compound has been crystallized with both monomeric Cdk2 in the Cdk2/Src-like inactive state[61] as well as the Cdk2:cyclinE complex in the active-like state[62], and has been shown to have a higher affinity for the pCdk2:cyclinA complex than the monomer[42]. For the purposes of this study, we have classified dinaciclib as a Cdk2 inhibitor.

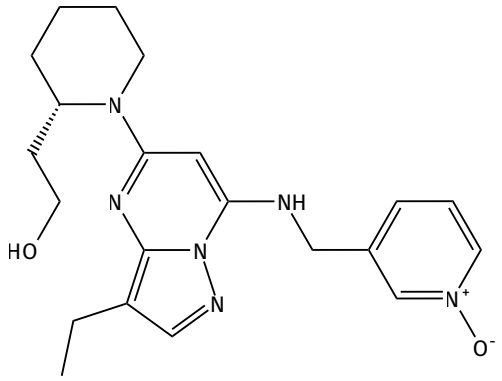

Figure 3.3: The chemical structure of the Cdk1/2/5/9 inhibitor dinaciclib.

4. **AZD5438** (Figure 3.4) was developed through a series of substitutions on imidazole compounds[63]. AZD5438 inhibits Cdks 1,2 and 9 at low nM concentrations[64]. The compound has undergone one clinical trial for the treatment of advanced tumors, but the trial was terminated due to tolerability issues[65]. AZD5438 has been crystallized with both monomeric Cdk2 in the Cdk2/Src-like inactive state (with evidence of a second inhibitor-driven conformation of the A-loop!) as well as with the Cdk2:cyclinA complex in the active-like state[42], and has been shown to have a higher affinity for the pCdk2:cyclinA complex than the monomer[42]. For the purposes of this study, we have classified AZD5438 as a Cdk2 inhibitor.

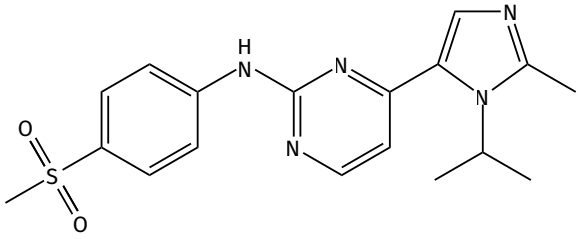

Figure 3.4: The chemical structure of the Cdk1/2/9 inhibitor AZD5438.

5. **Palbociclib** (Figure 3.5) is an FDA-approved[66] Cdk4/6 inhibitor therapy for HR+/HER2- breast cancer. The compound was developed through a series of

optimizations, specifically designed to maximize the selectivity for Cdk4:cyclinD over Cdk2:cyclinA, on a pyrido[2,3-d]pyrimidin-7-one core[67,68]. The resulting compound, palabociclib, exhibited a remarkable 450-fold difference in IC_{50} values between the Cdk4 and Cdk2 complexes, which is attributed to the differential interactions of the modified substituents with the kinase active sites. Palbociclib has been crystallized with both monomeric Cdk6[62] as well as a complex of Cdk6 and a cyclin from a herpesvirus[69]. Palbociclib is currently undergoing a large number of clinical trials for other types of cancer. For the purposes of this study, we have classified palbociclib as a Cdk4 inhibitor.

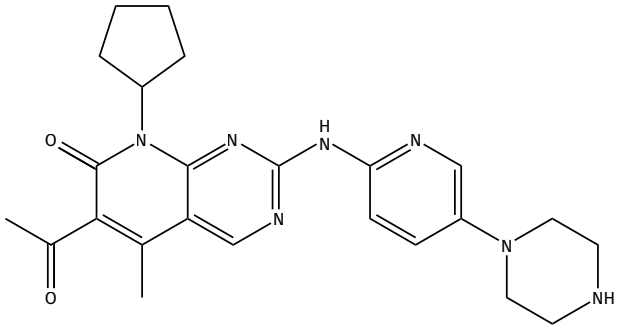

Figure 3.5: The chemical structure of the Cdk4/6 inhibitor palbociclib.

6. **Ribociclib** (Figure 3.6) is an FDA-approved[70] Cdk4/6 inhibitor therapy for HR+/HER2- breast cancer. Based on a pyrrolo[2,3-d]pyrimidine core (as opposed to the *pyrido*[2,3-d]pyrimidine core of palbociclib), the structure and activity of ribociclib are otherwise similar to those of palbociclib[71]. Ribociclib has been crystallized with monomeric Cdk6[62]. Ribociclib is currently undergoing a large number of clinical trials for other types of cancer. There are several known mechanisms for resistance to Cdk4/6 inhibitors such as ribociclib (and palbociclib), including an overexpression of cyclinE[72] as well as the formation of noncanonical Cdk2:cyclinD complexes[73] that override the inhibition of the primary targets. For

the purposes of this study, we have classified ribociclib as a Cdk4 inhibitor.

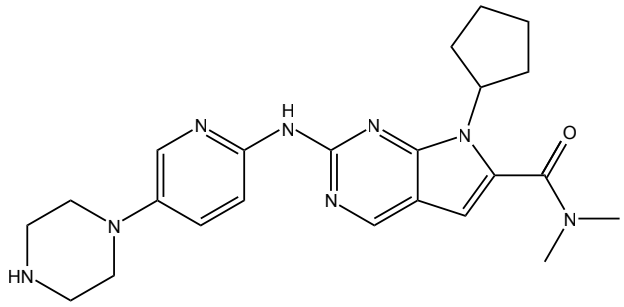

Figure 3.6: The chemical structure of the Cdk4/6 inhibitor ribociclib.

7. **Abemaciclib** (Figure 3.7) is a Cdk4/6 inhibitor therapy for HR+/HER2- breast cancer[74]. The compound was developed through the optimization of a 2-anilino-2,4-pyrimidine-[5-benzimidazole] scaffold that was discovered in a chemical screen[75]. Although it was approved for the same disease and mechanism of action as palbociclib and ribociclib, the inhibitor has a different selectivity profile for the CDKs, resulting in distinct therapeutic and toxicity outcomes[71]. Abemaciclib has been crystallized with the Cdk6 monomer[62]. For the purposes of this study, we have classified abemaciclib as a dual-specificity Cdk2/Cdk4 inhibitor.

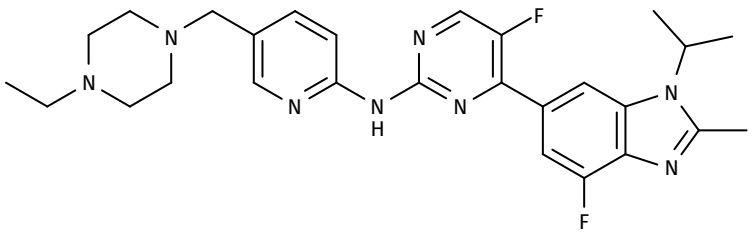

Figure 3.7: The chemical structure of the Cdk4/6 inhibitor abemaciclib.

3.1.1 A note on the Cdk2 FRET experiment

The steady-state FRET experiment used in this study is a relatively simple one that has been previously been described in detail[76]. The readout from the experiment is the *ratio* between the intensity of the donor and acceptor fluorophores, providing a relative measure of the distance between the two fluorophores (whereas the EPR experiments serve as the accurate "molecular ruler"). Importantly, this obviates the need for a set of donor-only samples that would otherwise be required in a typical FRET experiment. The benefits of this experiment are thus:

- it requires extremely small amounts of protein and inhibitor due to the high quantum yield of the attached fluorophores
- it can be infinitely scaled up
- it can generate many inhibitor titrations quickly in a high-throughput fashion

3.2 Results

3.2.1 Cdk2 inhibitors drive conformational shifts upon binding

We used DEER to probe the conformational effects of four ATP-competitive Cdk2 inhibitors: flavopiridol, roscovitine, AZD5438, and dinaciclib. All of the inhibitors increased the Aloop-out$_1$ subpopulation when bound to monomeric Cdk2, and also promoted the Aloop-out$_2$ subpopulation when bound to the Cdk2:cyclinA dimer (Figure 3.8 & 3.9 left, 3.10).

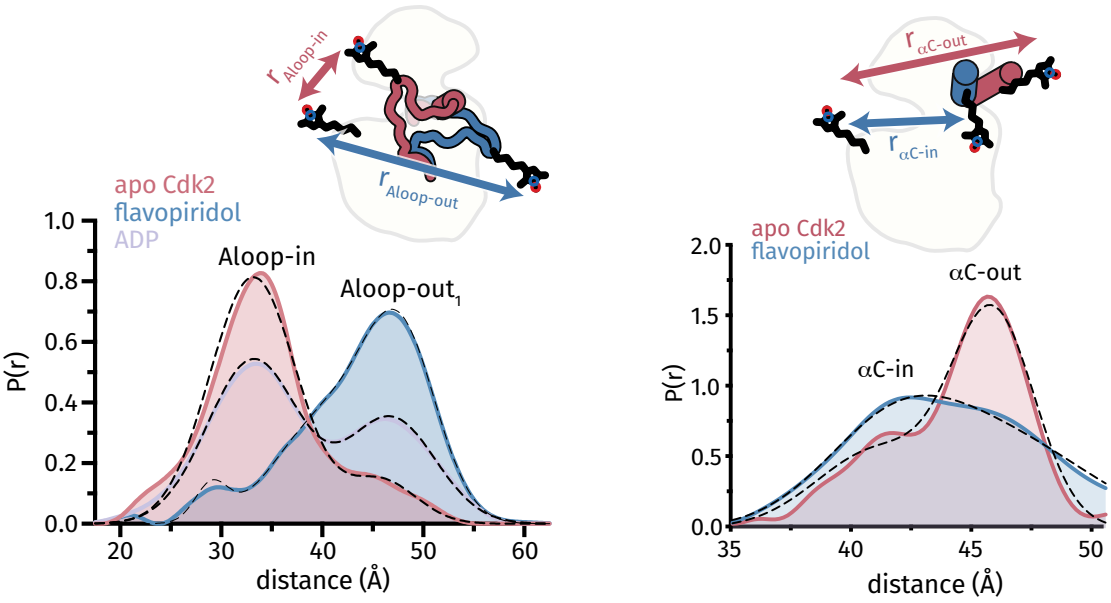

Figure 3.8: DEER experiments tracking the A-loop (left) and αC-helix (right) in the Cdk2 monomer, and Cdk2:flavopiridol complex. For the A-loop experiments, data are also shown for Cdk2 bound to ADP (bottom). Solid lines represent Tikhonov-derived distance distributions, while dashed black lines represent the Gaussian fits to the DEER data. Peak assignments are based on spin–spin distance calculations. The spin labeling schemes are represented schematically at the top.

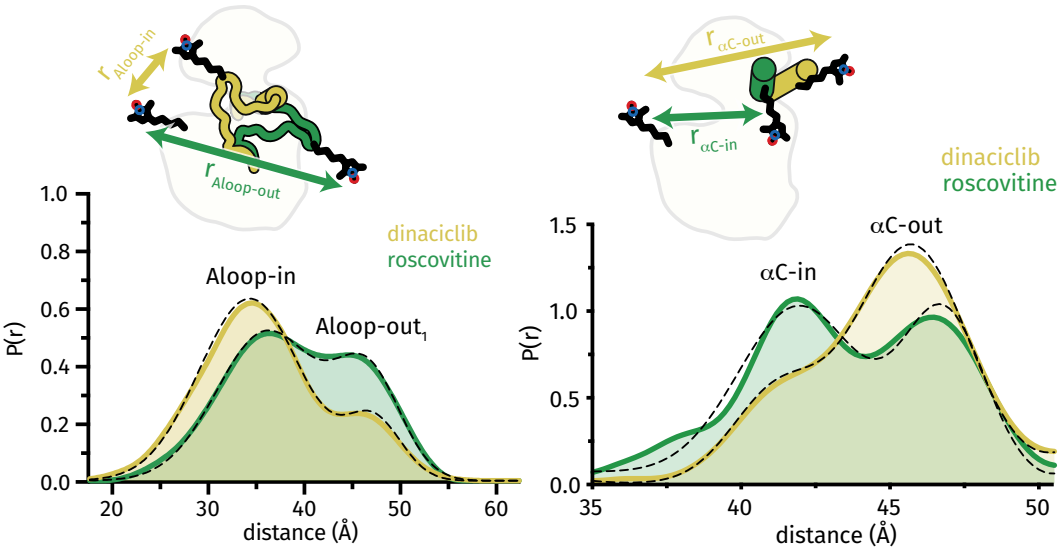

Figure 3.9: DEER experiments tracking the A-loop (left) and αC-helix (right) in the Cdk2:dinaciclib, and Cdk2:roscovitine complexes.

Corresponding population shifts toward the αC-in state were also observed (Figure 3.8 & 3.9 right, 3.11), demonstrating that the Cdk2 inhibitors promote concerted conformational shifts from the Aloop-in/αC-out state to the Aloop-out/αC-in state. These shifts can be described by an allosteric coupling parameter β, analogous to the parameter α for cyclin (Figure 3.12).

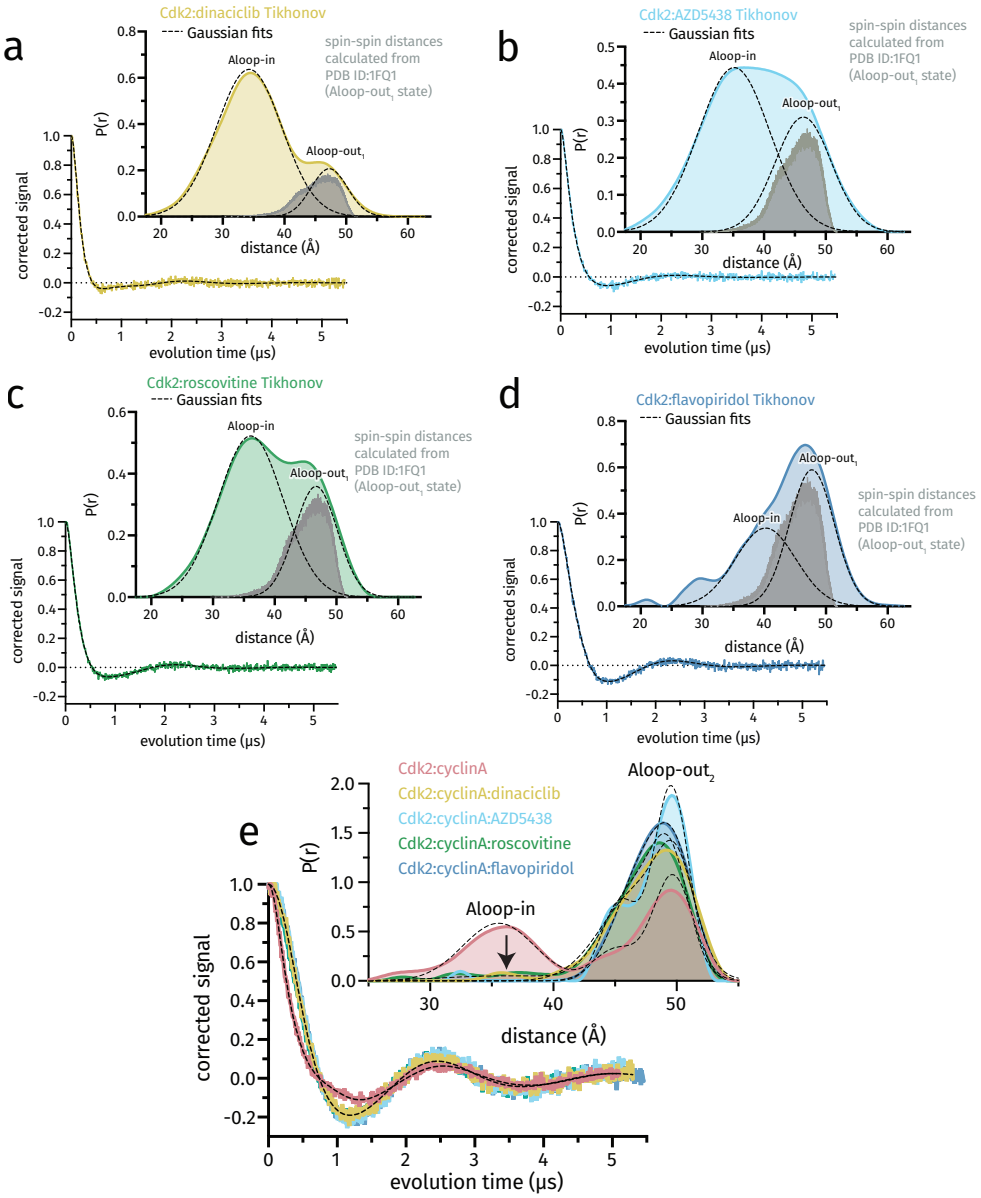

Figure 3.10: DEER spectra (bottom) and spin-spin distance distributions (top) for Cdk2 bound to four Cdk2 inhibitors. Distance distributions were acquired by fitting DEER spectra using Tikhonov regularization, and independently fitting to two Gaussian functions representing Aloop-in and Aloop-out$_1$ states. The calculated Aloop-out$_1$ distance distribution from the Cdk2:KAP structure (1FQ1) is shown in grey and scaled along the y-axis for clarity. DEER spectra, Tikhonov fits and decomposed Gaussian fits are shown for **a)** Cdk2:dinaciclib, **b)** Cdk2:AZD5438, **c)** Cdk2:roscovitine, **d)** Cdk2:flavopiridol. **e)** All four inhibitors promote the Aloop-out$_2$ state in the presence of cyclinA, as manifested by a loss of the Aloop-in subpopulation (arrow).

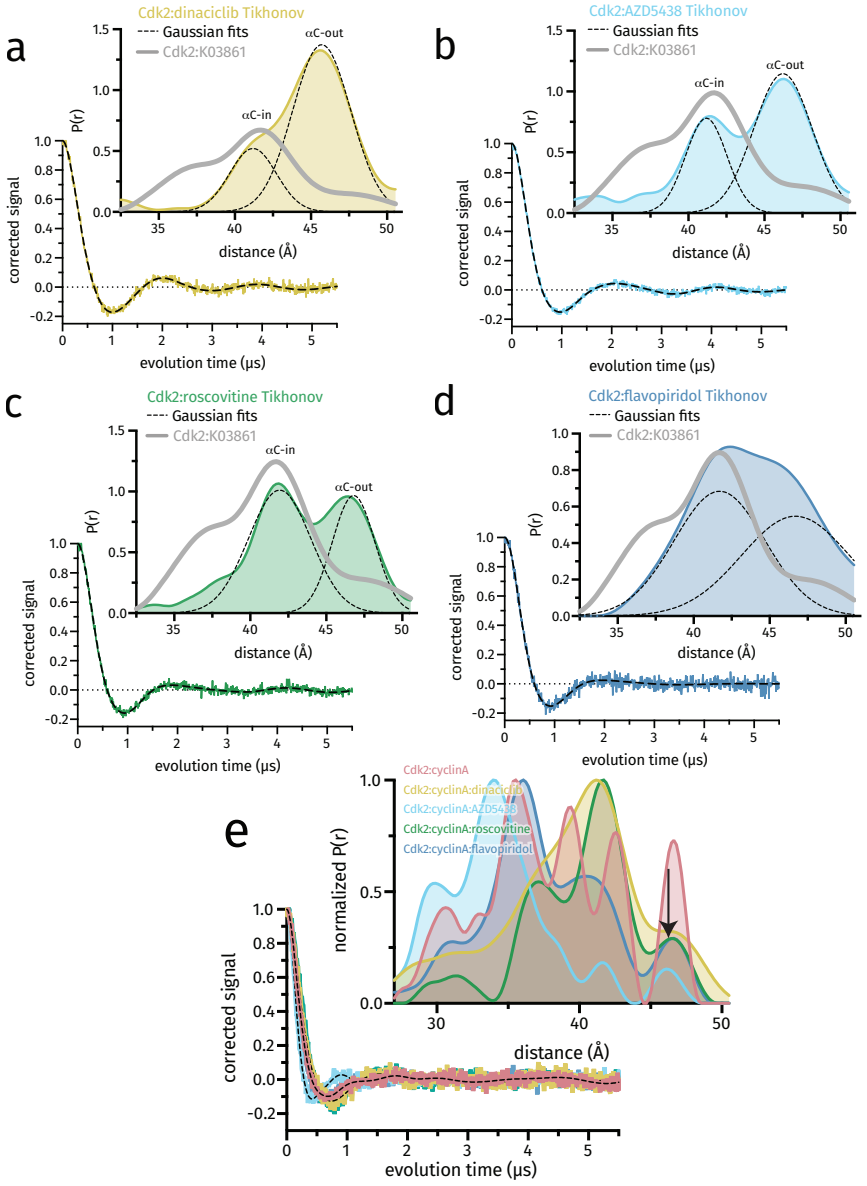

Figure 3.11: DEER spectra (bottom) and spin-spin distance distributions (top) for Cdk2 bound to four Cdk2 inhibitors. Distance distributions were acquired by fitting DEER spectra using Tikhonov regularization, and independently fitting to two Gaussian functions representing αC-out and αC-in states. The distance distribution from the αC-in state of Cdk2:K03861 is shown in grey and scaled along the y-axis for clarity. DEER spectra, Tikhonov fits and decomposed Gaussian fits are shown for **a)** Cdk2:dinaciclib, **b)** Cdk2:AZD5438, **c)** Cdk2:roscovitine, **d)** Cdk2:flavopiridol. **e)** All four inhibitors destabilize the αC-out state in the presence of cyclinA, as manifested by a loss of the αC-out subpopulation (arrow).

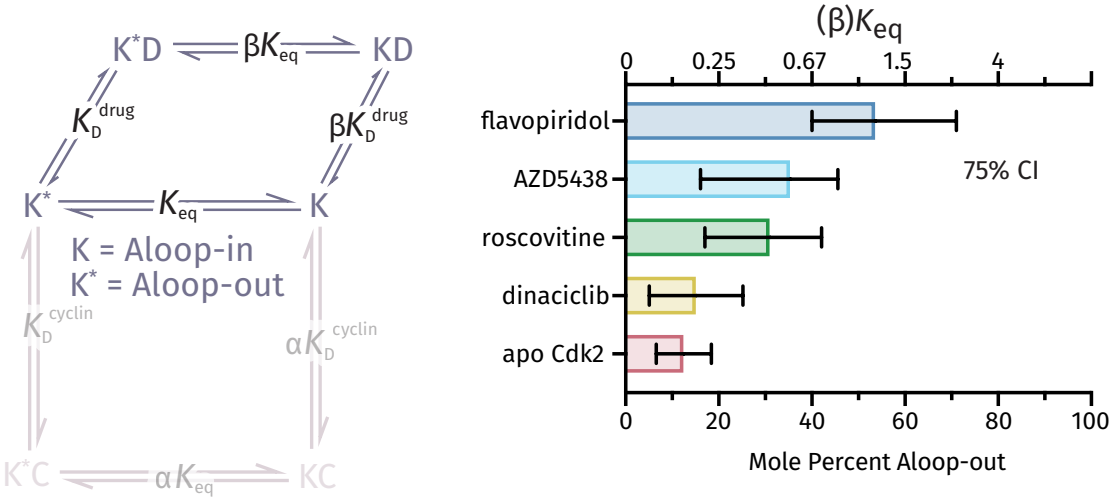

Figure 3.12: Allosteric two-state model for inhibitor binding to Cdk2, with K and K* representing the Aloop-in and Aloop-out states of the kinase, D representing the drug/inhibitor, K_{eq} the Aloop-in/out equilibrium constant and $K_{\mathrm{D}}^{\mathrm{drug}}$ and $\beta K_{\mathrm{D}}^{\mathrm{drug}}$ drug the microscopic equilibrium constants for inhibitor binding to Aloop-out and Aloop-in states, respectively. The coupling parameter β describes the fold change in K_{eq} upon inhibitor binding. The bar graph summarizes the values of K_{eq} and β derived from Gaussian fits of the A-loop DEER data. Error bars represent 75% CIs, calculated from 50,000 simulations of Gaussian fits to the primary data.

Although dinaciclib and roscovitine have similar chemical structures, roscovitine triggers a larger conformational shift. The x-ray structures of Cdk2 bound to dinaciclib and roscovitine are nearly identical, with the notable exception of a 3.5 angstrom shift of the ϵ-amino group of the catalytic lysine residue K33 (Figure 3.13)[52,61]. In the dinaciclib structure, K33 forms a salt bridge with D145 of the catalytic DFG motif, but the larger 9-isopropyl substituent of roscovitine compared to the 3-ethyl group of dinaciclib causes K33 to shift away from D145, breaking the salt bridge. Breakage of this salt bridge has been linked to conformational transitions away from the CDK/Src-like inactive state[77], and may explain the larger shift triggered by roscovitine. A similar mechanism may also explain the shift triggered by AZD5438, the 2-methylimidazole group of which, like the 9-isopropyl group of roscovitine, would clash with the position of the K33 lysine residue

seen in the dinaciclib complex (Figure 3.14).

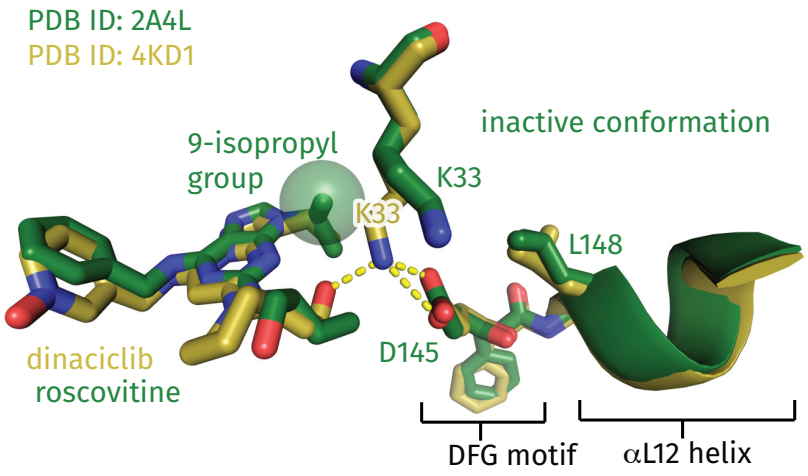

Figure 3.13: Aligned crystal structures of Cdk2 bound to dinaciclib and roscovitine. Hydrogen bonds are shown as yellow dashed lines.

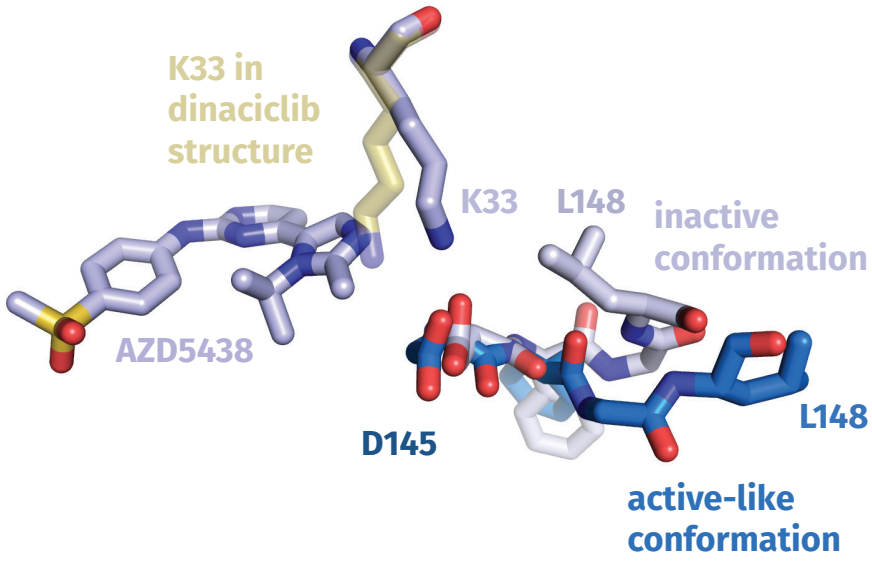

Figure 3.14: The x-ray structure of monomeric Cdk2 bound to AZD5438. The two conformations in the crystallographic model (PDB ID: 6GUH) are colored light blue for the inactive state and dark blue for the active-like state. The position of the catalytic lysine K33 in the corresponding dinaciclib structure is shown in light yellow for comparison.

Flavopiridol promotes the Aloop-out/αC-in state by a different mechanism. In the crystal structure of flavopiridol bound to the Cdk2:cyclinA dimer[42], the inhibitor forms hydrogen bonds with the K33 residue, the catalytic glutamate E51 and a water molecule (Figure 3.15, left). Water-mediated hydrogen bond networks at this site are important for catalytic function and inhibitor recognition[78,79], and structures of Cdk2:cyclinA[80] bound to nucleotides show a strikingly similar hydrogen bonding geometry (Figure 3.15, right). In DEER experiments, ADP binding also promoted the Aloop-out state (Figure 3.8), suggesting that flavopiridol and nucleotide trigger conformational shifts by stabilizing the active state.

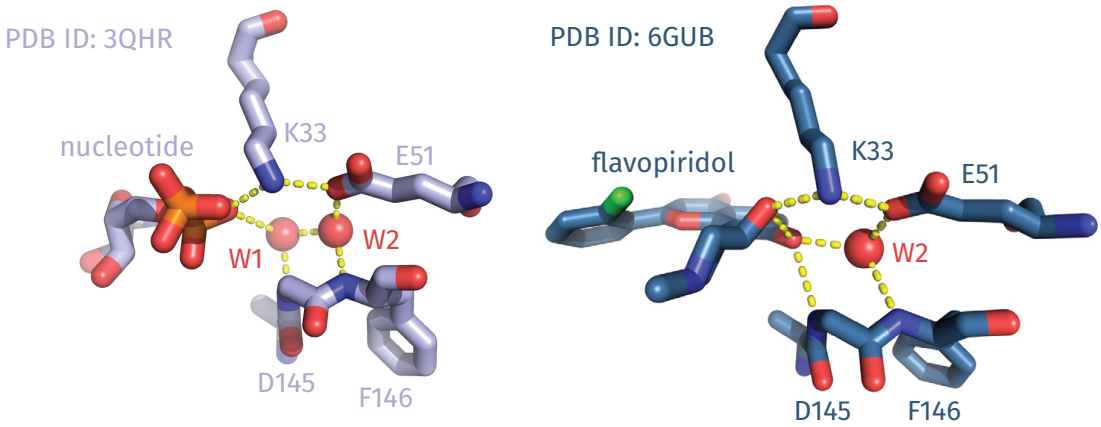

Figure 3.15: Structures of Cdk2:cyclinA bound to flavopiridol and ADP shown side by side. Hydrogen bonds are shown as yellow dashed lines, and structured water molecules as red spheres.

We also obtained DEER spectra of the Cdk2:cyclinA complex bound to the Cdk4 inhibitors palbociclib, ribociclib and abemaciclib (Figure 3.16). Although we had initially anticipated that the inhibitors would stabilize the Aloop-in subpopulation due to their tight binding to the inactive Cdk4:cyclinD complex, all three Cdk4 inhibitors drove relatively subtle shifts to the Aloop-in conformation, with abemaciclib having the largest effect. This was our first evidence that abemaciclib differs from the other two

Cdk4 inhibitors in the way it interacts with the Cdk2 conformational equilibrium.

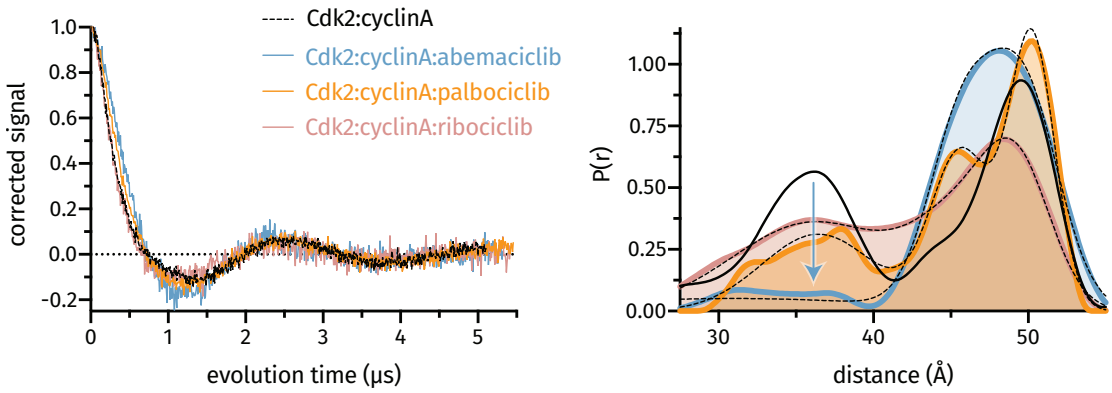

Figure 3.16: DEER experiments tracking the A-loop in the Cdk2:cyclinA:inhibitor complexes of palbociclib, ribociclib and abemaciclib. Solid lines represent Tikhonov-derived distance distributions, while dashed black lines represent the Gaussian fits to the DEER data. Of the three inhibitors, abemaciclib drives the largest shift to the Aloop-out state.

3.2.2 Inhibitor and cyclin binding are allosterically coupled

Several Cdk2 inhibitors bind more tightly in the presence of the cyclin subunit[42]. To simultaneously track inhibitor binding and conformational changes, we labeled Cdk2 with donor and acceptor dyes on the same sites used for conjugating spin labels for the A-loop DEER experiments, yielding high FRET for the Aloop-in state and low FRET for the Aloop-out state (Figure 3.17).

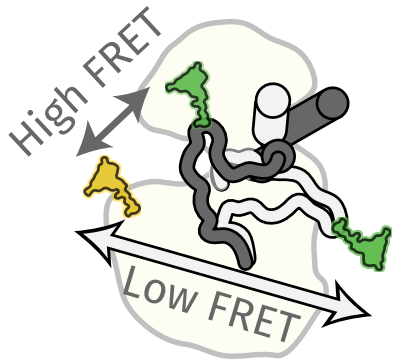

Figure 3.17: Schematic of the Cdk2 FRET sensor. Alexa 488 (donor) and Alexa 568 (acceptor) were conjugated to the same sites as the DEER spin probes.

Titrations of cyclinA and Cdk2 inhibitors both resulted in decreased FRET, consistent with shifts to the Aloop-out state (Figures 3.18 and 3.20), and the decrease triggered by cyclinA was larger for phosphorylated than unphosphorylated Cdk2, in agreement with the larger shift observed by DEER. The FRET data were analyzed by global fitting to an extended allosteric two-state model (ATSM)[36,81] (Figure 3.19) that describes the binding of cyclin and inhibitor and the effects thereof on the equilibrium between Aloop-in and Aloop-out states (see Methods). To map the FRET signal onto the conformational equilibrium, the model was parameterized using the Aloop-in/out equilibrium constants measured by DEER for apo and cyclin-bound Cdk2, thereby constraining the allosteric coupling parameter α. The resulting fits allowed the remaining thermodynamic parameters of the model to be defined, including the microscopic equilibrium constants for cyclin and inhibitor binding to Aloop-in and Aloop-out states, and the allosteric coupling parameters α,γ and δ. The values of β obtained from the model are similar to those measured by DEER and confirm that the Cdk2 inhibitors promote the Aloop-out state (Figure 3.21).

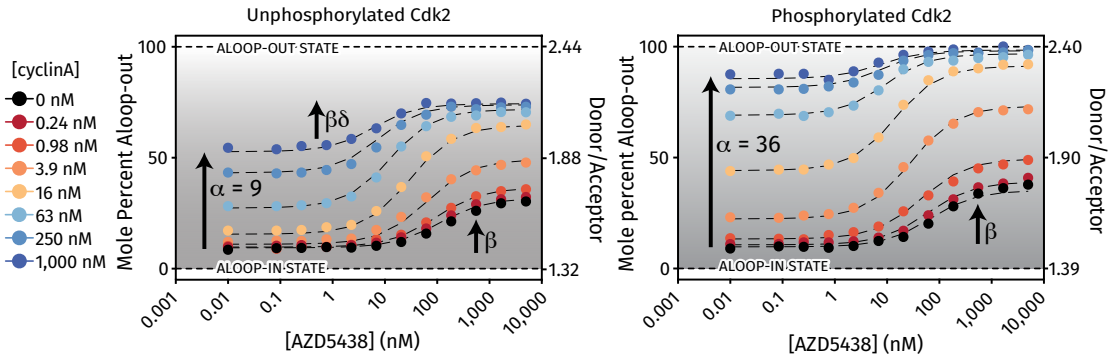

Figure 3.18: FRET measurements for AZD5438 binding to Cdk2 (left) and pCdk2 (right) at different cyclinA concentrations. The black dashed lines are the global fit to the allosteric model shown in Figure 3.19. The FRET values are shown on the right ordinate and the corresponding values of the conformational equilibrium on the left ordinate.

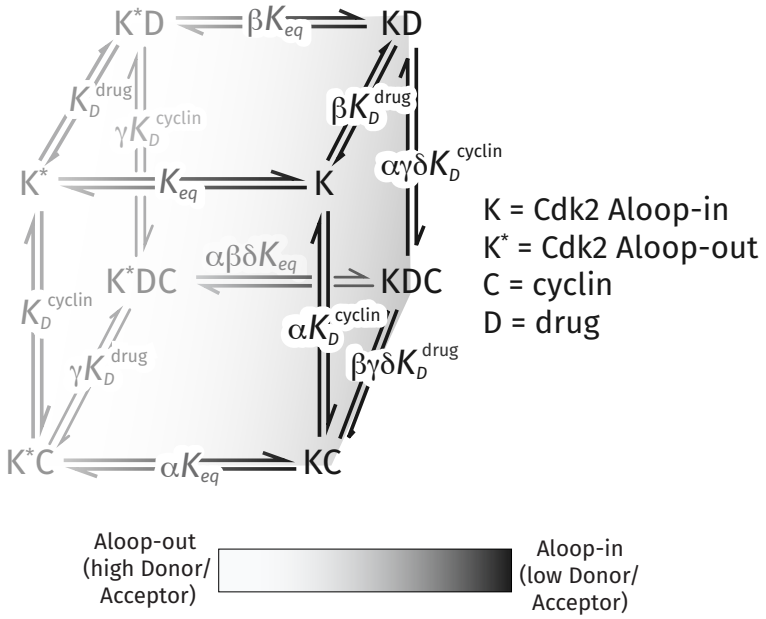

Figure 3.19: The allosteric model used to fit the FRET data. The model describes the binding of cyclin and inhibitor to the Aloop-in and Aloop-out states, with K_{eq} representing the Aloop-in/out equilibrium, $K_{\mathrm{eq}}^{\mathrm{cyclin}}$ and $K_{\mathrm{eq}}^{\mathrm{drug}}$ representing microscopic equilibrium constants for cyclin and inhibitor binding to the Aloop-out state, and the allosteric allosteric coupling described with α, β, γ and δ. The Aloop-in/out equilibrium is represented as a gray scale.

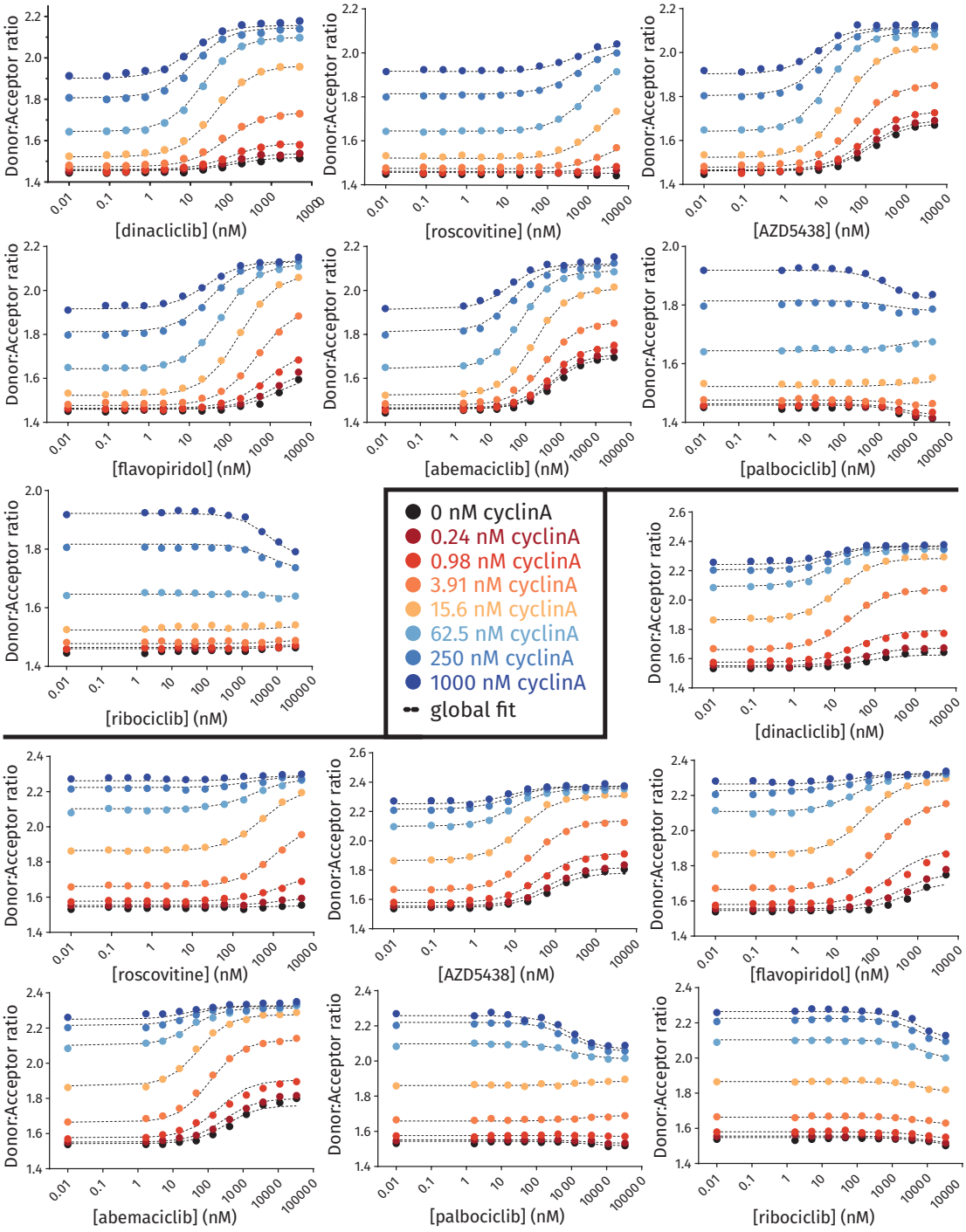

Figure 3.20: FRET measurements of inhibitor binding. Inhibitor and cyclin binding experiments with unphosophorylated Cdk2 (top) and phosphorylated Cdk2 (bottom). Ratiometric FRET measurements from representative experiments are shown along with the global fits (dashed black lines, see Methods).

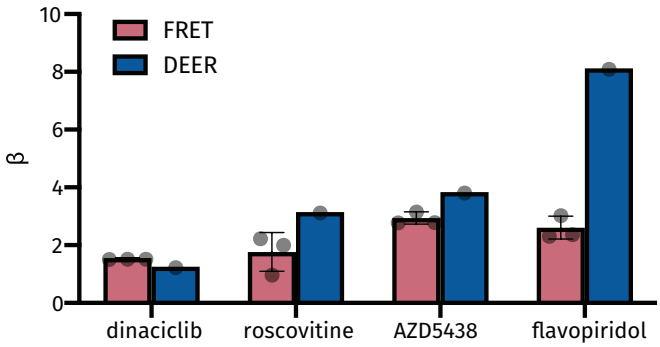

Figure 3.21: β values derived from fits of the FRET data to the extended allosteric two state model (black) and the corresponding values independently measured with DEER (blue), show that the four Cdk2 inhibitors drive a conformational shift to the Aloop-out state. Values for FRET experiments are mean ± S.E.M; n = 3 independent experiments.

Several insights emerge from this analysis. First, cyclin affinity for the Aloop-out state is enhanced ∼8-fold by phosphorylation (Figure 3.22). In contrast, phosphorylation has a modest effect on the affinity for cyclin binding to the Aloop-in state. This explains why phosphorylation enhances the allosteric shift triggered by cyclin binding. Second, the model recapitulates the positive binding cooperativity between cyclin and the Cdk2 inhibitors[42] and reveals that it can be partitioned into two allosteric effects, quantified by the allosteric coupling parameters β and γ (Figures 3.23 & 3.24). These can be understood as follows: the conformational shifts triggered by the inhibitors (β) arise from higher binding affinity for the Aloop-out state; since this state predominates when cyclin is bound, the inhibitor affinity is also enhanced by cyclin binding. However, even within the Aloop-out state there is allosteric cooperativity between inhibitor and cyclin (γ). This may arise from overlapping effects of the two ligands on the kinase conformational entropy, consistent with previous ITC experiments that showed a smaller entropic penalty for AZD5438 binding to the Cdk2:cyclin dimer than monomeric Cdk2[42]. Together, the two allosteric effects give rise to strong binding cooperativity: >10-fold in all four cases, and 50-fold for flavopiridol binding unphosphorylated Cdk2.

Without this cooperativity, these molecules would lack sufficient potency to effectively inhibit Cdk2 in cells, where they must compete with high concentrations of ATP.

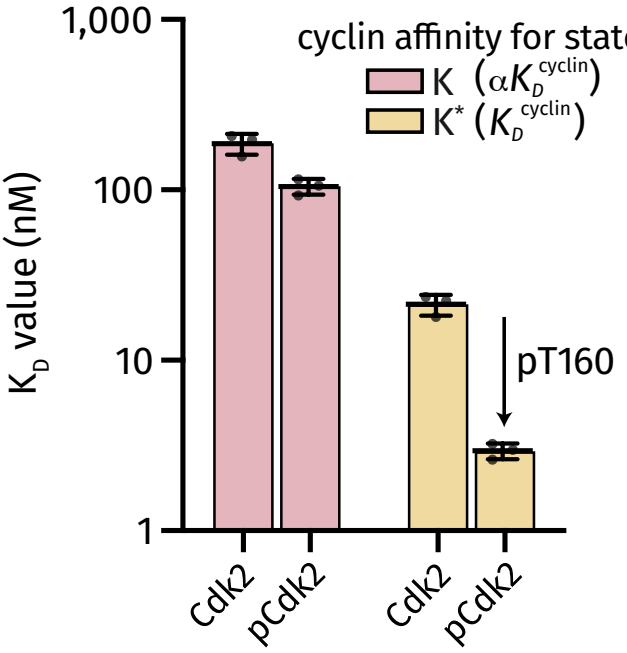

Figure 3.22: Microscopic equilibrium constants for cyclin binding to Aloop-in ($\alpha K_{\mathrm{D}}^{\mathrm{cyclin}}$) and Aloop-out ($K_{\mathrm{D}}^{\mathrm{cyclin}}$) states of unphosphorylated and phosphorylated Cdk2. Values are mean ± s.e.m.; n = 3 independent experiments.

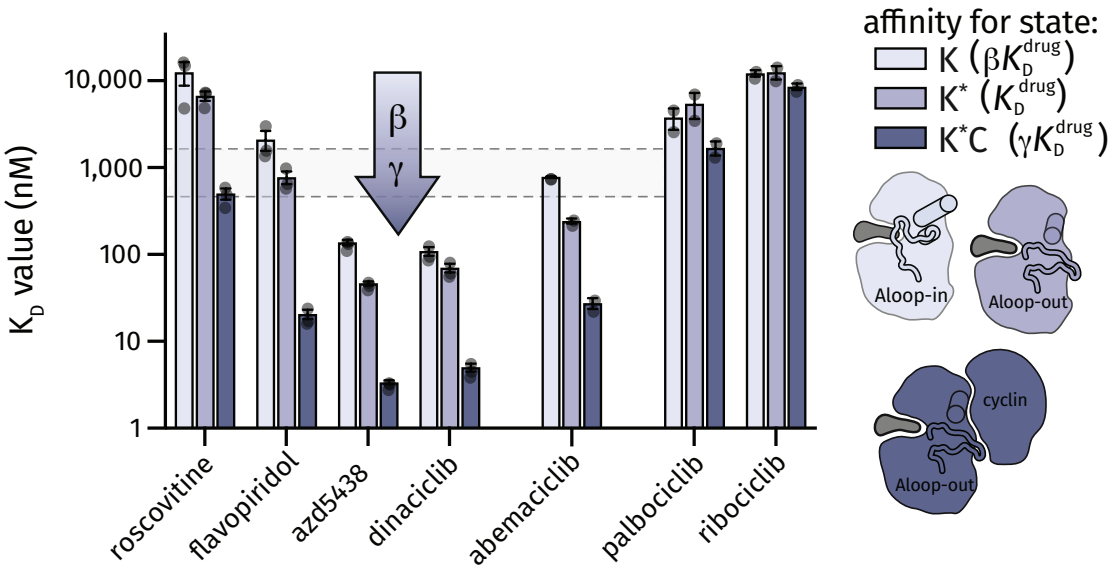

Figure 3.23: Microscopic equilibrium constants for inhibitor binding to three different structural states of unphosphorylated Cdk2. The arrow represents the allosteric coupling effects that drive cooperative binding of inhibitor and cyclin. Values are mean ± s.e.m.; n = 3 independent experiments.

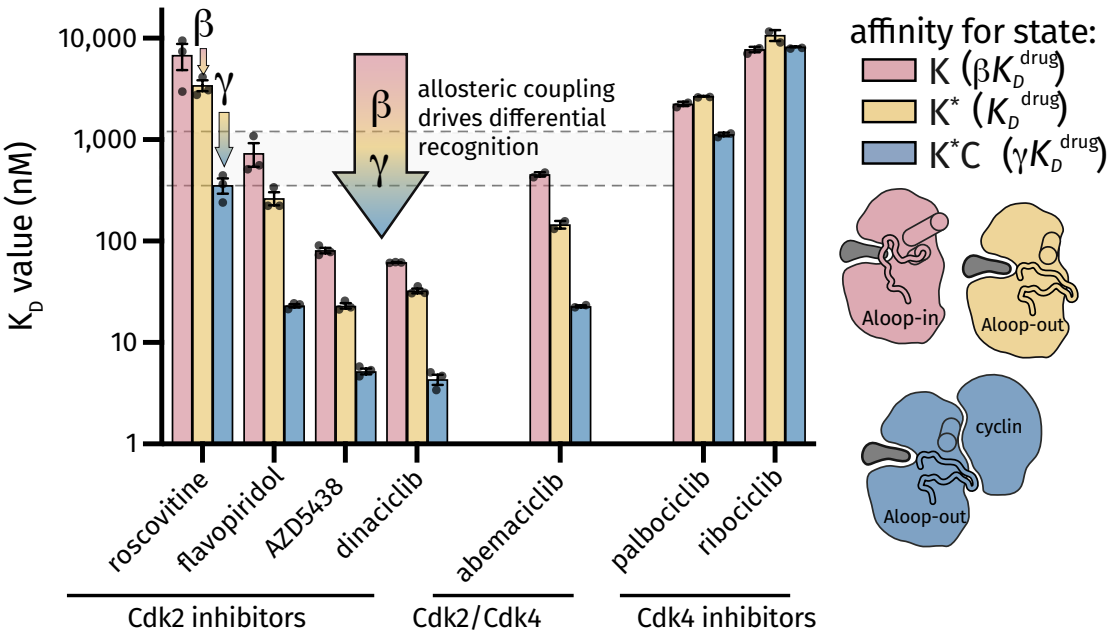

Figure 3.24: Microscopic equilibrium constants for inhibitor binding to three different structural states of phosphorylated Cdk2. The arrow represents the allosteric coupling effects that drive cooperative binding of inhibitor and cyclin. Values are mean ± s.e.m.; n = 3 independent experiments.

We also tested the Cdk4 inhibitors abemaciclib, palbociclib and ribociclib in our FRET assay (Figures 3.23 & 3.24). Palbociclib and ribociclib are selective for Cdk4, while abemaciclib inhibits both Cdk4 and Cdk2[62,71]. Abemaciclib behaved like the Cdk2 inhibitors, promoting the Aloop-out state and exhibiting binding cooperativity with cyclin that was similarly partitioned between β and γ effects, and without which the drug would likely lack efficacy against Cdk2. In striking contrast, palbociclib and ribociclib did not promote the Aloop-out state and lacked substantial binding cooperativity with cyclin.

While the Cdk4 inhibitors palbociclib and ribociclib are readily distinguished from the Cdk2 inhibitors by their weak affinities for the Cdk2:cyclinA dimer, the distinction between the two classes of inhibitor becomes blurred when considering their binding

affinities for the different conformational states of Cdk2. For example, the Cdk2 inhibitor roscovitine and the Cdk4 inhibitor ribociclib are predicted to bind with similar affinity to the Aloop-in state of monomeric Cdk2, and the same holds for flavopiridol and palbociclib. Thus, the clear separation between the Cdk4 and Cdk2 inhibitor classes apparent in IC50 inhibition values (Figure 3.25) is attributable to the strong allosteric coupling of the Cdk2 inhibitors.

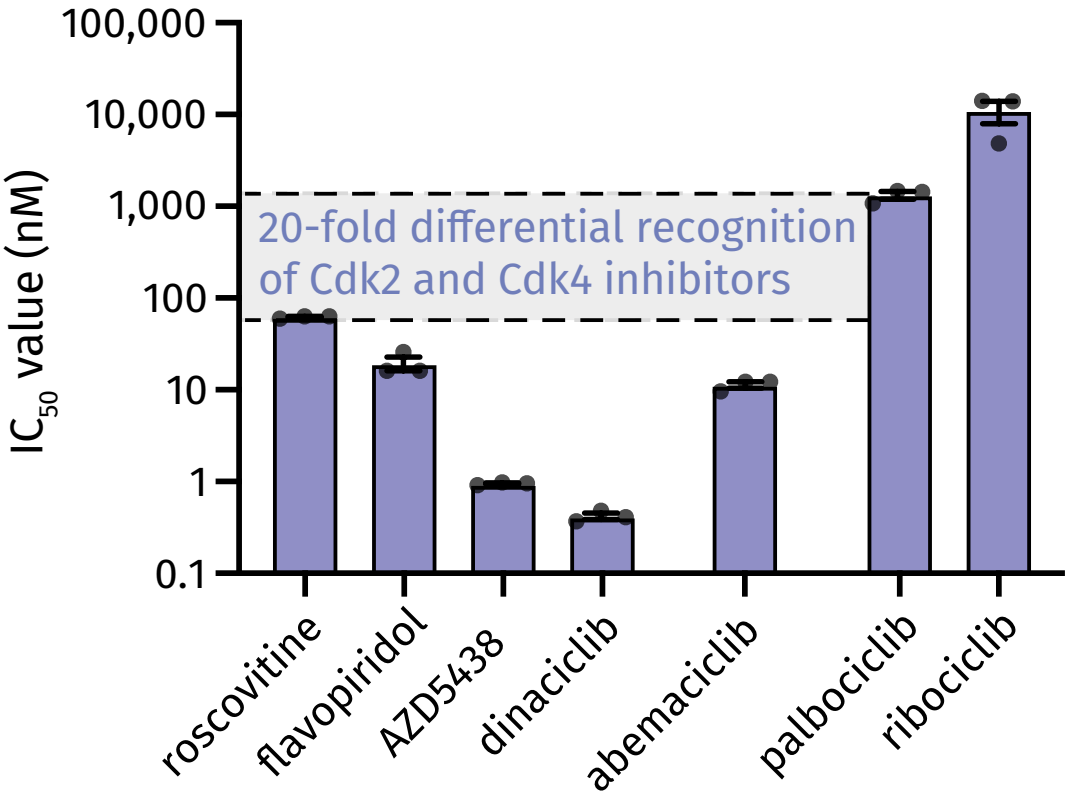

Figure 3.25: The IC_{50} values of the seven inhibitors for the pCdk2:cyclinA dimer.

3.3 Methods

FRET experiments tracking the A-loop

FRET samples were prepared by labeling "Cys-lite2" constructs of Cdk2 (C118A, C177S, A93C, R157C) with a 0.7:1 ratio of donor (AF488, Fluoroprobes) followed by a threefold excess of acceptor (AF568; Fluoroprobes) to ensure complete labeling. Labeled samples were purified by size exclusion chromatography into 1X PBS pH 7.4, 10 mM $MgCl_2$, 5 mM DTT and supplemented with 0.5 mg/ml bovine gamma globulins (Sigma) and 0.02% Tween-20. Inhibitor dose response titrations were prepared in 384-well plates using a mosquito liquid handling robot (ttp Labtech). Cdk2 FRET sensor (24 μL) was added to each well containing 1 μL of inhibitor in DMSO and incubated for 30 minutes prior to data collection. Steady-state fluorescence emission spectra were recorded with a fluorescence plate reader (Fluorescence Innovations), and the contributions of the donor and acceptor emission peaks to the measured emission spectra were unmixed by fitting each spectrum to basis functions for AF488, AF568 and the water Raman band[82]. For each inhibitor, binding experiments were performed using eight concentrations of cyclinA and twelve concentrations of inhibitor.

Global fit analysis of FRET data

FRET data were fit globally, using the numerical simulation package Kintek Explorer, to the extended allosteric two state model[36,81] shown in Figure 3.19. In this model, $K_{\mathrm{D}}^{\mathrm{cyclin}}$ and $K_{\mathrm{D}}^{\mathrm{drug}}$ represent the microscopic equilibrium constants for binding to the Aloop-out state of cyclinA and inhibitor, respectively, and $\alpha K_{\mathrm{D}}^{\mathrm{cyclin}}$ and $\beta K_{\mathrm{D}}^{\mathrm{drug}}$ the respective equilibrium constants for binding to the Aloop-in state.

$$K_{eq} = \frac{[\mathrm{Aloop_{out}}]}{[\mathrm{Aloop_{in}}]} \tag{3.1}$$

represents the conformational equilibrium constant for monomeric Cdk2, and α, β, γ, and δ represent the allosteric coupling factors that describe the coupling between cyclin binding and the conformational equilibrium (α), drug binding and the conformational equilibrium (β), the binding cooperativity between cyclin and drug in the Aloop-out state (γ) and the difference in binding cooperativity between the Aloop-in and Aloop-out states (δ).

The measured ratiometric FRET signal $F_{\mathrm{D/A}}$ was mapped onto the conformational equilibrium using one fluorescence coefficient, c1, to represent the Aloop-in state, and one coefficient, c2, for the Aloop-out state,

$$F_{\mathrm{D/A}} = c1 * ([\mathrm{K}] + [\mathrm{KC}] + [\mathrm{KD}] + [\mathrm{KDC}]) + c2 * ([\mathrm{K^*}] + [\mathrm{K^*C}] + [\mathrm{K^*D}] + [\mathrm{K^*DC}]) \quad (3.2)$$

where K and K* represent monomeric Cdk2 in the Aloop-in and Aloop-out states, respectively, KC and K*C Cdk2:cyclinA in the Aloop-in and Aloop-out states, KD and K*D Cdk2:inhibitor in the Aloop-in and Aloop-out states, and KDC and K*DC Cdk2 bound to both cyclinA and inhibitor in the Aloop-in and Aloop-out states. The values of K_{eq} and αK_{eq} were constrained to their values measured in the DEER experiments (Figures 2.15 and 3.26; $K_{\mathrm{eq}} = 0.143$ for Cdk2, $K_{\mathrm{eq}} = 0.178$ for pCdk2, $\alpha K_{\mathrm{eq}} = 1.26$ for Cdk2:cyclinA and $\alpha K_{\mathrm{eq}} = 6.4$ for pCdk2:cyclinA). For unphosphorylated Cdk2, fitting yielded well-constrained values for all remaining parameters of the model (β, γ, δ, $K_{\mathrm{D}}^{\mathrm{cyclin}}$ and $K_{\mathrm{D}}^{\mathrm{drug}}$) as judged by one- and two-dimensional error surface analysis (Figure 3.27). For phosphorylated Cdk2, the value of the allosteric coupling parameter δ, which determines the cyclin and inhibitor affinities for the inactive Aloop-in state of the pCdk2:cyclin dimer, was not well constrained in some datasets. We therefore chose not to interpret the value of δ. The values of $K_{\mathrm{D}}^{\mathrm{drug}}$, $\beta K_{\mathrm{D}}^{\mathrm{drug}}$ and $\delta K_{\mathrm{D}}^{\mathrm{drug}}$ shown in Figures 3.22, 3.23 and 3.24 represent the averages from three independent experiments.

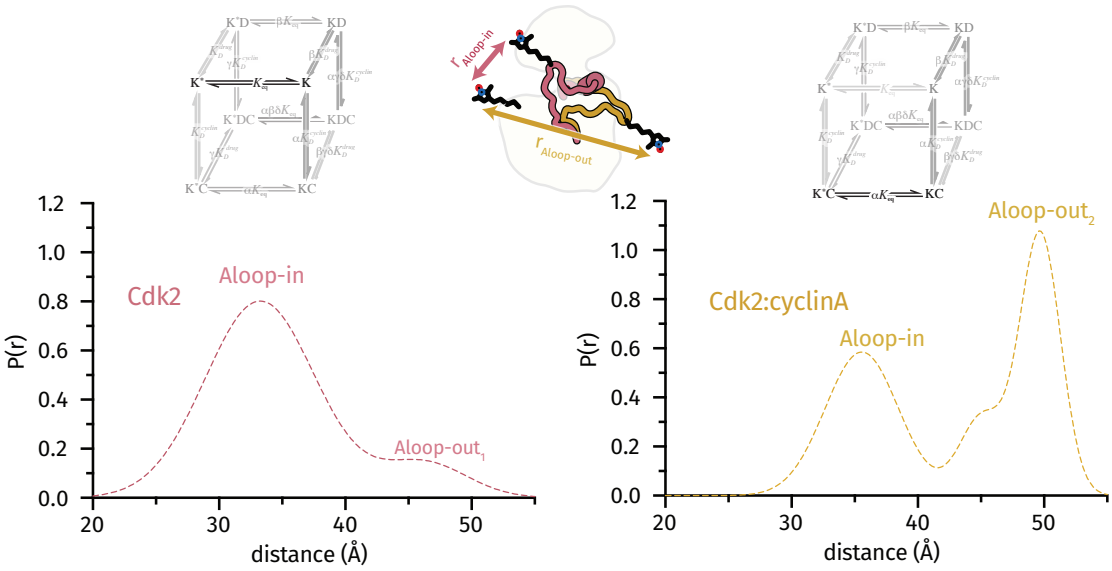

Figure 3.26: Gaussian populations derived from the DEER data for Cdk2 and Cdk2:cyclinA were used to constrain the values of the equilibrium constants K_{eq} and αK_{eq} in the fitting procedure.

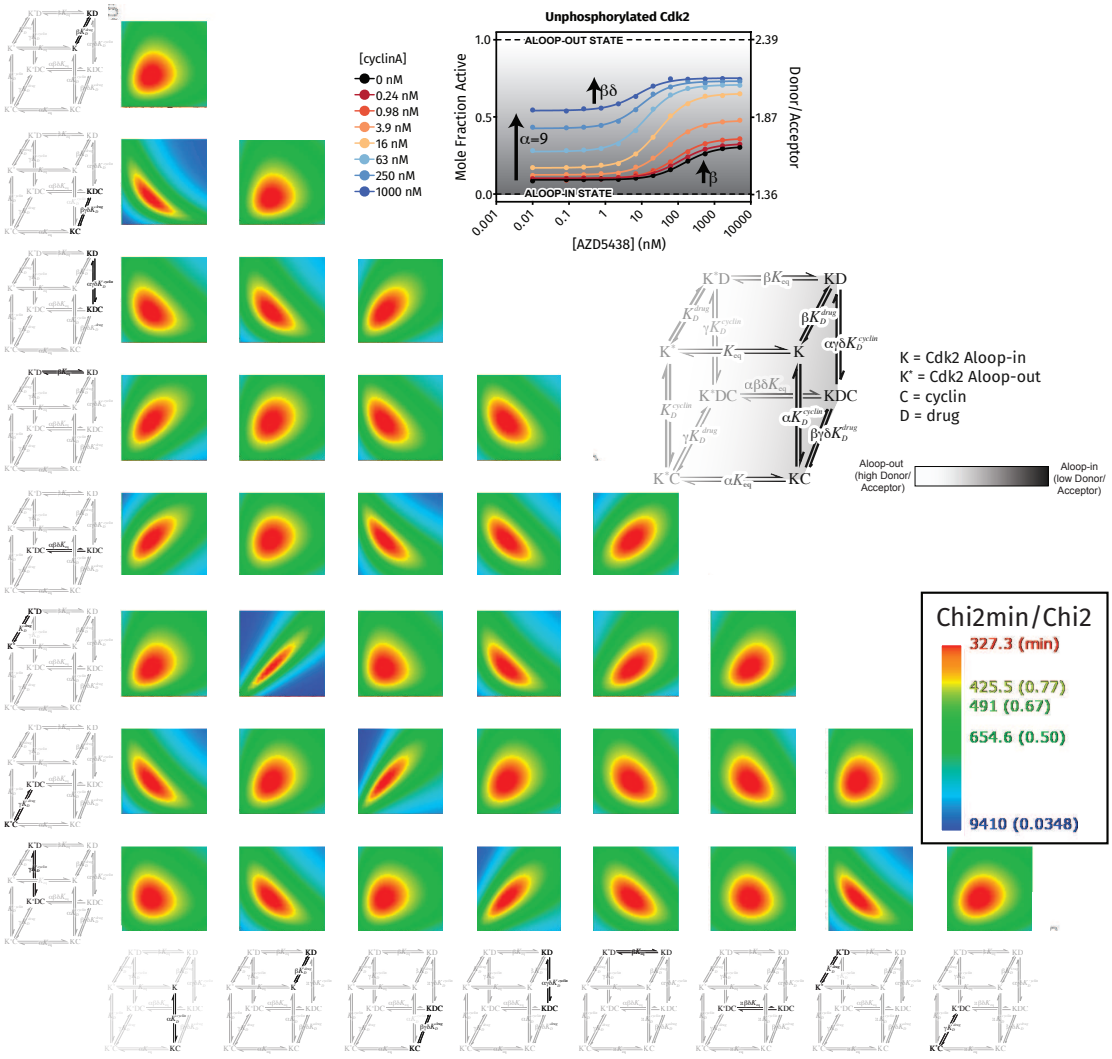

Figure 3.27: Error surface analysis of global fitting of FRET data to the extended allosteric two state model. A representative error surface analysis of the fit parameters performed in Kintek Explorer. Every pairwise combination of unconstrained parameters was explored and the ratio of the optimal fit χ^2 (chi2min) to the χ^2 obtained with a given combination of parameters is plotted on a color scale as shown in the legend.

Chapter 4

Allostery manifest in the architecture of Cdk2

4.1 Background

Despite a high degree of sequence conservation across the Cdk family (Figure 4.1), it is clear that the individual CDKs have adopted disparate activation mechanisms to regulate their activity. For example:

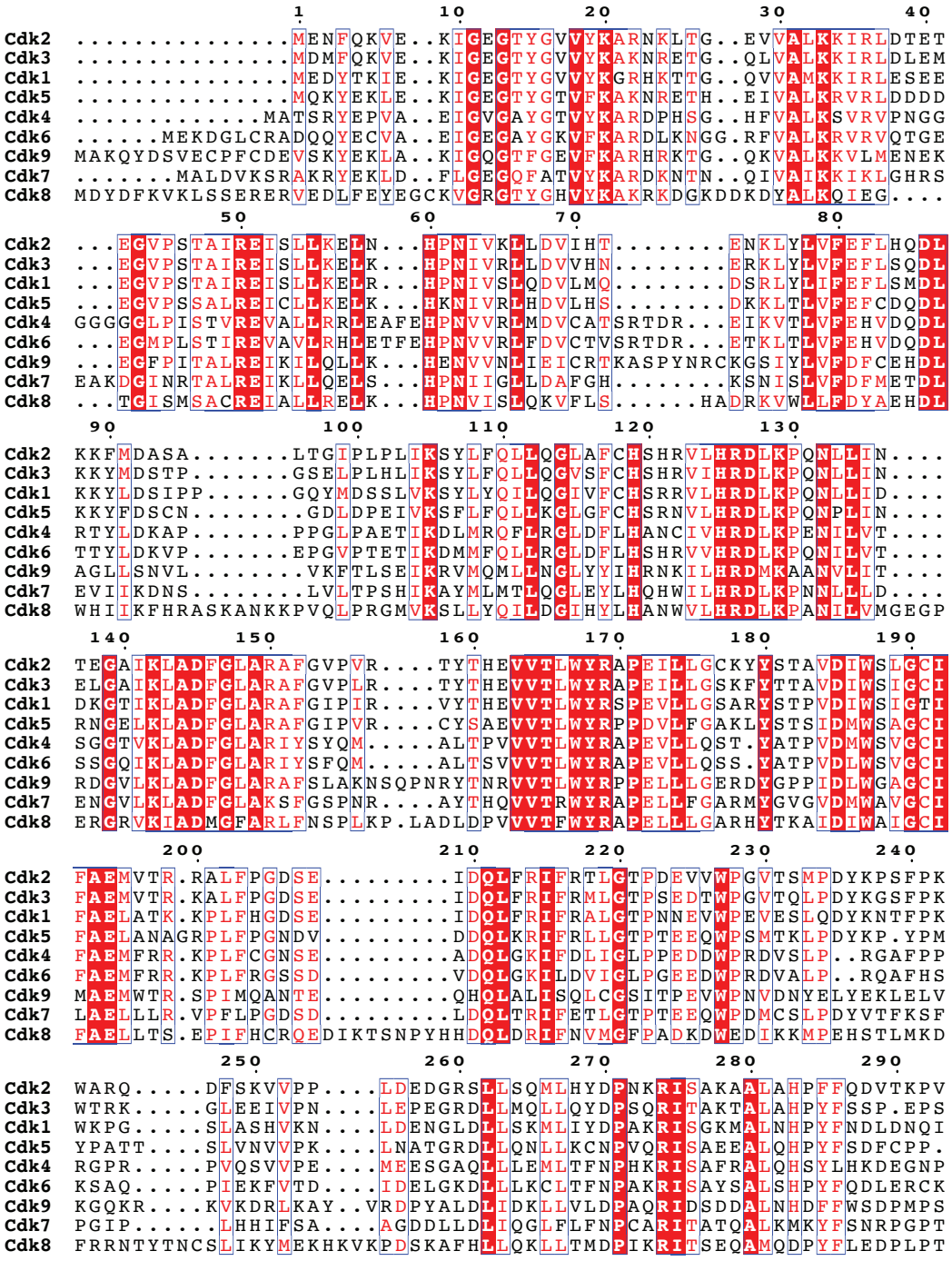

Figure 4.1: Sequence alignment of CDKs 1-9. Generated using [83] and [84].

- CDKs have preferred cyclin binding partners, with canonical CDK:cyclin pairings comprising vastly different binding interface surface areas[11,24,85–87], and dictating important signalling aspects such as cell cycle timing[88] and substrate recognition[89,90].

- CDKs differ in their requirement for non-cyclin accessory proteins for activation (e.g. Cks proteins for Cdk1[91] or MAT1 for Cdk7[92]).

- CDKs contain both activating and inactivating phosphorylation sites[93], but they vary in their requirement for phosphorylation to achieve a particular activation state[92], as well as in their ability to be continuously phosphorylated and dephosphorylated in cells.

- CDKs are known to associate with two different families of CDK-inhibitory proteins (INK4 and CIP/KIP families) for additional control of kinase activity in the cell cycle[94,95].

Each of these topics comprises its own line of investigation spanning decades of work, and is therefore largely beyond the scope of this study. However, each mechanism loosely ties into the questions at hand: how does the *architecture of the kinase itself* regulate its conformation and activity?

4.2 Results

4.2.1 The autoinhibitory hub of Cdk2 differs from that of Cdk4

The impetus for this study was the observation that, unlike in Cdk2, where cyclin binding and phosphorylation are enough to drive the kinase into the active conformation, T172-phosphorylated, cyclinD-bound Cdk4 remains in the Cdk2/Src-like inactive conformation (Figure 4.2)[24,25].

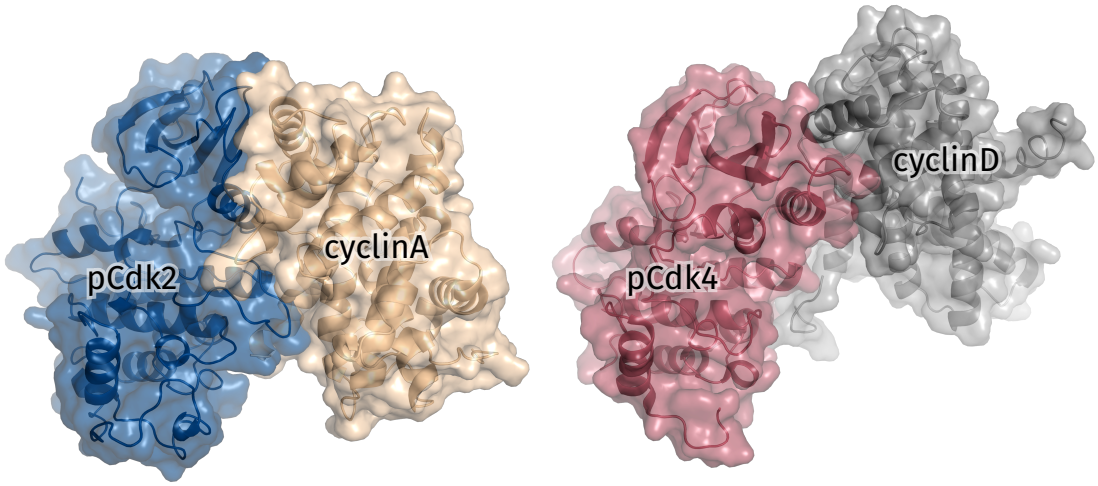

Figure 4.2: X-ray structures depicting the pCdk2:cyclinA complex (1JST) in an active-like conformation and the pCdk4:cyclinD complex (2W96) in the inactive conformation.

Since Cdk4 is not exempt from the requirement to adopt the active conformation in order to perform catalysis, several studies have investigated other biochemical determinants of Cdk4:cyclinD activation, pointing to both substrate[89] and, paradoxically, the CDK inhibitory protein p27[96]. In comparing the structures of human Cdk2 and Cdk4, we noticed differences in a particular set of hydrophobic residues in the core of the kinase (the "hub;" Figure (4.3), leading us to wonder how much they contribute to the ability of cyclin and phosphorylation to activate the CDKs, how they affect substrate recognition, and whether they affect inhibitor binding.

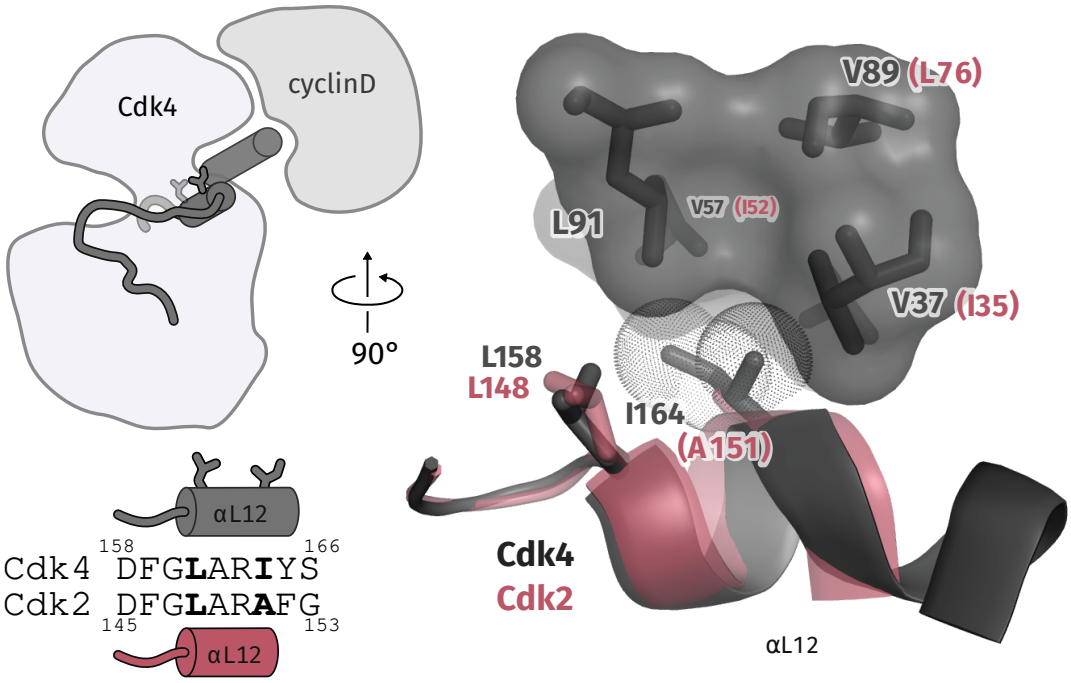

Figure 4.3: A comparison of the hydrophobic residues that comprise the autoinhibitory "hub" of Cdk2 and Cdk4.

4.2.2 A divergent hub controls allosteric coupling in Cdk2

To investigate the origins of the distinct allosteric wiring of Cdk2 and Cdk4, we performed a phylogenetic analysis of Cdk1, Cdk2 and the Cdk4/6 family across metazoan lineages (Figure 4.4). Mapping the metazoan sequence conservation within the respective CDK families onto the structures of Cdk2 and Cdk4 in the Aloop-in state revealed that the entire kinase domain interior was conserved in the Cdk1 and Cdk2 families, but that there was a hotspot of conservative amino acid substitutions in Cdk4/6 clustered in and around the αL12 helical turn of the A-loop (Figure 4.5). The variable residues are hydrophobic and interact with one another across the interface between the αL12 helix and the N-terminal lobe (the "hub"). These interactions are broken when the αL12 helix unfolds to form anchor 1 in the Aloop-out state. The residue at the center

of the hub is on the αL12 helix and is strictly conserved as an alanine in Cdk1 and Cdk2 (A151 in human Cdk2). In vertebrate Cdk4/6, this residue is instead conserved as an isoleucine (I164 in human Cdk4) and engages in more extensive hydrophobic interactions with the rest of the hub than the corresponding alanine residue of Cdk2 (Figure 4.5). The isoleucine in vertebrate Cdk4/6 is substituted in more basal clades with either valine or threonine (Figure 4.6). An enlarged β-branched residue at this position is thus a characteristic feature of Cdk4/6 kinases conserved across most metazoan life.

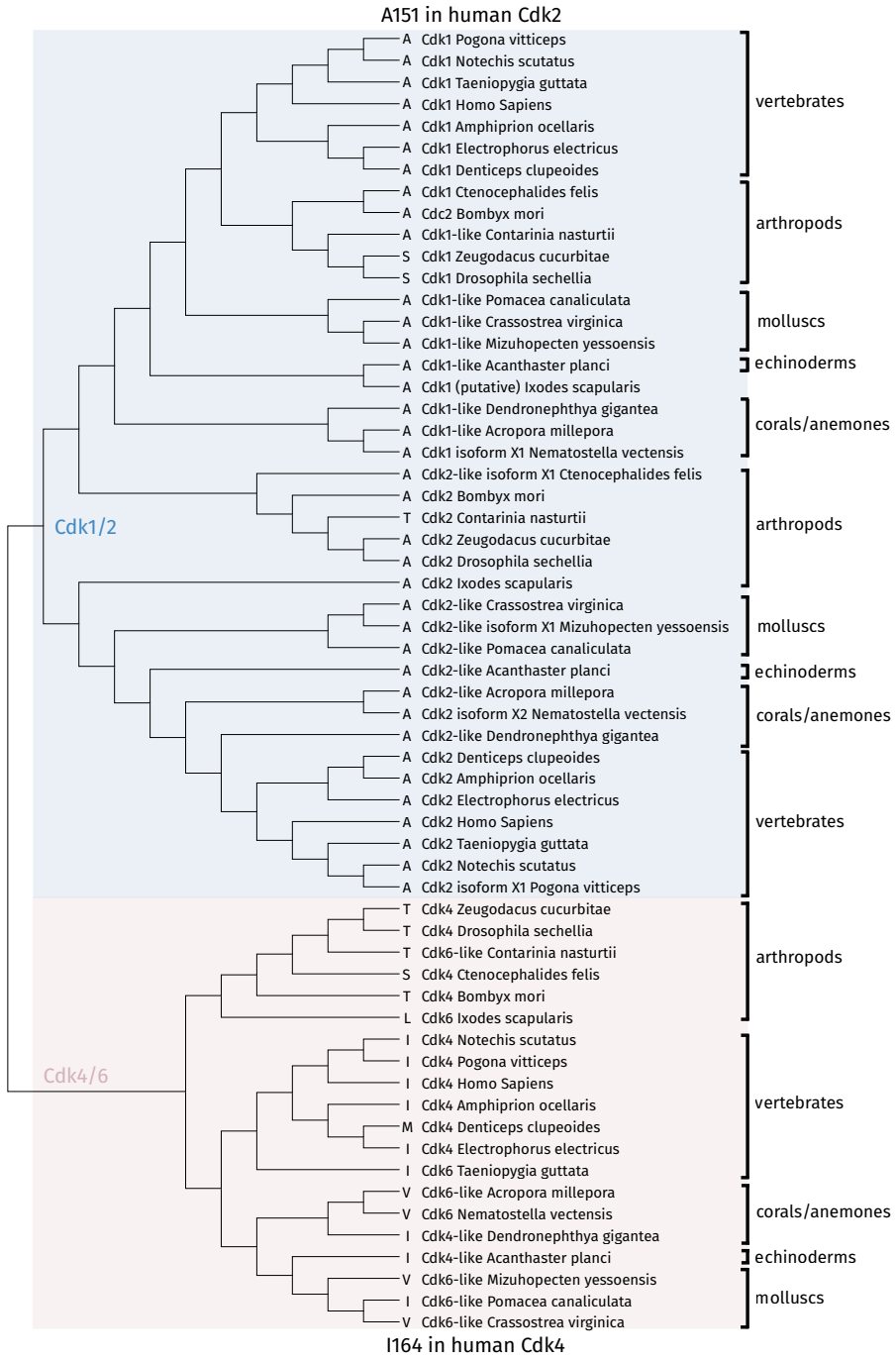

Figure 4.4: The phylogenetic tree was generated using the maximum likelihood method in MEGA X. The amino acid residue found at the central hub location (A151 in human Cdk2, I164 in human Cdk4)is shown for each species. There is a clear divergence of this position between Cdk2 and Cdk4 lineages.

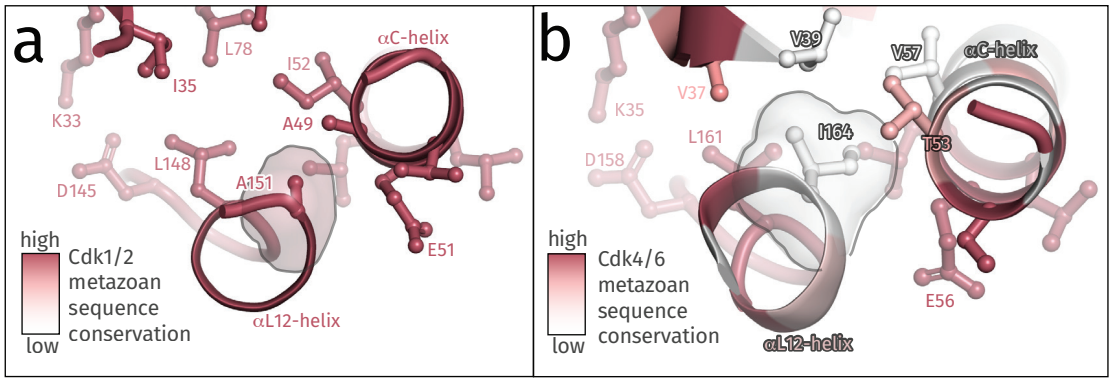

Figure 4.5: Metazoan sequence conservation in Cdk1/2 (a) and Cdk4/6 (b), determined from a set of 20 sequences (Figure 4.4) is mapped onto the structures of Cdk2 (left) and Cdk4 (right) in the Aloop-in conformation. Red represents strict conservation and white represents lower conservation.

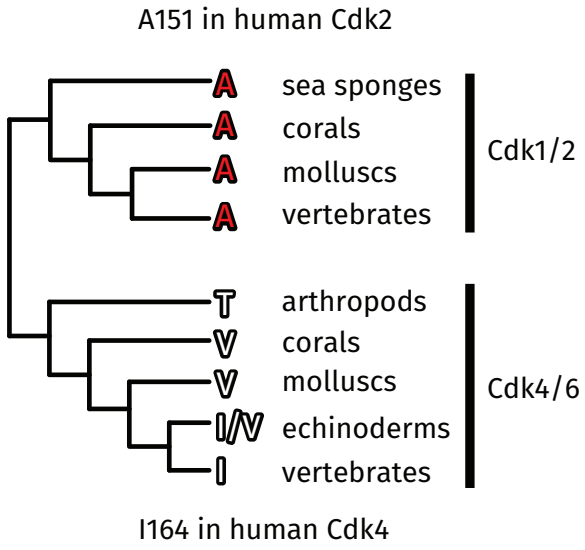

Figure 4.6: Divergence of the central hub residue (A151 in Cdk2, I164 in Cdk4) between Cdk1/2 and Cdk4/6 lineages.

We prepared a mutant of Cdk2 in which five hub residues were replaced with those of human Cdk4 ($Cdk2^{cdk4hub}$; Figure 4.7). We also prepared a second mutant in which the L148 residue was replaced with arginine to destabilize the hub (Cdk2L148R), inspired by a similar oncogenic mutation in EGFR[97]. DEER experiments revealed opposite

effects of these mutations on the kinase conformation (Figure 4.8). In the monomeric form, the pCdk2^{cdk4hub} mutant was fully in the Aloop-in state, with no evidence of the Aloop-out subpopulation observed in WT Cdk2 (Figure 4.9). Addition of saturating cyclinA resulted in the appearance of an Aloop-out subpopulation, but it remained the minor population (19 ± 9 %). Results with the phosphorylated and unphosphorylated Cdk2^{cdk4hub} mutant were similar, indicating that phosphorylation was no longer coupled to the structural change. Thus, the Cdk2cdk4hub mutant remains predominantly in the Aloop-in state even when bound to cyclin and phosphorylated on the A-loop, as has been reported for Cdk4[24,25]. In contrast, monomeric pCdk2^{L148R} displayed an increased Aloop-out subpopulation compared to WT Cdk2, and addition of cyclinA resulted in homogeneous adoption of the Aloop-out state with no evidence of a residual Aloop-in subpopulation, unlike WT Cdk2 (Figure 4.10). The two sets of mutations also had opposite effects on the affinity of cyclin binding measured by FRET (Figure 4.11). These results demonstrate that the residues of the hub play an important role in controlling the Aloop-in/out equilibrium and the degree to which cyclin binding is coupled to this equilibrium. The hub residues found in Cdk4/6 appear to weaken this allosteric coupling.

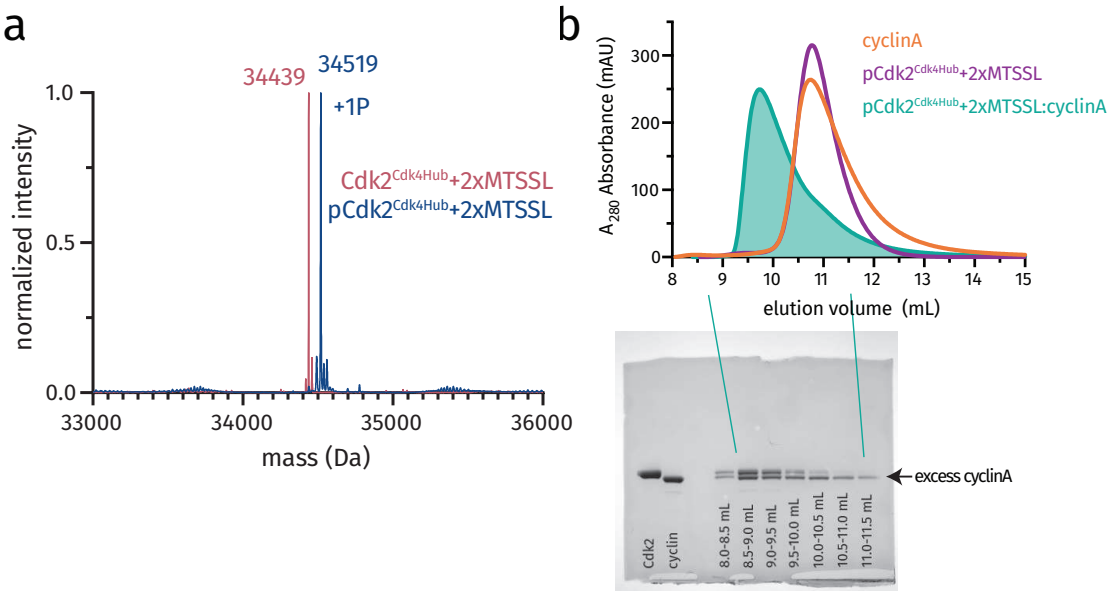

Figure 4.7: Validation of the Cdk2^{cdk4hub} construct, phosphorylation, cyclinA binding and folding. **a)** Mass spectrum of unphosphorylated and phosphorylated Cdk2^{cdk4hub} homogeneously labeled with 2 MTSSL spin labels (expected masses: 34439 Da and 34519 Da, respectively). **b)** Size exclusion chromatograms for spin-labeled monomeric Cdk2^{cdk4hub} (blue), MTSSL-labeledCdk2^{cdk4hub}:cyclinA complex (green), and free cyclinA. The SDS-PAGE gel shows the fractions from the size exclusion run on the Cdk2^{cdk4hub}:cyclinA complex, confirming the formation of the 1:1 complex and demonstrating the presence of excess cyclinA in the sample used for DEER experiments. Protein samples used for reference Cdk2 and cyclinA markers (lanes 1 and 2) had been previously validated. This analysis was performed on the sample used for the DEER experiment.

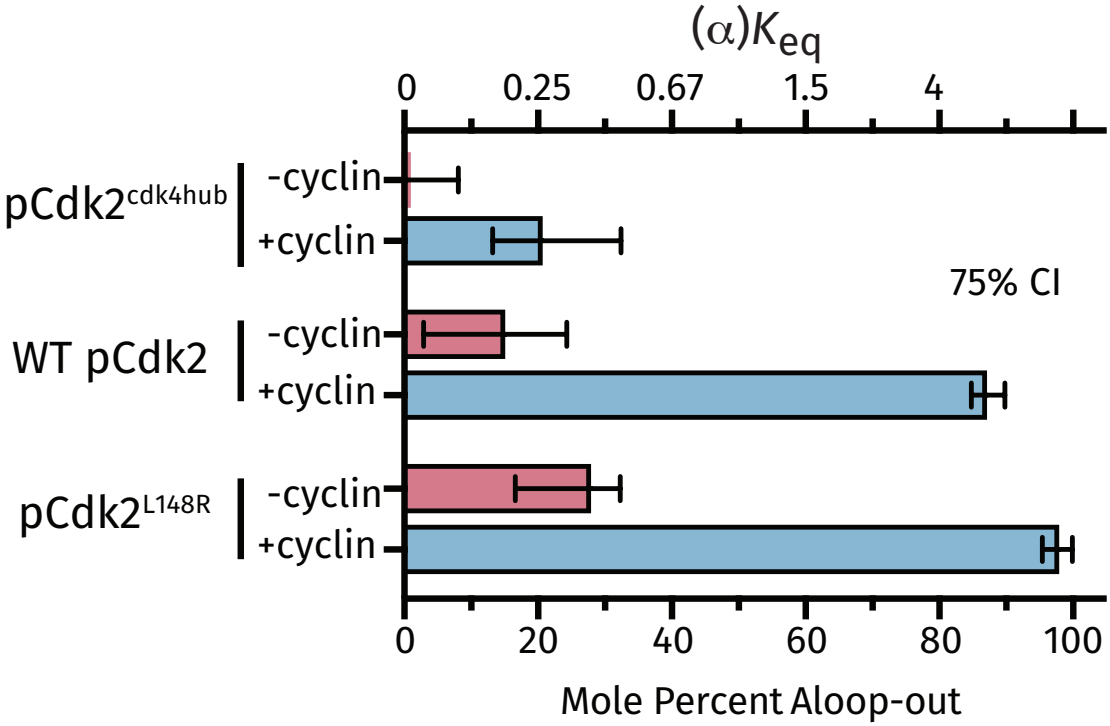

Figure 4.8: Conformational equilibrium values for WT Cdk2, pCdk2^{L148R} and pCdk2^{cdk4hub}. Error bars represent 75% CIs, calculated from 50,000 simulations of Gaussian fits to the primary data.

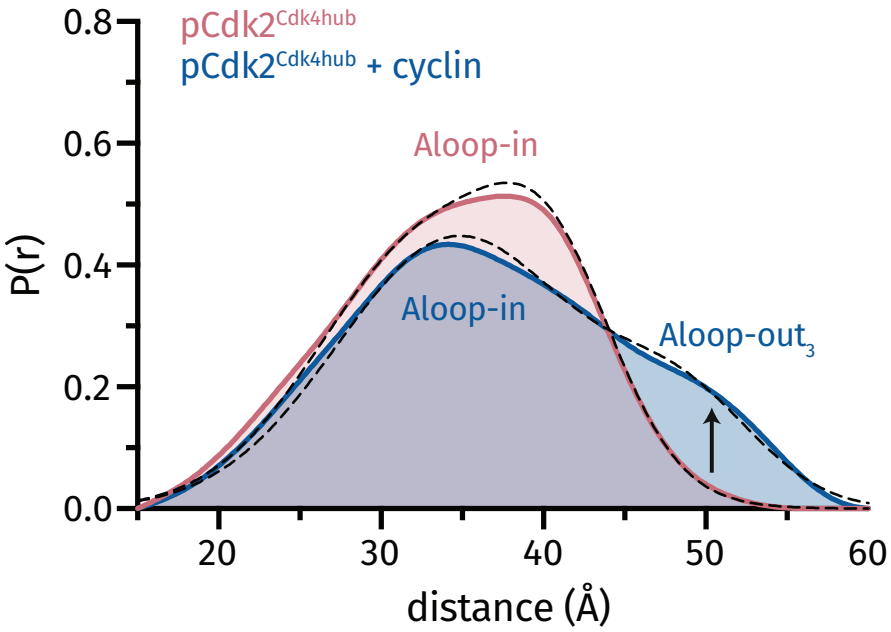

Figure 4.9: DEER data for the phosphorylated pCdk2$^{\text{cdk4hub}}$ mutant.

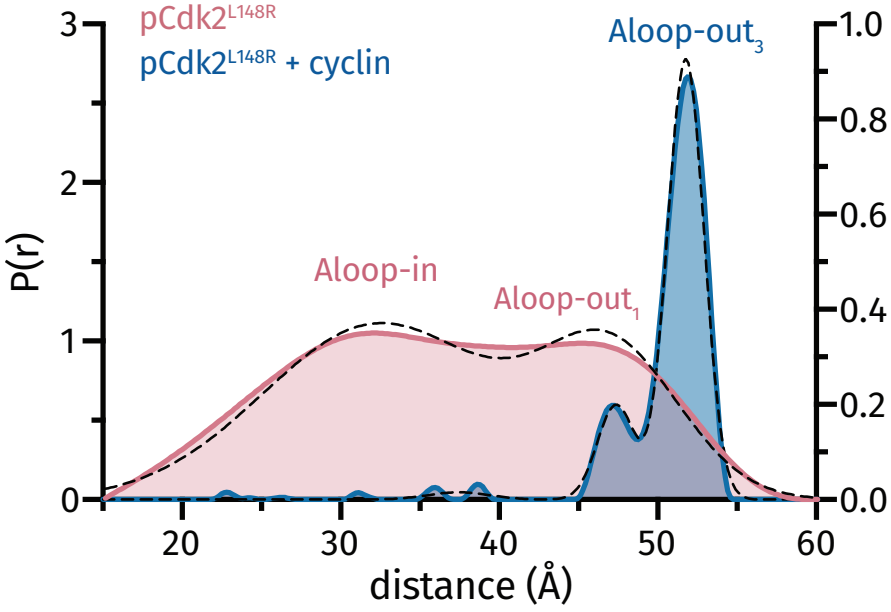

Figure 4.10: DEER data for the phosphorylated pCdk2$^{\text{L148R}}$ mutant. The monomer data are plotted on a different y axis scale for clarity.

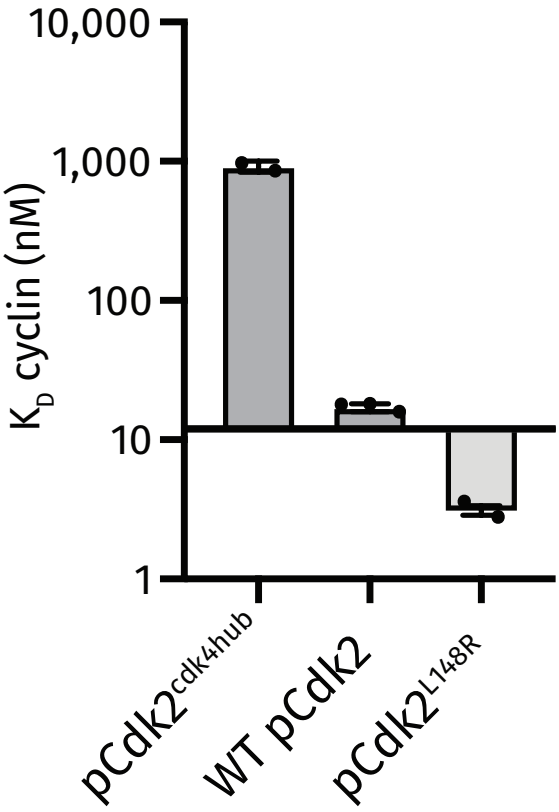

Figure 4.11: Cyclin binding affinities measured by FRET for WT Cdk2, Cdk2^{L148R} and Cdk2^{cdk4hub} mutants. Values are mean ± s.e.m.; n = 3 independent experiments.

For the Cdk2^{cdk4hub} mutant we also probed the effects of the hub mutations on inhibitor affinities. The affinities of the Cdk2 inhibitors and abemaciclib for the cyclin-bound mutant were markedly decreased compared to WT Cdk2, whereas the affinities of the Cdk4 inhibitors were unaffected (Figure 4.12). Consequently, the discrimination between the Cdk2 and Cdk4 inhibitor classes, so apparent with WT Cdk2, was diminished. These changes in affinity arise specifically from loss of allosteric coupling with the cyclin subunit, as they were not observed with the monomeric Cdk2^{cdk4hub} mutant (Figure 4.13). We measured IC_{50} values for all 7 inhibitors against both pCdk2:cyclinA and

pCdk4:cyclinD. The IC_{50} values obtained for Cdk2 show the expected >20-fold discrimination between the Cdk2 and Cdk4 inhibitors (Figure 4.14), but the values measured for Cdk4 show a strikingly different pattern. As expected, palbociclib, ribociclib and abemaciclib inhibit Cdk4 potently, but so do the majority of the Cdk2 inhibitors. With the exception of roscovitine, the Cdk2 inhibitors inhibit Cdk4 with IC_{50} values within 10-fold of palbociclib and ribociclib. Unlike Cdk2, Cdk4 does not differentiate clearly between Cdk2 and Cdk4 inhibitors. Thus, by uncoupling cyclin binding from the structural change, the altered hub residues of Cdk4 have also removed a major mechanism for distinguishing the two inhibitor classes.

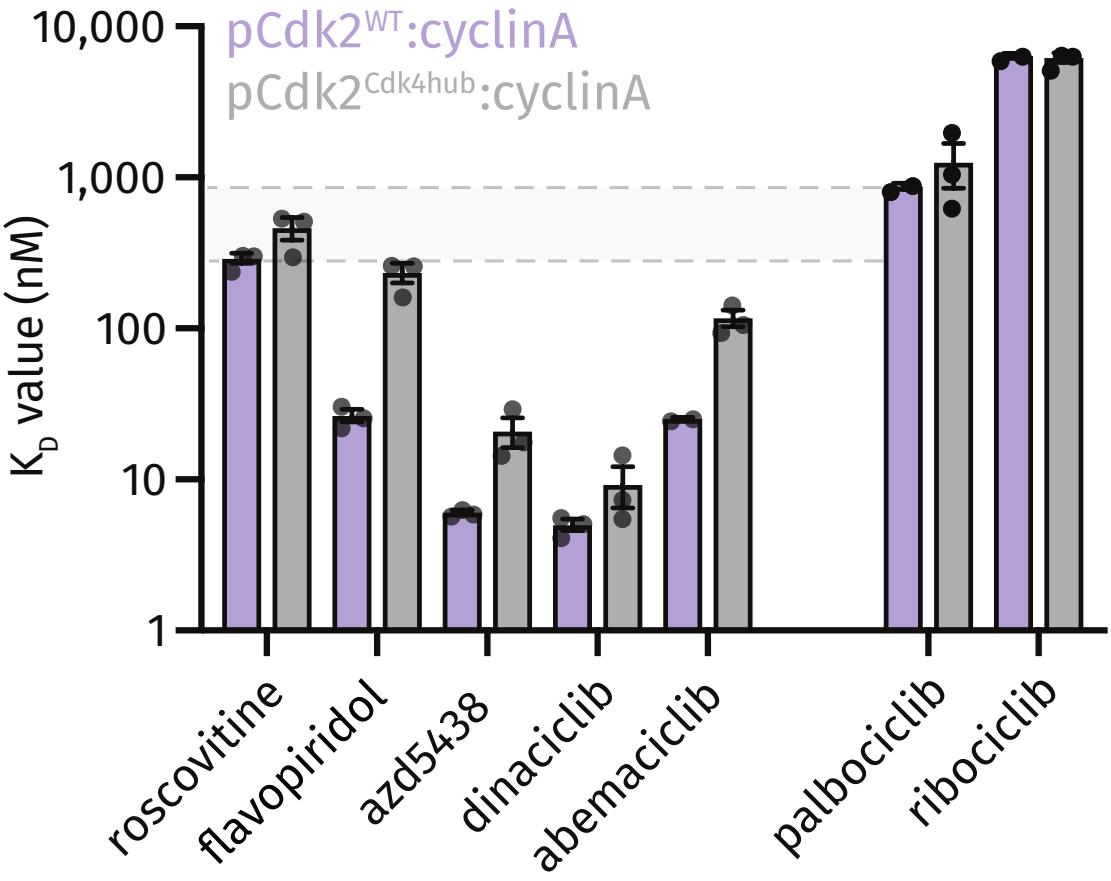

Figure 4.12: Inhibitor K_D values measured by FRET for WT pCdk2–cyclinA and pCdk2^{cdk4hub}–cyclinA. Values are mean ± s.e.m.; n = 3 independent experiments.

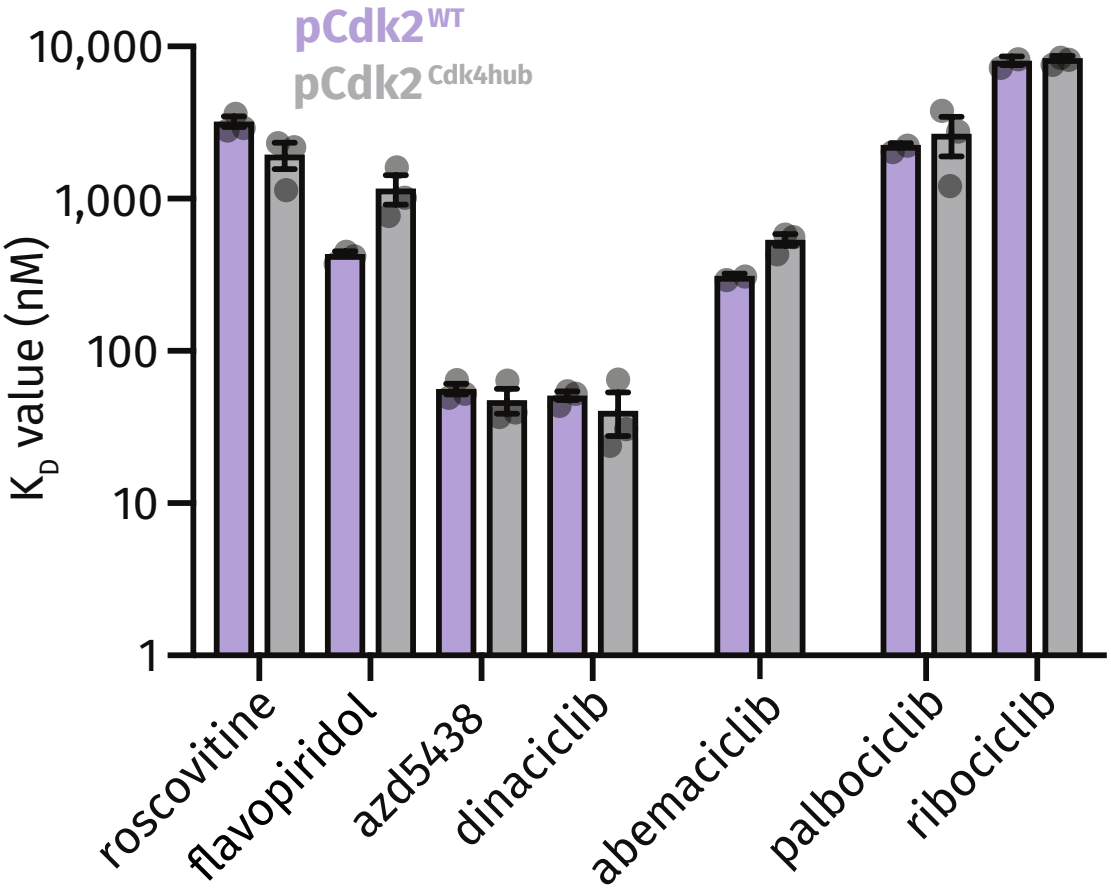

Figure 4.13: Inhibitor K_{D} values measured by FRET for WT pCdk2 and pCdk2$^{\mathrm{cdk4hub}}$. Values are mean ± s.e.m.; n = 3 independent experiments.

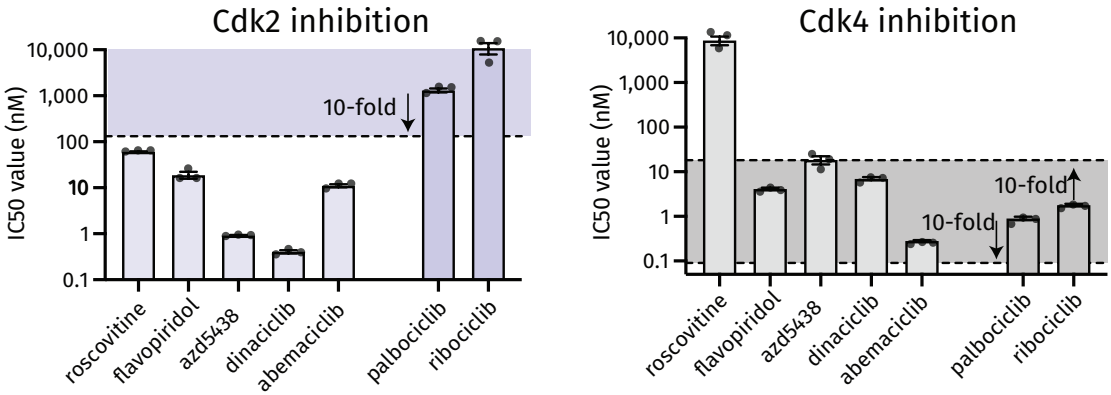

Figure 4.14: IC_{50} values measured in kinase assays for the seven inhibitors for pCdk2–cyclinA (left) and pCdk4–cyclinD (right). The shaded areas represent the range of IC_{50} values within tenfold of the IC_{50} values for palbociclib and ribociclib. Values are mean ± s.e.m.; n = 3 independent experiments.

In kinase assays, WT Cdk2, the Cdk2^{cdk4hub} mutant, and Cdk4 itself showed similar K_M values toward the physiological substrate RB (Figure 4.15). However, the K_M value of Cdk4 for a short peptide substrate was 8-fold higher than that of Cdk2, and the K_M value of the Cdk2^{cdk4hub} mutant was in between that of WT Cdk2 and Cdk4. This is likely attributable to Cdk4 and the Cdk2^{cdk4hub} mutant favoring the Aloop-in state, in which the peptide binding site is disassembled. In DEER experiments with the Cdk2^{cdk4hub} mutant, the addition of the short peptide substrate increased the population of the Aloop-out$_3$ state (Figure 4.16). This indicates that when binding to the Cdk2^{cdk4hub} mutant, and presumably to Cdk4 itself, substrates pay an energetic penalty to induce the Aloop-out$_3$ state, leading to compromised substrate recognition. RB possesses a secondary docking site specific for Cdk4 and essential for phosphorylation by Cdk4, but not Cdk2[89]. A central function of this site may be to compensate for the intrinsically poor substrate binding of Cdk4, driving the comparative specialization of Cdk4 toward RB relative to Cdk2[98].

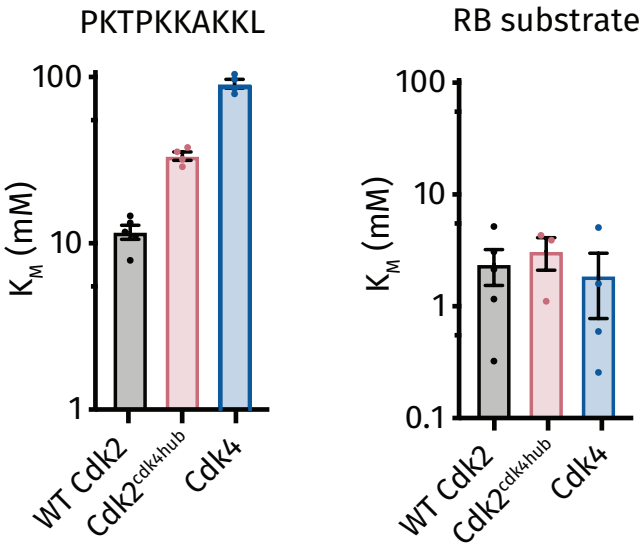

Figure 4.15: K_{M} values for phosphorylation of a short peptide substrate (left) and RB (right), measured for WT pCdk2, pCdk2$^{\mathrm{cdk4hub}}$ and pCdk4. Values are mean ± S.E.M; n = 4 independent experiments.

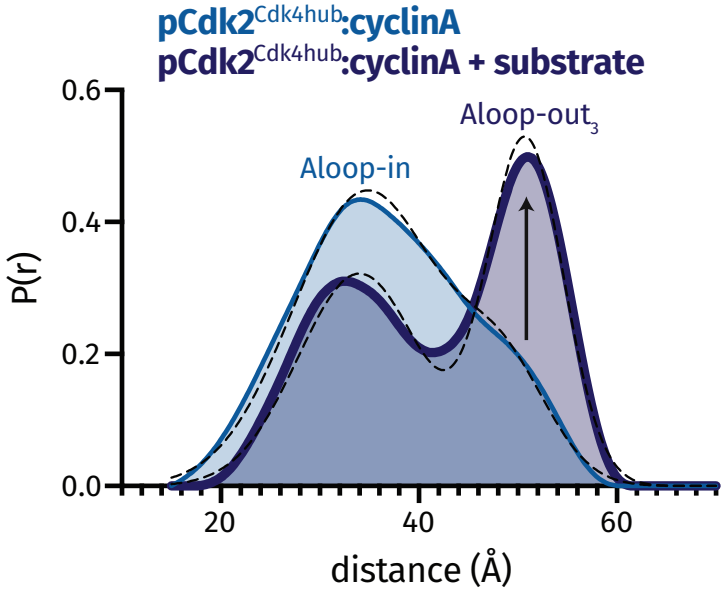

Figure 4.16: DEER data for the Cdk2$^{\mathrm{cdk4hub}}$ mutant bound to cyclinA with and without addition of saturating peptide substrate and AMPPNP.

4.3 Methods

Protein expression and purification

Cdk2 constructs were prepared as detailed in chapter 2. The Cdk2^{cdk4hub} mutant contained the I35V, I52V, L76V, A151I and F152Y mutations derived from the sequence of human Cdk4.

Human RB (residues 771-928 in a PGEX-3T vector) was expressed overnight in BL21 (DE3) *Escherichia coli*. Harvested cells were resuspended in 1X PBS, 10% glycerol, 1 mM DTT, pH 7.4, lysed with a homogenizer, and lysates clarified by centrifugation at 20,000 rpm. Clarified lysate was loaded onto 2 5mL GSTrap columns (GE), washed with 1X PBS, 10% glycerol, 1 mM DTT, pH 7.4, and eluted with 50 mM Tris, 10% glycerol, 20 mM reduced glutathione, 5 mM DTT, pH 8. Eluted protein was desalted into 20 mM sodium phosphate pH 7.4, loaded onto 2 5 mL SP columns and eluted with 20 mM sodium phosphate, 1 M NaCl, pH 7.4.

Kinase activity assays

Kinase activities of WT and mutant recombinant pCdk2–cyclinA and commercial pCdk4:cyclinD (Thermo Fisher) were determined using the ADP Quest accumulation assay (Eurofins). Reactions were performed with 5 nM kinase and 200 μM ATP in 384-well plates using a fluorescence plate reader and the Magellan Standard software (Tecan) at 20 °C. Rates were determined from time-dependent fluorescence traces by linear regression using Prism 8 (Graphpad).

Reactions were performed in the presence and absence of substrate, and rates were corrected for nonspecific ATP turnover by subtracting the rates measured in the absence of substrate. Substrates used include RB residues 771–928, which includes the

C-terminal Cdk4 docking site, and the histone H1-derived short peptide substrate PK-TPKKAKKL[99,100]. IC_{50} values for the seven inhibitors were measured using a γ-^{33}P radioactivity assay with RB as a substrate and 10 μM ATP (Reaction Biology).

Chapter 5

Conclusion and Discussion

5.1 Summary

In cycling cells, monomeric Cdk2 is subject to a continuous cycle of phosphorylation and dephosphorylation on T160[88]. Our results show that regardless of its phosphorylation state, monomeric Cdk2 samples the Aloop-out$_1$ conformation that is optimized for dephosphorylation rather than for substrate binding, thereby avoiding any residual kinase activity arising from the Aloop-out subpopulation. This permits a small energy barrier for the global structural change, promoting facile regulation while preventing kinase activity from being uncoupled from the expression of cyclins A and E in G1 and S phase. The effects of T160 phosphorylation are only unmasked in the presence of the cyclin subunit, where it enhances the cyclin-driven conformational shift and favors the Aloop-out$_3$ state, trapping the kinase in the catalytically active form. This explains why cyclin binding renders Cdk2 resistant to dephosphorylation in cells, a property that is thought to be important for switch-like activation of the kinase at the G1/S boundary[23]. In contrast, the graded activation of Cdk4 by growth factor signaling has been linked to the A-loop phosphorylation site remaining accessible to both CAK and phosphatases in

Cdk4:cyclinD complexes[23]. Our results with the Cdk2^{cdk4hub} mutant suggest that this is due to the altered allosteric wiring of Cdk4, in which the cyclin-driven conformational shift is reduced and the enhancement of this shift by A-loop phosphorylation, observed in Cdk2, is lost. The resulting disassembly of the peptide binding site in Cdk4:cyclinD complexes also leads to weak activity toward generic substrates and dependence on the secondary docking site of RB. We have traced the contrasting allosteric properties of Cdk2 and Cdk4 to evolutionary divergence within the allosteric hub, and shown that these differences have important implications for inhibitor recognition.

The advent of Cdk4 inhibitors transformed the treatment of hormone-responsive breast cancer[70,101], but the clinical experience with Cdk2 inhibitors has been less favorable. This has been attributed in part to the greater selectivity and therapeutic window of Cdk4 inhibitors. Our results show that the active sites of Cdk2 and Cdk4 do not inherently differentiate between Cdk2 and Cdk4 inhibitors. Instead, the distinction between these two drug classes arises from their differential recognition of particular conformational states. The allosteric properties of the Cdk2 inhibitors reflect the fact that cyclin binding is tightly coupled to the Aloop-out/αC-in state in Cdk2. By similarly coupling to this conformational state, Cdk2 inhibitors are able to target the catalytically active Cdk2:cyclin complexes with high affinity despite binding monomeric Cdk2 relatively weakly. The Cdk4 inhibitors palbociclib and ribociclib are not allosterically coupled in this way because cyclin binding is not tightly coupled to the structural change in Cdk4. This lack of allosteric coupling ensures that palbociclib and ribociclib bind both monomeric Cdk2 and Cdk2:cyclin complexes weakly, and is likely the result of the development process of these drugs in which selectivity for Cdk4 over Cdk2 was prioritized[67,68]. The importance of allostery is underscored by the contrasting example of abemaciclib, which has greater potency for Cdk4 than either palbociclib or ribociclib, but possesses the allosteric properties of a Cdk2 inhibitor and consequently targets Cdk2

as well. This ability of abemaciclib to target CDKs other than Cdk4/6 has been associated with a superior cytotoxicity profile and the ability to override clinical resistance to palbociclib arising from overexpression of cyclinE[71].

The allosteric effects of the Cdk2 inhibitors and abemaciclib have implications for CDK scaffolding interactions, analogous to those reported for palbociclib[96]. The cognate pairing of CDK and cyclin subunits is relatively labile in cells. For example, enhancing or blocking A-loop phosphorylation of Cdk1 shunts cyclinA onto Cdk1 or cyclinB onto Cdk2, respectively[88]. The enhancement of cyclinA affinity by Cdk2 inhibitors is likely to apply to other cyclin subunits, which could become sequestered in non-cognate Cdk2:cyclin complexes. Sequestration of cyclinB in such a manner may explain why abemaciclib blocks Cdk1 substrate phosphorylation and triggers a G2 arrest in cells[71] despite lacking potent activity against Cdk1 in vitro[62]. Thus, the contrasting allosteric properties of Cdk4 and Cdk2 inhibitors reported here may play a central role in the therapeutic efficacy of these drugs.

5.2 The role of cyclins in the conformational balance of CDKs

CyclinE associates with Cdk2 to drive the G1-S transition in the cell cycle, and the Cdk2:cyclinE binding interface is larger than that of Cdk2:cyclinA[102,103]. This raises the questions of whether the two cyclins differ in their ability to activate Cdk2 and whether inhibitors would bind differently to the Cdk2:cyclinE complex. Furthermore, the elucidation of the effects of the low molecular weight isoform of cyclinE[21] by the allosteric two-state model (ATSM) would serve as an instructive comparison for how cyclinE activates its CDK partner.

For all of the experiments in this study, we were only able to use cyclinA. This

was in large part due to the relative ease with which we could express, purify and store monomeric cyclinA. It is unlikely that recombinant expression of other cyclins in a monomeric form is an insurmountable problem, and therefore the effect of the other cyclins warrants further study.

Although CDKs have preferences for which cyclins they bind to, they are known to form noncanonical binding interactions with other members of the cyclin family, particularly in pathological contexts. This, too, would make for an interesting line of investigation: the ATSM treatment applied to various combinations of CDK and cyclin partners would provide a detailed insight into how the specific interactions at the CDK-cyclin interface contribute to CDK activation. It is likely that in addition to the variable timing of cyclin expression in the cell, each cyclin may also be characterized by a different α value.

5.3 The importance of considering the conformational equilibrium in drug discovery

One of the key insights from this study is the variability in the degree to which active site inhibitors are allosterically coupled to the conformational equilibrium of Cdk2. The development of kinase inhibitors typically involves a process of winnowing drug candidates through molecular docking and compound screening, followed by an iterative optimization process by which substituents on a lead compound are modified and tested against kinase activity. *This is inherently a flawed process:* in the case of Cdk2, for example, the active pCdk2:cyclinA complex against which drug candidates are tested happens to be locked in the most rigid conformational state the kinase is capable of achieving. This process selects for inhibitors in an unfortunate way: not only does it come at the expense of compounds that would bind tightly to an inactive state

of the kinase, but it also exacerbates the problem of selectivity because the active conformation, the one which permits every kinase to catalyze *exactly the same reaction*, is naturally the one that is most highly conserved across the kinome. It is therefore unsurprising that Cdk2 inhibitors such as dinaciclib have virtually indistinguishable IC_{50} values for both Cdk1 and Cdk2, which likely limits the dosing regimen (and thus limits efficacy) so as to avoid Cdk1-associated cytotoxicity in clinical trials.

In hindsight, it is also not surprising that Cdk4 inhibitors were the first (and to this day, only) CDK inhibitors to be approved for clinical use. In this case, the typical inhibitor development process described above was unknowingly aided by a quirk specific to the drug target itself: unlike in pCdk2:cyclinA, the conformational balance of the pCdk4:cyclinD complex is highly skewed towards the inactive conformation, thereby making it possible to select for inhibitors (i.e. palbociclib, ribociclib and to a lesser degree, abemaciclib) that are agnostic to the conformation of the kinase. Note that while this analysis could easily be read as a dismissal of Cdk4 inhibitor development as "easy," it is not intended as such; the selectivity profiles of palbociclib, ribociclib and abemaciclib are truly remarkable, and their availability helped provide us with important insights into how kinase inhibitors truly interact with their targets.

Nevertheless, the explicit consideration of the conformational states of drug targets is a necessity in any drug discovery pipeline, and the FRET assays in this study, as well as prior work from our lab on Aurora A[76], have laid a foundation for achieving this. Compound screens that measure the structural states of drug targets in addition to biological activity may very well lead to drug candidates that would otherwise never have been identified in a screen for activity alone. Knowledge of the ability of inhibitors to interact with the kinase conformational equilibrium also has another important consequence: many researchers use inhibitors as controls, or as a means to achieve a precondition for studies of other effects in cells (e.g. using a CDK inhibitor to

block cell cycle progression). It is eminently possible to introduce confounding variables (e.g. sequestration of other cyclins by the inhibitor-bound CDK) without realizing it. The added dimension of conformational data would allow researchers to better account for the unintended effects of inhibitor treatment.

Finally, there are significant efforts underway to develop "true" allosteric inhibitors of Cdk2 that bind away from the active site[104,105]. Theoretically, these inhibitors would be more selective for Cdk2 because they target pockets that are less conserved than the active site. An ATSM analysis of Cdk2 in the presence of allosteric drug candidates is critical, and may very well uncover molecules that are negatively cooperative with cyclins (i.e. having $\beta < 1$), thus circumventing problems associated with cyclin sequestration by Cdk2:inhibitor complexes.

5.4 Towards an understanding of the role of hub mutations in the evolution of the eukaryotic cell cycle

There is a fascinating tension between the requirement for cellular signalling sensitivity, which allows the cell to respond to small changes in the environment, and the requirement for robustness, which allows the cell to absorb the effects of genetic and environmental aberrations. There are dramatic examples of each extreme: relatively small changes in PKCα kinase activity have been shown to propagate to disastrous effect in an Alzheimer's model[106]. In contrast, it has also been shown that a single Cdk:cyclin complex can drive the whole cell cycle in fission yeast[107], thus demonstrating the significant redundancy built into the eukaryotic cell cycle. The link between particular somatic point mutations and the resulting constitutively active kinases have been well studied in cancer[108,109], but the effects (if any) of many subtle mutations remain unknown.

Although the Cdk2^{cdk4hub} mutations resulted in dramatic changes in kinase conformation, inhibitor recognition, and catalytic activity, the Cdk2^{cdk4hub} construct only represents a difference of five residues between human Cdk2 and Cdk4. Our sequence analysis of Cdk4 across different lineages uncovered a variety of conservative mutations of hydrophobic residues in the hub; their effects on the conformation and catalytic activity of the kinase, cell cycle timing, and their ultimate role in the evolution of the eukaryotic cell cycle remain to be seen.

Bibliography

1. Cohen, P. The origins of protein phosphorylation. *Nature Cell Biology* **4,** E127–E130. ISSN: 1476-4679. http://www.nature.com/articles/ncb0502-e127 (May 2002).
2. Knighton, D. R. *et al.* Crystal Structure of the Catalytic Subunit of Cyclic Adenosine Monophosphate-Dependent Protein Kinase. *Science* **253,** 407–414. ISSN: 0036-8075. http://www.jstor.org/stable/2878883 (1991).
3. Huse, M. & Kuriyan, J. The Conformational Plasticity of Protein Kinases. *Cell* **109,** 275–282. ISSN: 0092-8674. https://www.sciencedirect.com/science/article/pii/S0092867402007419 (May 3, 2002).
4. Rahman, R., Ung, P. M.-U. & Schlessinger, A. KinaMetrix: a web resource to investigate kinase conformations and inhibitor space. *Nucleic Acids Research* **47,** D361–D366. ISSN: 0305-1048. https://doi.org/10.1093/nar/gky916 (D1 Jan. 8, 2019).
5. Might, M. *The illustrated guide to a Ph.D.* http://matt.might.net/articles/phd-school-in-pictures/.
6. Morgan, D. O. CYCLIN-DEPENDENT KINASES: Engines, Clocks, and Microprocessors. *Annu. Rev. Cell Dev. Biol.* **13,** 261–291. ISSN: 1081-0706. https://www.annualreviews.org/doi/10.1146/annurev.cellbio.13.1.261 (Nov. 1, 1997).
7. Hochegger, H., Takeda, S. & Hunt, T. Cyclin-dependent kinases and cell-cycle transitions: does one fit all? *Nature Reviews Molecular Cell Biology* **9,** 910–916. ISSN: 1471-0080. https://www.nature.com/articles/nrm2510 (Nov. 2008).
8. Fisher, R. P. & Morgan, D. O. A novel cyclin associates with M015/CDK7 to form the CDK-activating kinase. *Cell* **78,** 713–724. ISSN: 0092-8674. http://www.sciencedirect.com/science/article/pii/0092867494905355 (Aug. 26, 1994).

9. Desai, D., Wessling, H. C., Fisher, R. P. & Morgan, D. O. Effects of phosphorylation by CAK on cyclin binding by CDC2 and CDK2. *Molecular and Cellular Biology* **15,** 345–350. ISSN: 0270-7306, 1098-5549. https://mcb.asm.org/content/15/1/345 (Jan. 1, 1995).

10. De Bondt, H. L. *et al.* Crystal structure of cyclin-dependent kinase 2. *Nature* **363,** 595–602. ISSN: 1476-4687. http://www.nature.com/articles/363595a0 (June 1993).

11. Jeffrey, P. D. *et al.* Mechanism of CDK activation revealed by the structure of a cyclinA-CDK2 complex. *Nature* **376,** 313–320. ISSN: 1476-4687. http://www.nature.com/articles/376313a0 (July 1995).

12. Russo, A. A., Jeffrey, P. D. & Pavletich, N. P. Structural basis of cyclin-dependent kinase activation by phosphorylation. *Nat. Struct. Biol.* **3,** 696–700. ISSN: 1072-8368 (Aug. 1996).

13. Majumdar, A. *et al.* Allostery governs Cdk2 activation and differential recognition of CDK inhibitors. *Nature Chemical Biology,* 1–9. ISSN: 1552-4469. https://www.nature.com/articles/s41589-020-00725-y (Feb. 1, 2021).

14. Nowell, C. The minute chromosome (Ph1) in chronic granulocytic leukemia. *Blut* **8,** 65–66. ISSN: 1432-0584. https://doi.org/10.1007/BF01630378 (Apr. 1, 1962).

15. Lugo, T. G., Pendergast, A. M., Muller, A. J. & Witte, O. N. Tyrosine kinase activity and transformation potency of bcr-abl oncogene products. *Science* **247,** 1079–1082. ISSN: 0036-8075, 1095-9203. http://science.sciencemag.org/content/247/4946/1079 (Mar. 2, 1990).

16. Druker, B. J. *et al.* Efficacy and Safety of a Specific Inhibitor of the BCR-ABL Tyrosine Kinase in Chronic Myeloid Leukemia. *New England Journal of Medicine* **344,** 1031–1037. ISSN: 0028-4793. https://doi.org/10.1056/NEJM200104053441401 (Apr. 5, 2001).

17. Hantschel, O. Structure, Regulation, Signaling, and Targeting of Abl Kinases in Cancer. *Genes Cancer* **3,** 436–446. ISSN: 1947-6019. https://www.ncbi.nlm.nih.gov/pmc/articles/PMC3513796/ (May 2012).

18. Roskoski, R. Properties of FDA-approved small molecule protein kinase inhibitors: A 2021 update. *Pharmacological Research,* 105463. ISSN: 1043-6618. https://www.sciencedirect.com/science/article/pii/S1043661821000463 (Jan. 26, 2021).

19. Karst, A. M. *et al.* Cyclin E1 Deregulation Occurs Early in Secretory Cell Transformation to Promote Formation of Fallopian Tube–Derived High-Grade Serous Ovarian Cancers. *Cancer Res* **74,** 1141–1152. ISSN: 0008-5472, 1538-7445. http://cancerres.aacrjournals.org/content/74/4/1141 (Feb. 15, 2014).

20. Hunt, K. K. *et al.* Cytoplasmic Cyclin E Predicts Recurrence in Patients with Breast Cancer. *Clin Cancer Res* **23,** 2991–3002. ISSN: 1078-0432, 1557-3265. https://clincancerres.aacrjournals.org/content/23/12/2991 (June 15, 2017).

21. Keyomarsi, K. *et al.* Cyclin E, a Potential Prognostic Marker for Breast Cancer. *Cancer Res* **54,** 380–385. ISSN: 0008-5472, 1538-7445. http://cancerres.aacrjournals.org/content/54/2/380 (Jan. 15, 1994).

22. Wang, J. *et al.* Cyclin-Dependent Kinase 2 Promotes Tumor Proliferation and Induces Radio Resistance in Glioblastoma. *Translational Oncology* **9,** 548–556. ISSN: 1936-5233. http://www.sciencedirect.com/science/article/pii/S1936523316301073 (Dec. 1, 2016).

23. Schachter, M. M. *et al.* A Cdk7-Cdk4 T-Loop Phosphorylation Cascade Promotes G1 Progression. *Molecular Cell* **50,** 250–260. ISSN: 1097-2765. http://www.cell.com/molecular-cell/abstract/S1097-2765(13)00284-0 (Apr. 25, 2013).

24. Day, P. J. *et al.* Crystal structure of human CDK4 in complex with a D-type cyclin. *PNAS* **106,** 4166–4170. ISSN: 0027-8424, 1091-6490. http://www.pnas.org/content/106/11/4166 (Mar. 17, 2009).

25. Takaki, T. *et al.* The structure of CDK4/cyclin D3 has implications for models of CDK activation. *PNAS* **106,** 4171–4176. ISSN: 0027-8424, 1091-6490. http://www.pnas.org/content/106/11/4171 (Mar. 17, 2009).

26. Stevenson, L. M., Deal, M. S., Hagopian, J. C. & Lew, J. Activation mechanism of CDK2: role of cyclin binding versus phosphorylation. *Biochemistry* **41,** 8528–8534. ISSN: 0006-2960 (July 2, 2002).

27. Lakowicz, J. R. *Principles of Fluorescence Spectroscopy* 3rd ed. ISBN: 978-0-387-31278-1. https://www.springer.com/gp/book/9780387312781 (Springer US, 2006).

28. Evans, E. G. & Millhauser, G. L. Genetic Incorporation of the Unnatural Amino Acid p-Acetyl Phenylalanine into Proteins for Site-Directed Spin Labeling. *Methods Enzymol* **563,** 503–527. ISSN: 0076-6879. https://www.ncbi.nlm.nih.gov/pmc/articles/PMC4841275/ (2015).

29. Jeschke, G. DEER distance measurements on proteins. *Annu Rev Phys Chem* **63,** 419–446. ISSN: 1545-1593 (2012).

30. MacArthur, M. W. & Thornton, J. M. Influence of proline residues on protein conformation. *J Mol Biol* **218,** 397–412. ISSN: 0022-2836 (Mar. 20, 1991).

31. Chiang, Y.-W., Borbat, P. P. & Freed, J. H. The determination of pair distance distributions by pulsed ESR using Tikhonov regularization. *Journal of Magnetic Resonance* **172,** 279–295. ISSN: 1090-7807. http://www.sciencedirect.com/science/article/pii/S1090780704003532 (Feb. 1, 2005).

32. Hagelueken, G., Ward, R., Naismith, J. H. & Schiemann, O. MtsslWizard: In Silico Spin-Labeling and Generation of Distance Distributions in PyMOL. *Appl Magn Reson* **42,** 377–391. ISSN: 0937-9347, 1613-7507. http://link.springer.com/10.1007/s00723-012-0314-0 (Apr. 2012).

33. Pisani, P., Caporuscio, F., Carlino, L. & Rastelli, G. Molecular Dynamics Simulations and Classical Multidimensional Scaling Unveil New Metastable States in the Conformational Landscape of CDK2. *PLOS ONE* **11,** e0154066. ISSN: 1932-6203. https://journals.plos.org/plosone/article?id=10.1371/journal.pone.0154066 (Apr. 21, 2016).

34. Brown, N. R. *et al.* Effects of Phosphorylation of Threonine 160 on Cyclin-dependent Kinase 2 Structure and Activity. *J. Biol. Chem.* **274,** 8746–8756. ISSN: 0021-9258, 1083-351X. http://www.jbc.org/content/274/13/8746 (Mar. 26, 1999).

35. Alexander, L. T. *et al.* Type II Inhibitors Targeting CDK2. *ACS Chem. Biol.* **10,** 2116–2125. ISSN: 1554-8929. https://doi.org/10.1021/acschembio.5b00398 (Sept. 18, 2015).

36. Tsai, C.-J. & Nussinov, R. A Unified View of "How Allostery Works". *PLOS Computational Biology* **10,** e1003394. ISSN: 1553-7358. https://journals.plos.org/ploscompbiol/article?id=10.1371/journal.pcbi.1003394 (Feb. 6, 2014).

37. Battiste, J. L. & Wagner, G. Utilization of Site-Directed Spin Labeling and High-Resolution Heteronuclear Nuclear Magnetic Resonance for Global Fold Determination of Large Proteins with Limited Nuclear Overhauser Effect Data. *Biochemistry* **39,** 5355–5365. ISSN: 0006-2960. https://doi.org/10.1021/bi000060h (May 1, 2000).

38. Song, H. *et al.* Phosphoprotein–Protein Interactions Revealed by the Crystal Structure of Kinase-Associated Phosphatase in Complex with PhosphoCDK2. *Molecular Cell* **7,** 615–626. ISSN: 1097-2765. http://www.sciencedirect.com/science/article/pii/S1097276501002088 (Mar. 1, 2001).

39. Levinson, N. M. The multifaceted allosteric regulation of Aurora kinase A. *Biochemical Journal* **475,** 2025–2042. ISSN: 0264-6021. https://doi.org/10.1042/BCJ20170771 (June 26, 2018).

40. Pannier, M., Veit, S., Godt, A., Jeschke, G. & Spiess, H. W. Dead-Time Free Measurement of Dipole–Dipole Interactions between Electron Spins. *Journal of Magnetic Resonance* **142,** 331–340. ISSN: 1090-7807. https://www.sciencedirect.com/science/article/pii/S1090780799919444 (Feb. 1, 2000).

41. Priestley, M. *Spectral Analysis and Time Series* 890 pp. ISBN: 978-0-08-057055-6 (Academic Press, London, 1982).

42. Wood, D. J. *et al.* Differences in the Conformational Energy Landscape of CDK1 and CDK2 Suggest a Mechanism for Achieving Selective CDK Inhibition. *Cell Chemical Biology* **0.** ISSN: 2451-9456, 2451-9448. https://www.cell.com/cell-chemical-biology/abstract/S2451-9456(18)30375-1 (Nov. 21, 2018).

43. Shapiro, G. I. Preclinical and Clinical Development of the Cyclin-Dependent Kinase Inhibitor Flavopiridol. *Clin Cancer Res* **10,** 4270s–4275s. ISSN: 1078-0432, 1557-3265. https://clincancerres.aacrjournals.org/content/10/12/4270s (June 15, 2004).

44. Harmon, A. D., Weiss, U. & Silverton, J. The structure of rohitukine, the main alkaloid of Amoora rohituka (Syn. Aphanamixis polystachya) (meliaceae). *Tetrahedron Letters* **20,** 721–724. ISSN: 00404039. https://linkinghub.elsevier.com/retrieve/pii/S0040403901935567 (Jan. 1979).

45. Naik, R. G. *et al.* An antiinflammatory cum immunomodulatory piperidinylbenzopyranone from dysoxylum binectariferum : isolation, structure and total synthesis. *Tetrahedron* **44,** 2081–2086. ISSN: 00404020. https://linkinghub.elsevier.com/retrieve/pii/S0040402001903527 (Jan. 1988).

46. Losiewicz, M. D., Carlson, B. A., Kaur, G., Sausville, E. A. & Worland, P. J. Potent inhibition of CDC2 kinase activity by the flavonoid L86-8275. *Biochem Biophys Res Commun* **201,** 589–595. ISSN: 0006-291X (June 15, 1994).

47. Carlson, B. A., Dubay, M. M., Sausville, E. A., Brizuela, L. & Worland, P. J. Flavopiridol induces G1 arrest with inhibition of cyclin-dependent kinase (CDK) 2 and CDK4 in human breast carcinoma cells. *Cancer Res* **56,** 2973–2978. ISSN: 0008-5472 (July 1, 1996).

48. Sedlacek, H. *et al.* Flavopiridol (L86 8275; NSC 649890), a new kinase inhibitor for tumor therapy. *Int J Oncol* **9,** 1143–1168. ISSN: 1019-6439 (Dec. 1996).

49. Phelps, M. A. *et al.* Clinical response and pharmacokinetics from a phase 1 study of an active dosing schedule of flavopiridol in relapsed chronic lymphocytic leukemia. *Blood* **113,** 2637–2645. ISSN: 0006-4971. https://doi.org/10.1182/blood-2008-07-168583 (Mar. 19, 2009).

50. Havlíček, L. *et al.* Cytokinin-Derived Cyclin-Dependent Kinase Inhibitors: Synthesis and cdc2 Inhibitory Activity of Olomoucine and Related Compounds. *J. Med. Chem.* **40,** 408–412. ISSN: 0022-2623. https://doi.org/10.1021/jm960666x (Feb. 1, 1997).

51. Khalil, H. S., Mitev, V., Vlaykova, T., Cavicchi, L. & Zhelev, N. Discovery and development of Seliciclib. How systems biology approaches can lead to better drug performance. *Journal of Biotechnology. Progress in Biotechnology: EuroBiotech 2014* **202,** 40–49. ISSN: 0168-1656. https://www.sciencedirect.com/science/article/pii/S0168165615000942 (May 20, 2015).

52. Azevedo, W. F. D. *et al.* Inhibition of Cyclin-Dependent Kinases by Purine Analogues. *European Journal of Biochemistry* **243,** 518–526. ISSN: 1432-1033. https://febs.onlinelibrary.wiley.com/doi/abs/10.1111/j.1432-1033.1997.0518a.x (1997).

53. Bettayeb, K. *et al.* CR8, a potent and selective, roscovitine-derived inhibitor of cyclin-dependent kinases. *Oncogene* **27,** 5797–5807. ISSN: 1476-5594 (Oct. 2, 2008).

54. Le Tourneau, C. *et al.* Phase I evaluation of seliciclib (R-roscovitine), a novel oral cyclin-dependent kinase inhibitor, in patients with advanced malignancies. *European Journal of Cancer* **46,** 3243–3250. ISSN: 0959-8049. https://www.sciencedirect.com/science/article/pii/S0959804910007823 (Dec. 1, 2010).

55. Paruch, K. *et al.* Discovery of Dinaciclib (SCH 727965): A Potent and Selective Inhibitor of Cyclin-Dependent Kinases. *ACS Med. Chem. Lett.* **1,** 204–208. ISSN: 1948-5875, 1948-5875. http://pubs.acs.org/doi/10.1021/ml100051d (Aug. 12, 2010).

56. Parry, D. *et al.* Dinaciclib (SCH 727965), a Novel and Potent Cyclin-Dependent Kinase Inhibitor. *Mol Cancer Ther* **9,** 2344–2353. ISSN: 1535-7163, 1538-8514. https://mct.aacrjournals.org/content/9/8/2344 (Aug. 1, 2010).

57. Mita, M. M. *et al.* Randomized phase II trial of the cyclin-dependent kinase inhibitor dinaciclib (MK-7965) versus capecitabine in patients with advanced breast cancer. *Clin Breast Cancer* **14,** 169–176. ISSN: 1938-0666 (June 2014).

58. Stephenson, J. J. *et al.* Randomized phase 2 study of the cyclin-dependent kinase inhibitor dinaciclib (MK-7965) versus erlotinib in patients with non-small cell lung cancer. *Lung Cancer* **83,** 219–223. ISSN: 1872-8332 (Feb. 2014).

59. Ghia, P. *et al.* Efficacy and safety of dinaciclib vs ofatumumab in patients with relapsed/refractory chronic lymphocytic leukemia. *Blood* **129,** 1876–1878. ISSN: 0006-4971. https://doi.org/10.1182/blood-2016-10-748210 (Mar. 30, 2017).

60. Flynn, J. *et al.* Dinaciclib is a novel cyclin-dependent kinase inhibitor with significant clinical activity in relapsed and refractory chronic lymphocytic leukemia. *Leukemia* **29,** 1524–1529. ISSN: 1476-5551. https://www.nature.com/articles/leu201531 (July 2015).

61. Martin, M. P., Olesen, S. H., Georg, G. I. & Schönbrunn, E. Cyclin-Dependent Kinase Inhibitor Dinaciclib Interacts with the Acetyl-Lysine Recognition Site of Bromodomains. *ACS Chem. Biol.* **8,** 2360–2365. ISSN: 1554-8929. https://doi.org/10.1021/cb4003283 (Nov. 15, 2013).

62. Chen, P. *et al.* Spectrum and Degree of CDK Drug Interactions Predicts Clinical Performance. *Molecular Cancer Therapeutics* **15,** 2273–2281. ISSN: 1535-7163, 1538-8514. http://mct.aacrjournals.org/cgi/doi/10.1158/1535-7163.MCT-16-0300 (Oct. 1, 2016).

63. Anderson, M. *et al.* Imidazoles: SAR and development of a potent class of cyclin-dependent kinase inhibitors. *Bioorganic & Medicinal Chemistry Letters* **18,** 5487–5492. ISSN: 0960-894X. https://www.sciencedirect.com/science/article/pii/S0960894X08010792 (Oct. 15, 2008).

64. Byth, K. F. *et al.* AZD5438, a potent oral inhibitor of cyclin-dependent kinases 1, 2, and 9, leads to pharmacodynamic changes and potent antitumor effects in human tumor xenografts. *Mol Cancer Ther* **8,** 1856–1866. ISSN: 1535-7163, 1538-8514. https://mct.aacrjournals.org/content/8/7/1856 (July 1, 2009).

65. Boss, D. S. *et al.* Safety, tolerability, pharmacokinetics and pharmacodynamics of the oral cyclin-dependent kinase inhibitor AZD5438 when administered at intermittent and continuous dosing schedules in patients with advanced solid tumours. *Annals of Oncology* **21,** 884–894. ISSN: 0923-7534. https://www.sciencedirect.com/science/article/pii/S0923753419389355 (Apr. 1, 2010).

66. Cristofanilli, M. *et al.* Fulvestrant plus palbociclib versus fulvestrant plus placebo for treatment of hormone-receptor-positive, HER2-negative metastatic breast cancer that progressed on previous endocrine therapy (PALOMA-3): final analysis of the multicentre, double-blind, phase 3 randomised controlled trial. *The Lancet*

Oncology **17,** 425–439. ISSN: 1470-2045. https://www.sciencedirect.com/science/article/pii/S1470204515006130 (Apr. 1, 2016).

67. VanderWel, S. N. *et al.* Pyrido[2,3-d]pyrimidin-7-ones as Specific Inhibitors of Cyclin-Dependent Kinase 4. *J. Med. Chem.* **48,** 2371–2387. ISSN: 0022-2623. https://doi.org/10.1021/jm049355+ (Apr. 1, 2005).

68. Toogood, P. L. *et al.* Discovery of a Potent and Selective Inhibitor of Cyclin-Dependent Kinase 4/6. *J. Med. Chem.* **48,** 2388–2406. ISSN: 0022-2623. https://doi.org/10.1021/jm049354h (Apr. 1, 2005).

69. Lu, H. & Schulze-Gahmen, U. Toward understanding the structural basis of cyclin-dependent kinase 6 specific inhibition. *J Med Chem* **49,** 3826–3831. ISSN: 0022-2623 (June 29, 2006).

70. Hortobagyi, G. N. *et al.* Ribociclib as First-Line Therapy for HR-Positive, Advanced Breast Cancer. *New England Journal of Medicine* **375,** 1738–1748. ISSN: 0028-4793. https://doi.org/10.1056/NEJMoa1609709 (Nov. 3, 2016).

71. Hafner, M. *et al.* Multiomics Profiling Establishes the Polypharmacology of FDA-Approved CDK4/6 Inhibitors and the Potential for Differential Clinical Activity. *Cell Chemical Biology* **26,** 1067–1080.e8. ISSN: 2451-9456, 2451-9448. http://www.cell.com/cell-chemical-biology/abstract/S2451-9456(19)30174-6 (Aug. 15, 2019).

72. Taylor-Harding, B. *et al.* Cyclin E1 and RTK/RAS signaling drive CDK inhibitor resistance via activation of E2F and ETS. *Oncotarget* **6,** 696–714. ISSN: 1949-2553 (Jan. 20, 2015).

73. Herrera-Abreu, M. T. *et al.* Early Adaptation and Acquired Resistance to CDK4/6 Inhibition in Estrogen Receptor-Positive Breast Cancer. *Cancer Res* **76,** 2301–2313. ISSN: 1538-7445 (Apr. 15, 2016).

74. Dickler, M. N. *et al.* MONARCH1: Results from a phase II study of abemaciclib, a CDK4 and CDK6 inhibitor, as monotherapy, in patients with HR+/HER2- breast cancer, after chemotherapy for advanced disease. *JCO* **34,** 510–510. ISSN: 0732-183X. https://ascopubs.org/doi/abs/10.1200/jco.2016.34.15_suppl.510 (May 20, 2016).

75. Gelbert, L. M. *et al.* Preclinical characterization of the CDK4/6 inhibitor LY2835219: in-vivo cell cycle-dependent/independent anti-tumor activities alone/in combination with gemcitabine. *Invest New Drugs* **32,** 825–837. ISSN: 1573-0646. https://doi.org/10.1007/s10637-014-0120-7 (Oct. 1, 2014).

76. Lake, E. W. *et al.* Quantitative conformational profiling of kinase inhibitors reveals origins of selectivity for Aurora kinase activation states. *PNAS* **115,** E11894–E11903. ISSN: 0027-8424, 1091-6490. https://www.pnas.org/content/115/51/E11894 (Dec. 18, 2018).

77. Levinson, N. M. *et al.* A Src-Like Inactive Conformation in the Abl Tyrosine Kinase Domain. *PLOS Biology* **4,** e144. ISSN: 1545-7885. https://journals.plos.org/plosbiology/article?id=10.1371/journal.pbio.0040144 (May 2, 2006).

78. Levinson, N. M. & Boxer, S. G. A conserved water-mediated hydrogen bond network defines bosutinib's kinase selectivity. *Nature Chemical Biology* **10,** 127–132. ISSN: 1552-4469. https://www.nature.com/articles/nchembio.1404 (Feb. 2014).

79. Cyphers, S., Ruff, E. F., Behr, J. M., Chodera, J. D. & Levinson, N. M. A water-mediated allosteric network governs activation of Aurora kinase A. *Nature Chemical Biology* **13,** 402–408. ISSN: 1552-4469. https://www.nature.com/articles/nchembio.2296 (Apr. 2017).

80. Bao, Z. Q., Jacobsen, D. M. & Young, M. A. Briefly Bound to Activate: Transient Binding of a Second Catalytic Magnesium Activates the Structure and Dynamics of CDK2 Kinase for Catalysis. *Structure* **19,** 675–690. ISSN: 0969-2126. http://www.cell.com/structure/abstract/S0969-2126(11)00132-8 (May 11, 2011).

81. Hall, D. A. Modeling the Functional Effects of Allosteric Modulators at Pharmacological Receptors: An Extension of the Two-State Model of Receptor Activation. *Mol Pharmacol* **58,** 1412–1423. ISSN: 0026-895X, 1521-0111. https://molpharm.aspetjournals.org/content/58/6/1412 (Dec. 1, 2000).

82. Schaaf, T. M., Peterson, K. C., Grant, B. D., Thomas, D. D. & Gillispie, G. D. Spectral Unmixing Plate Reader: High-Throughput, High-Precision FRET Assays in Living Cells. *SLAS DISCOVERY: Advancing the Science of Drug Discovery* **22,** 250–261. ISSN: 2472-5552. https://doi.org/10.1177/1087057116679637 (Mar. 1, 2017).

83. Sievers, F. *et al.* Fast, scalable generation of high-quality protein multiple sequence alignments using Clustal Omega. *Molecular Systems Biology* **7,** 539. ISSN: 1744-4292. https://www.embopress.org/doi/full/10.1038/msb.2011.75 (Jan. 1, 2011).

84. Robert, X. & Gouet, P. Deciphering key features in protein structures with the new ENDscript server. *Nucleic Acids Research* **42,** W320–W324. ISSN: 0305-1048. https://doi.org/10.1093/nar/gku316 (W1 July 1, 2014).

85. Echalier, A., Endicott, J. A. & Noble, M. E. M. Recent developments in cyclin-dependent kinase biochemical and structural studies. *Biochimica et Biophysica Acta (BBA) - Proteins and Proteomics. Inhibitors of Protein Kinases* **1804,** 511–519. ISSN: 1570-9639. https://www.sciencedirect.com/science/article/pii/S157096390900291X (Mar. 1, 2010).

86. Brown, N. R. *et al.* CDK1 structures reveal conserved and unique features of the essential cell cycle CDK. *Nature Communications* **6,** 6769. ISSN: 2041-1723. https://www.nature.com/articles/ncomms7769 (Apr. 13, 2015).

87. Greber, B. J. *et al.* The cryoelectron microscopy structure of the human CDK-activating kinase. *PNAS* **117,** 22849–22857. ISSN: 0027-8424, 1091-6490. https://www.pnas.org/content/117/37/22849 (Sept. 15, 2020).

88. Merrick, K. A. *et al.* Distinct Activation Pathways Confer Cyclin-Binding Specificity on Cdk1 and Cdk2 in Human Cells. *Molecular Cell* **32,** 662–672. ISSN: 1097-2765. http://www.sciencedirect.com/science/article/pii/S1097276508007636 (Dec. 5, 2008).

89. Topacio, B. R. *et al.* Cyclin D-Cdk4,6 Drives Cell-Cycle Progression via the Retinoblastoma Protein's C-Terminal Helix. *Molecular Cell* **74,** 758–770.e4. ISSN: 1097-2765. https://www.sciencedirect.com/science/article/pii/S1097276519302242 (May 16, 2019).

90. Takeda, D. Y., Wohlschlegel, J. A. & Dutta, A. A Bipartite Substrate Recognition Motif for Cyclin-dependent Kinases *. *Journal of Biological Chemistry* **276.** Publisher: Elsevier, 1993–1997. ISSN: 0021-9258, 1083-351X. https://www.jbc.org/article/S0021-9258(18)46703-8/abstract (Jan. 19, 2001).

91. Patra, D., Wang, S. X., Kumagai, A. & Dunphy, W. G. The Xenopus Suc1/Cks Protein Promotes the Phosphorylation of G2/M Regulators*. *Journal of Biological Chemistry* **274,** 36839–36842. ISSN: 0021-9258. https://www.sciencedirect.com/science/article/pii/S0021925819530307 (Dec. 24, 1999).

92. Fisher, R. P., Jin, P., Chamberlin, H. M. & Morgan, D. O. Alternative mechanisms of CAK assembly require an assembly factor or an Activating Kinase. *Cell* **83,** 47–57. ISSN: 00928674. https://linkinghub.elsevier.com/retrieve/pii/0092867495902333 (Oct. 1995).

93. Gu, Y., Rosenblatt, J. & Morgan, D. O. Cell cycle regulation of CDK2 activity by phosphorylation of Thr160 and Tyr15. *EMBO J* **11,** 3995–4005. ISSN: 0261-4189 (Nov. 1992).

94. Sherr, C. J. & Roberts, J. M. CDK inhibitors: positive and negative regulators of G1-phase progression. *Genes Dev.* **13,** 1501–1512. ISSN: 0890-9369, 1549-5477. http://genesdev.cshlp.org/content/13/12/1501 (June 15, 1999).

95. Besson, A., Dowdy, S. F. & Roberts, J. M. CDK Inhibitors: Cell Cycle Regulators and Beyond. *Developmental Cell* **14,** 159–169. ISSN: 1534-5807. https://www.sciencedirect.com/science/article/pii/S1534580708000415 (Feb. 12, 2008).

96. Guiley, K. Z. *et al.* p27 allosterically activates cyclin-dependent kinase 4 and antagonizes palbociclib inhibition. *Science* **366.** ISSN: 0036-8075, 1095-9203. http://science.sciencemag.org/content/366/6471/eaaw2106 (Dec. 13, 2019).

97. Paez, J. G. *et al.* EGFR Mutations in Lung Cancer: Correlation with Clinical Response to Gefitinib Therapy. *Science* **304,** 1497–1500. ISSN: 0036-8075, 1095-9203. https://science.sciencemag.org/content/304/5676/1497 (June 4, 2004).

98. Chi, Y. *et al.* Identification of CDK2 substrates in human cell lysates. *Genome Biology* **9,** R149. ISSN: 1474-760X. https://doi.org/10.1186/gb-2008-9-10-r149 (Oct. 13, 2008).

99. Hagopian, J. C. *et al.* Kinetic Basis for Activation of CDK2/Cyclin A by Phosphorylation. *Journal of Biological Chemistry* **276,** 275–280. ISSN: 0021-9258, 1083-351X. https://www.jbc.org/article/S0021-9258(18)44235-4/abstract (Jan. 5, 2001).

100. Stevenson-Lindert, L. M., Fowler, P. & Lew, J. Substrate Specificity of CDK2-Cyclin A WHAT IS OPTIMAL? *J. Biol. Chem.* **278,** 50956–50960. ISSN: 0021-9258, 1083-351X. http://www.jbc.org/content/278/51/50956 (Dec. 19, 2003).

101. Finn, R. S. *et al.* The cyclin-dependent kinase 4/6 inhibitor palbociclib in combination with letrozole versus letrozole alone as first-line treatment of oestrogen receptor-positive, HER2-negative, advanced breast cancer (PALOMA-1/TRIO-18): a randomised phase 2 study. *The Lancet Oncology* **16,** 25–35. ISSN: 1470-2045, 1474-5488. http://www.thelancet.com/journals/lanonc/article/PIIS1470-2045(14)71159-3/abstract (Jan. 1, 2015).

102. Lolli, G. Structural dissection of cyclin dependent kinases regulation and protein recognition properties. *Cell Cycle* **9,** 1551–1561. ISSN: 1551-4005 (Apr. 15, 2010).

103. Honda, R. *et al.* The structure of cyclin E1/CDK2: implications for CDK2 activation and CDK2-independent roles. *EMBO J* **24,** 452–463. ISSN: 0261-4189 (Feb. 9, 2005).

104. Betzi, S. *et al.* Discovery of a potential allosteric ligand binding site in CDK2. *ACS Chem Biol* **6,** 492–501. ISSN: 1554-8937 (May 20, 2011).

105. Christodoulou, M. S. *et al.* Probing an Allosteric Pocket of CDK2 with Small Molecules. *ChemMedChem* **12,** 33–41. ISSN: 1860-7187 (Jan. 5, 2017).

106. Callender, J. A. *et al.* Protein kinase Cα gain-of-function variant in Alzheimer's disease displays enhanced catalysis by a mechanism that evades down-regulation. *PNAS* **115,** E5497–E5505. ISSN: 0027-8424, 1091-6490. `https://www.pnas.org/content/115/24/E5497` (June 12, 2018).

107. Gutiérrez-Escribano, P. & Nurse, P. A single cyclin–CDK complex is sufficient for both mitotic and meiotic progression in fission yeast. *Nature Communications* **6,** 6871. ISSN: 2041-1723. `http://www.nature.com/articles/ncomms7871` (Apr. 20, 2015).

108. Davies, H. *et al.* Mutations of the BRAF gene in human cancer. *Nature* **417,** 949–954. ISSN: 0028-0836 (June 27, 2002).

109. Lynch, T. J. *et al.* Activating Mutations in the Epidermal Growth Factor Receptor Underlying Responsiveness of Non–Small-Cell Lung Cancer to Gefitinib. *New England Journal of Medicine* **350,** 2129–2139. ISSN: 0028-4793. `https://doi.org/10.1056/NEJMoa040938` (May 20, 2004).

Appendix A

A brief comparison of Cdk2 and AurA DEER results

An important consideration in measuring effects of inhibitors on kinase conformation is the value of *context*. A single DEER measurement will provide a distance distribution for a sample, but it is extremely difficult to extract meaning from a single distance distribution in isolation; the power of this study is derived from our ability to measure multiple inhibitors bound to the same protein and order them by their ability to effect conformational change (Figure A.1).

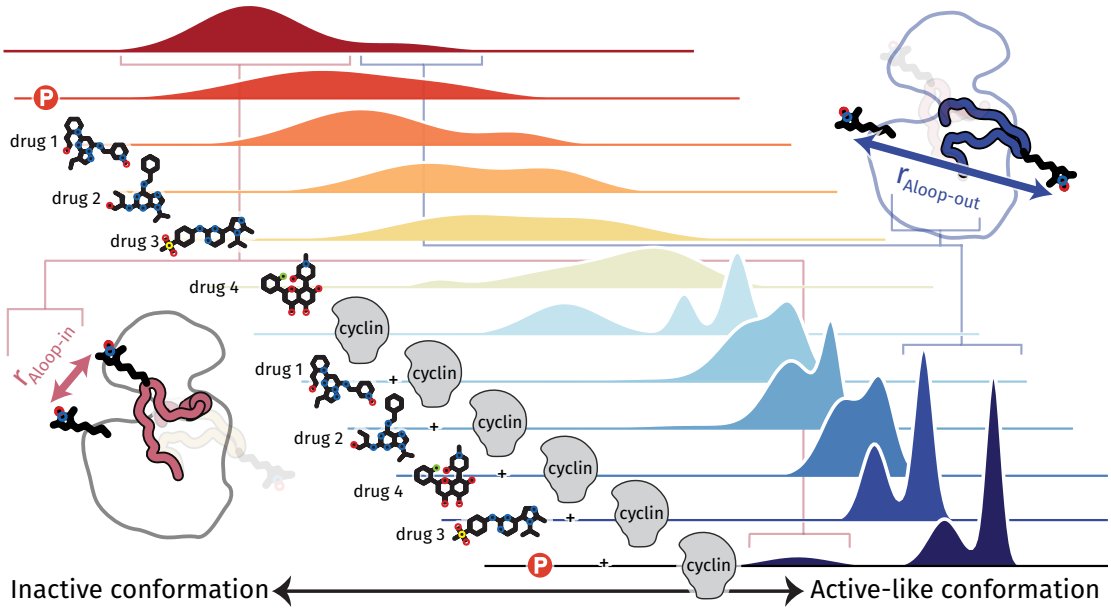

Figure A.1: Cdk2 inhibitors ordered by their ability to shift the balance between the Aloop-in and Aloop-out states of Cdk2 with and without cyclinA. Not only does this make for a pleasing visual, but it also drives home the point that the kinase is emphatically not switch-like, but rather transitions in a graded fashion.

The conserved nature of the kinase fold facilitates interesting comparisons across different kinases as well. For example, we performed a set of DEER experiments on phosphorylated, monomeric Aurora A (pAurA), a kinase that regulates cell cycle centrosome maturation and microtubule assembly, in the presence of several inhibitors (Figure A.2)[76]. The results look superficially similar to those of Cdk2; pAurA samples a continuum of conformational states intermediate between the DFG-in and DFG-out extremes. It is important to notice that although AurA is also regulated by the binding of other proteins (somewhat analogous to cyclins for the CDKs), unlike with Cdk2, monomeric pAurA seems more conformationally flexible than monomeric Cdk2 and is perfectly capable of adopting a full DFG-in state when bound to the inhibitor SNS-314.

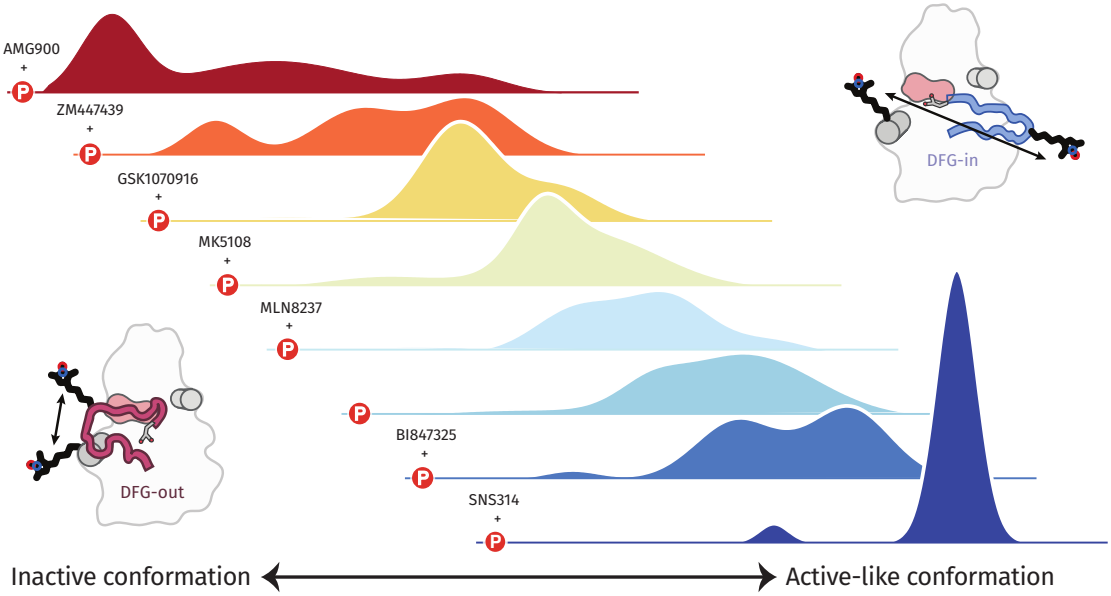

Figure A.2: A sampling of Aurora A inhibitors ordered by their ability to shift the balance between the DFG-in and DFG-out conformations of monomeric, phosphorylated Aurora A. Adapted from [76].